Addis Ababa University

Addis Ababa Institute of Technology

School of Mechanical and Industrial Engineering

Optimization of process parameters in Friction Stir Welding of dissimilar aluminum alloys (AA6061–T6 and AA5052–H32)

A Master Thesis Submitted to Graduate School of Addis Ababa University in Partial Fulfillment of the Requirements for the Award of Degree of Masters of Science (M.Sc.) in Mechanical Engineering (Manufacturing Engineering)

By: **Wondu Tesfaye Heramo**

Advisor**: Mr. Henok Zewdu (Ph.D. Candidate)**

Addis Ababa, Ethiopia

March, 2023

Addis Ababa University
Addis Ababa Institute of Technology
School of Mechanical and Industrial Engineering

Optimization of process parameters in FSW of dissimilar aluminum alloys (AA6061–T6 and AA5052–H32)

By: Wondu Tesfaye Heramo

Submitted for the requirements of the degree

Master of Science (M.Sc.)

Approved by: Board of Examiners

Henok Zewdu		28-03-2023
Advisor	Signature	date
Co – Advisor	Signature	date
Desalegn Wogaso (PhD)		28-03-2023
Internal examiner	Signature	date
Mesfin Gebeyaw (PhD)		28-03-2023
External examiner	Signature	date
Dr. Tenaya Abera		28/03/2023
Dean of the School	Signature	date

DECLARATION

I now declare that this thesis entitled **"Optimization of process parameters in Friction Stir Welding of dissimilar aluminum alloys (AA6061–T6 and AA5052–H32)"** is prepared by me with the guidance of my advisor the work contained here is my own except where explicitly stated otherwise in the text. This work had never been submitted in a complete or part, for any other degree or professional qualification.

Wondu Tesfaye Heramo		28/03/2023
Student Name	Signature	date

This is to certify that the above declaration made by the candidate is correct to the best of our knowledge and belief. It has been submitted for examination with our approval.

Henok Zewdu		28-03-2023
Advisor	Signature	date
Co – Advisor	Signature	date

ACKNOWLEDGEMENT

First, I want to give thanks to the Almighty God, who gave me the strength to overcome several challenges and complete my thesis. I want to express my gratitude to my advisors Professor Shantha Kumar and Mr. Henok Zewdu, for their essential guidance, ongoing inspiration, and patience throughout my MSc thesis. Their knowledge and experience have continuously inspired me while I work on my thesis.

I would like to thank Dr. Yilma Tadesse and Dr. Bikila Teklu for writing support letters for Ethiopia's customs and revenue authorities to get aluminum plates imported from China.

I must thank all the staff members of SMIE, especially the manufacturing stream, for their assistance and support to complete my work. I would also like to thank Mr. Israel and Mr. Masresha for their technical support during the fabrication of the fixture and tool.

I would like to thank my best friend, Mr. Wubishet Abera, who encouraged me during my thesis work.

I would like to thank the instructors of Federal TVET College, Mr. Gezae Mebratu, Mr. Tewodros Alem, and Mr. Kemhu for facilitating the experimental workplace and machines and giving important feedback on my work.

Finally, I'd like to thank my family, friends, and classmates. Without their support and understanding throughout the previous few years, I would not have been able to complete my thesis work.

ABSTRACT

Friction stir welding (FSW) is a solid-state welding method mostly used to join aluminum and aluminum alloys that has been used in aerospace, railway, automotive, and marine applications. This process is used for welding dissimilar aluminum alloys. Solid-state welding processes solve several problems that occur during fusion welding of Al-alloys like heat affected zone liquation cracking, porosity, and segregation.

Aluminum Alloys of two different series AA5052 and AA6061 thickness of 6mm are Friction Stir welded using process parameters like tool rotational speed (900,1100,1400) rpm, transverse speed (40,50,60) mm/min, and pin profiles (cylindrical, conical, and square). This thesis aims to optimize the mechanical and metallurgical properties of the above dissimilar combination to evaluate the performance and characteristics of the welded joints. The combined Taguchi and Grey relation analysis experimental method was chosen to construct the number of welding experiments. Analysis of variance was performed to obtain the effect of the parameters on the Friction Stir welded joints strength.

The plates are successfully welded, and the welded plates are tested at room temperature to examine their tensile strength and hardness. The findings indicate that the square pin profile, the rotational speed of 1400 rpm, and the transverse speed of 40 mm/min are the optimum parameters for joining these dissimilar joints. A fine and uniform distribution of strengthening precipitates was found in the stir zone.

Keywords: Friction Stir Welding, Parameter Optimization, Microstructure, Grey relation analysis, Pin profile, AA6061–T6 and AA5052–H32.

TABLE OF CONTENTS

LIST OF FIGURES

LIST OF TABLES

LIST OF ABBREVIATIONS

3D	Three Dimensional
AA	Aluminum Alloy
CMM	Convectional Milling Machine
CNC	Computer Numerical Control
DOE	Design of Experiment
FSW	Friction Stir Welding
FSWP	Friction Stir Welding Process
GMAW	Gas Metal Arc Welding
GRA	Gray Relation Analysis
GTAW	Gas Tungsten Arc Welding
HAZ	Heat Affected Zone
HRC	Rockwell Hardness
HSS	High Speed Steel
HV	Vickers Hardness
MIG	Metal Inert Gas
OA	Orthogonal Array
PCA	Principal Component Analysis
SEM	Scanning Electron Microscope
SZ	Stir Zone
TIG	Tungsten Inert Gas
TMAZ	Thermo mechanical Heat Affected Zone
UK	United Kingdom
UTM	Universal Testing Machine
WS	Welding Speed

CHAPTER ONE

1. INTRODUCTION

1.1 Background of the Study

Friction-stir welding is an advanced solid-state joining technique, and it is an environment-friendly process because of the low emission of fumes during the process when compared to that fusion welding processes. This welding technique makes use of a non-consumable welding tool to generate heat by friction between the tool and the material. The process has an advancing side and a retreating side, as the tool gets in contact with the plate. The pin will have impinged to the plate while the shoulder of the tool encounters the workpiece. As a result, the material gets plasticized due to stirring action and material movement takes place because of frictional heat generated in the process from the retreating side to the advancing side. The tool used in the FSW process can be straight, cylindrical, tapered, threaded, or unthreaded pins [1,2].

FSW was first introduced by Thomas and Nicholas at the Welding Institute, Cambridge, UK in 1991 [3]. FSW uses a rotating tool with a pin and shoulder for heat generation, which is used for softening the base materials. The process has two welded sides. The advanced side is found in the direction of the tool, and the weld axis is in the same direction. The retreating side is the direction of the tool, and the weld axis is in the opposite direction [4].

The applications of aluminum and aluminum alloys are mostly in the aircraft, shipping, defense, and transportation industries as they possess certain properties, like being lightweight, having high corrosion resistance, good mechanical properties, and a good strength-to-weight ratio [4]. Joining soft materials by fusion welding is difficult and results in low mechanical and metallurgical properties due to the formation of a brittle inter-metallic compound at the weld joint. FSW is used to solve this problem. In this process, the joint is produced at a low temperature and with high strength compared with fusion welding [5–7].

Nowadays, AA6061 is categorized under the 6000 series moderate strength, which has the alloying elements magnesium and silicon (Al–Mg–Si) and is used for external body panels in the automotive sector. AA5052 is categorized under the 5000 series of strong work hardening alloys, which have alloying element magnesium (Al-Mg) and are used for internal body panels in the automotive sector. Both alloys are used in the shipbuilding and automotive sectors due to their lightweight and higher strength [4].

However, it needs appropriate process control. Therefore, the aim of this thesis deals with finding optimum process parameters for the tensile and hardness strength of the dissimilar FSW of the above materials.

1.2 Problem Statement

Aluminum alloys, have lightweight and high strength, are used for industries like shipbuilding, automotive, and railway. Aluminum alloys meet the demand for lightweight materials in the shipbuilding and automotive industries. The aluminum alloys AA6xxx and AA5xxx are widely utilized in shipbuilding, automobile manufacturing, and other structural applications [8]. For instance, the 5xxx series is used in automobiles in the inner part of door panels and the outer hulls of ships for good corrosion resistance. Similarly, the 6xxx series is used in the outer part of door panels and inner structural parts of shipbuilding for appearance and strength [4]. Dissimilar joining of both series of aluminum alloys is required. Dissimilar welding of these two alloys is frequently encountered in those structures. Structural parts and frames composed of these aluminum alloys can be welded using sound welding techniques commonly used in industries. Non-ferrous materials, especially aluminum and its alloys, join permanently using rivets and/or fusion welding. Besides adding more weights to the material, using rivets require different manufacturing processes: locating drill holes; punching; drilling, and finally riveting. It requires a high labor force and a slow production rate. In addition, rivets are exposed to corrosion and unwanted stresses. Many welding defects occur when fusion welding of aluminum alloys, including voids, spatters, hot cracking, distortions, precipitate dissolution, work hardening loss, and lack of penetration in the joints [9]. As a result, using a solid-state joining technique is especially recommended to overcome those problems.

The selection of exact and suitable process parameters to make proper joints is a challenging task for manufacturing units and structural engineers. The mechanical and microstructural properties of the joints are influenced by FSW process parameters such as tool rotational speed, transverse speed, and tool pin profile. However, process parameter optimization in dissimilar aluminum and its alloys is not adequately done. Hence, this research work aims the optimization process parameters of dissimilar 6061-T6 and 5052-H32 aluminum alloys often used in the transportation sector by making use of a new approach, FSW.

1.3 Objective of the Study

1.3.1. General Objective

The main objective of this study is the optimization of the process parameters in friction stir welding of dissimilar 6061-T6 and 5052-H32 aluminum plates.

1.3.2. Specific objectives

- ✓ Design and fabricate fixtures and backing plates for the FSW process setup, which is simple to assemble onto a CNC milling machine bed.
- ✓ Prepare FSW tool (Conical, square, and cylindrical) shape from high speed steel for friction Stir welding process.
- ✓ Conduct FSW experiments at different process parameters such as rotational speed, welding speed (transverse speed), and tool profile (conical, square, and cylindrical).
- ✓ To investigate the optimum parameter for FSW of dissimilar Al-alloys by combined Taguchi and Grey relation analysis method L9; 3 factors and 3 levels.
- ✓ Evaluate the mechanical properties of friction stir welded joints using destructive testing such as hardness and tensile tests.
- ✓ Evaluate the microstructure for each welded joint.

1.4 Scope of the Study

The scope of this research work was successfully to join dissimilar 6061-T6 and 5052-H32 aluminum plates by using the FSW process. Weld-quality and joint integrity was quantified through metallurgical evaluation and mechanical testing.

1.5 Significance of the Study

The importance of the study is FSW has many advantages over fusion welding. FSW is used for the joining of similar and dissimilar materials in the aerospace, automobile, ship, building industries, and so on. FSW machine is not available in any industries in Ethiopia and are expensive. This is not favorable for the small industries, university laboratories, or any person to invest this amount of money in expensive FSW machines. So, the study helps introduce the

possibility of the FSW process easily joining nonferrous material by preparing the setup of CNC milling machines for small industries, universities, laboratories, and so on.

1.6 Research Questions

1) Which process parameters give maximum mechanical properties of FSW joint?
2) What is the most tool pin profile that affects the mechanical properties and microstructure of welded joint?
3) Which optimization techniques are suitable for a multi-response study?

1.7 Limitations of the Study

In this thesis, in the SEM image, some scratches occur due to the lack of sufficient grinding paper with different grit sizes.

1.8 Thesis Organization

This thesis is organized into five chapters and its content is about the optimization of process parameters in FSW of AA6061-T6 and AA5052-H32.The thesis is structured as follows:

Chapter one: describes the background of the study, problem statement, objectives of the study, scope of the study, etc.

Chapter two: describes the theory and trend of research related to optimization of FSW and identifies the research gaps.

Chapter three: This chapter describes the thesis' methodology, materials, and equipment, including the material to be used, dimension, design of experiment, mechanical testing, metallurgical analysis, and method of analysis.

Chapter four: presents the experimental results and discussion of the analysis in chapter three.

Chapter Five: presents the conclusion, recommendation, and future work of the thesis.

CHAPTER TWO

2. LITERATURE REVIEW

2.1 Introduction

In this chapter, basic knowledge of the Friction Stir Welding process parameters is presented, and relevant literature has been conducted on previous work on FSW process parameters on similar and dissimilar aluminum alloys. This chapter discusses the findings of the previous researches.

2.2 FSW process

Friction Stir Welding uses a non-consumable tool consisting of a pin and shoulder that are inserted to be joined at the butt edges of the plates and traversed along the direction of the weld axis as shown in figure 2.1. The function of the rotating tool is heating the workpiece and movement of material to produce the joint. Plastic deformation occurs during the heating of workpieces generated by friction between the rotating tool and the base material. Tool rotation and translational movement produce heating which softens the material. Therefore, the joint is produced in a solid state. In the FSW process, dynamic recrystallization of the base metal occurs due to the stirring action of the tool pin. This results in the generation of fine equalized recrystallized grains, and the FSW joints that have better mechanical properties. There are two sides concerning the welding tool during FSW. On the advancing side, the direction of tool rotation and traverse is the same, and on the retreating side, the direction of tool rotation and traverse is the opposite direction [4,10].

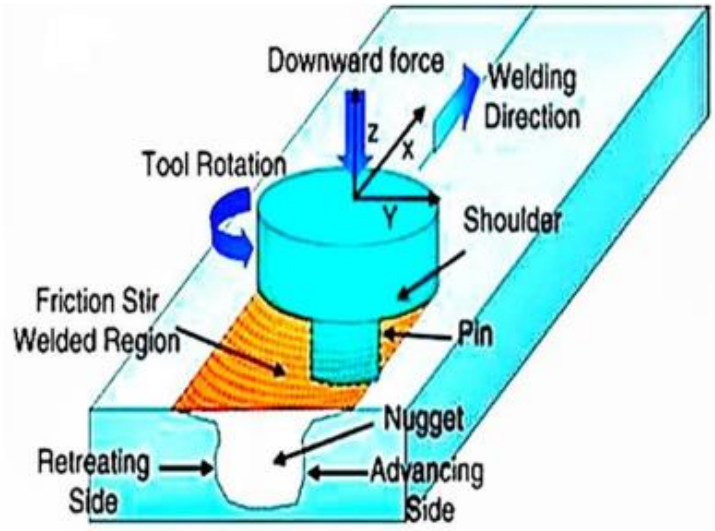

Figure 2. 1: Schematic diagram of the Friction Stir Welding Process [1]

2.3 Significance of FSW process

Friction stir welding is used to join effectively similar and dissimilar aluminum alloys. This process of joining materials is beneficial for humans, needs no consumables like (filler material, or fluxes) doesn't generate any harmful gases and is energy-efficient and environmentally beneficial [10], as summarized in Table 2.1 and Fig. 2.2. Better mechanical properties, minimal residual stress, and deformation are benefits of the FSW process [11].

Table 2. 1: Metallurgical and environmental benefits of FSW [12]

Metallurgical benefits	Environmental benefits
➢ Solid phase process ➢ Low distortion ➢ Good dimensional stability and repeatability ➢ No loss of alloying elements ➢ Excellent mechanical properties in joint area ➢ Fine recrystallized microstructure ➢ Absence of solidification cracking ➢ Post FSW formability	➢ No shielding gas required ➢ Minimal surface cleaning ➢ No harmful emission ➢ Eliminate the solvent requirement ➢ Consumable material saving such as rugs, wire, or any other gases ➢ Only 2.5 % of the energy needed compared with a laser weld.

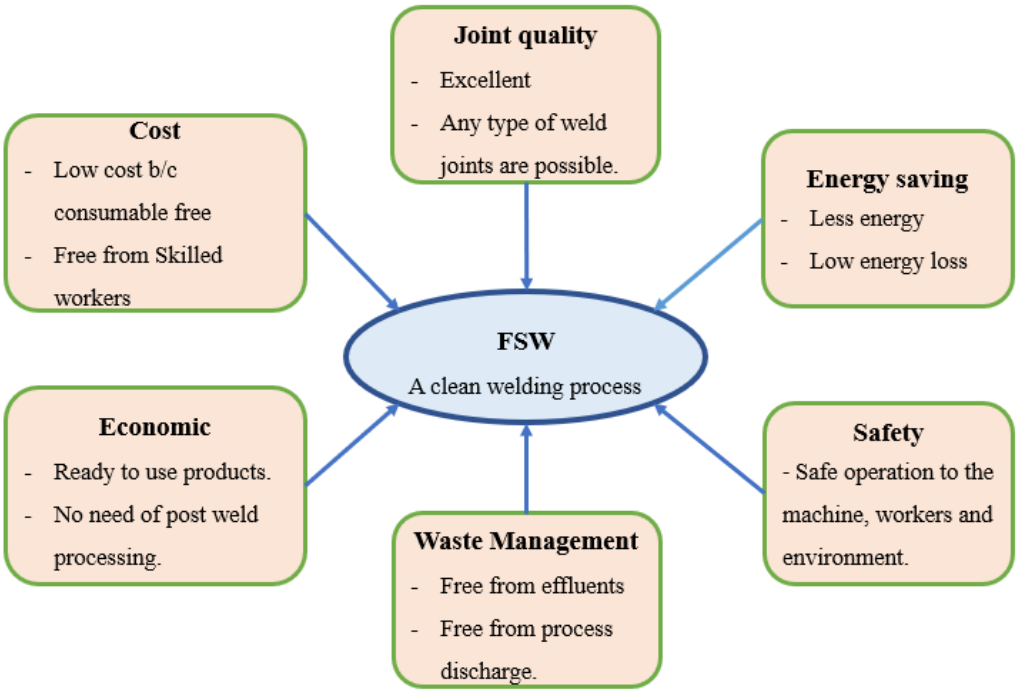

Figure 2. 2: Significance of FSW [12]

2.4 FSW process parameters

Friction Stir Welding encompasses complex material movement and plastic deformation. The microstructural evolution of the material is influenced by process parameters such as tool geometry and joint design, which have significant effects on the material flow and temperature distribution [10]. In the FSW process, major process parameters such as rotational tool, tool pin, tool shoulder, and welding parameters that affect the process are discussed in this section.

The process parameters for FSW are generally classified into three groups: The first is tooling-related parameters: such as tool material, shoulder diameter, pin length, pin diameter, feature geometry, thread pitch, D/d ratio, etc. The second is machine-related parameters: such as welding speed, plunge force or depth, spindle speed, tool tilt angle, etc.; and the third is other parameters: such as anvil material, anvil size, workpiece size, and workpiece properties [2]. The process parameters play a significant role in affecting the mechanical as well as the metallurgical properties of the welded joints are shown in Fig. 2.3.

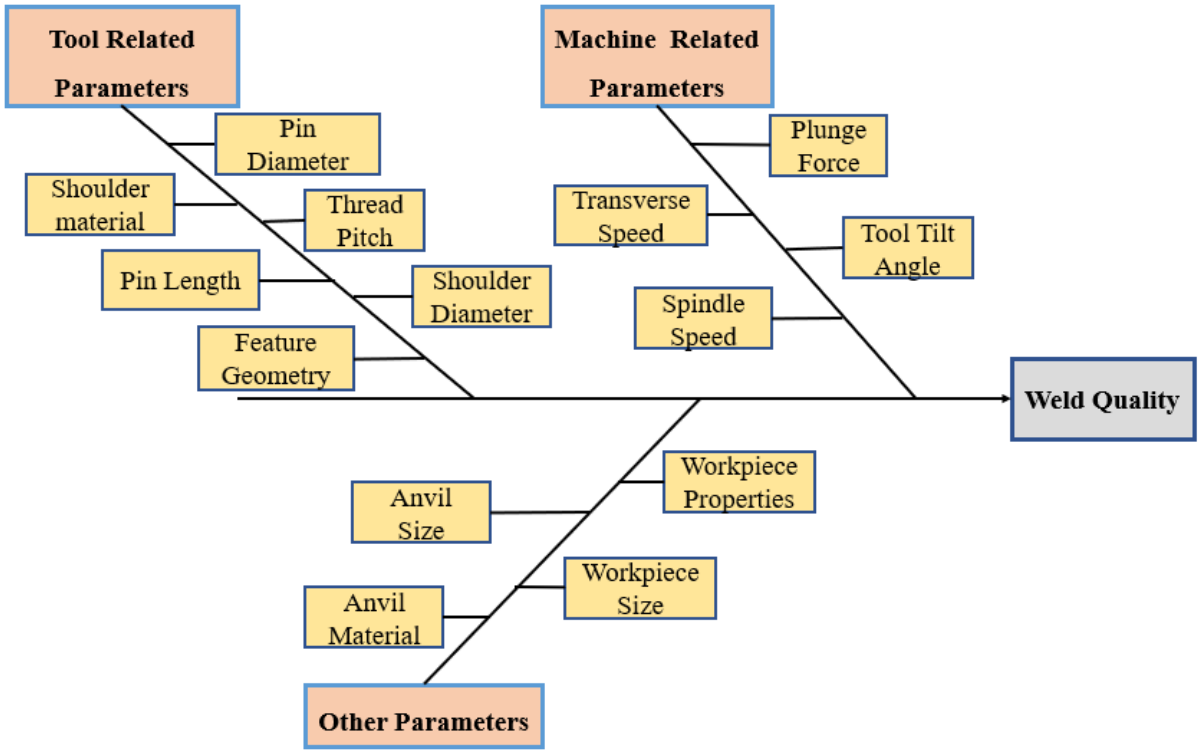

Figure 2. 3: Cause and effect diagram for FSW process [2]

2.4.1 Rotational tool

In the FSW process, a non-consumable rotating tool is used to join materials that are fabricated from high temperature resistance materials. The tool pin is placed against the workpieces on butting sides and rotated to produce frictional heat. This heat softens the plasticized region around the immersed pin and at the point in which the tool shoulder contacts the workpiece. The shoulder is used to give the workpiece additional frictional heat and prevent plasticized material from leaving the weld. As the temperature increases, the strength of the metal at the point where the rotating tool and workpiece contact decreases below the applied shear stress, producing plasticized material to be extruded from the tool's advancing side to its retreating side. The joint line is then slowly moved along with the tool to produce a continuous weld [13].

During the FSW process, the welding material must be stirred and then mixed to get sound welded joints. The gap between the tip of the pin and the bottom of the welding workpiece is 0.1–0.2 mm. This gap was used to avoid contact between the tool and the backing plate and protect the tool or backing plate from damage. However, the practical distance between the tip of the pin and the bottom of the work piece is longer or shorter than 0.1–0.2 mm, which results in a change in the work piece thickness or the plunging depth of the tool. The longer distance may result in the appearance of welded joints because of the lack of material flow [14].

2.4.2 Tool pin/probe

Friction stirring pins play significant roles in material flow during the FSW process. The pines designed to disrupt the fraying surface of the workpiece. The tool used was made from heat-treated H13 tool steel with pin profile such as a threaded pin, square, cylindrical, cylindrical grooved with a concave shoulder [14].

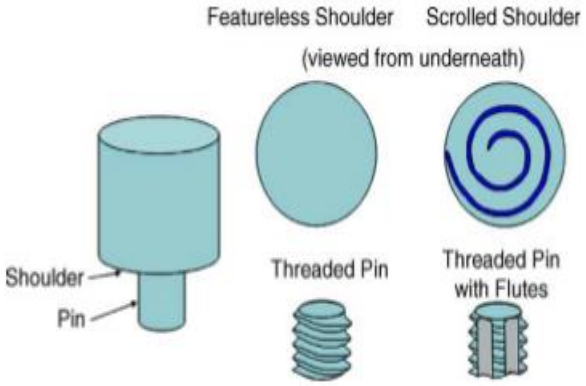

Figure 2. 4: Schematic drawing of the FSW tool [14]

2.4.3 Tool shoulder

Tool shoulders are used to provide the downward forging motion required for welding consolidation and to prevent the hot metal beneath the bottom shoulder surface. In the FSW process, the welding quality is influenced by the shape of the shoulder outer surface because the shoulder plunge depth is small, which is (1-5%) of the workpiece thickness. The material is fed into the tool shoulder cavity during tool plunging, with a small angle ($6\text{-}10^0$) inclined to the flat shoulder end surface from the concave shoulder. As a result, the tool shoulder concave surface profile serves as the reservoir or escape volume for the probe-displaced material. The displaced material stored in the concave shoulder profile generates a forging action on the material behind the tool while downward pressure is applied to the tool. The tool moves forward, pushing new material into the cavity under the shoulder. The proper operation of this shoulder requires the tilting of the tool $1–3^0$ from the normal of the work piece against the direction of travel. The shoulder diameter is 2.2 times the work piece thickness plus a constant of 7.3 mm. This relationship is reasonable considering that with increasing thickness, more energy input is necessary and hence a larger shoulder diameter is required to generate the heat. Similarly, the probe diameter is 0.8 times the sample thickness plus a constant of 2.2 mm. However, the most used ratio of shoulder-to-probe diameter is 3 [10].

2.4.4 Downward force and plunge depth

To ensure quality welded joints, there must be proper selection of vertical force during the FSW process. The vertical force is an important factor in heat generation during the process. As shown in Fig.2.5, the penetration of the shoulder surface into the work piece is known as the plunge depth. The forging of flow material in the nugget zone is controlled by increasing the plunge depth for heat generation. When increasing plunge depth, the axial force also increases due to this high heat generates. This high amount of heat affects grain growth in the nugget zone. Low plunge depth decreases the axial load, which leads to low heat supply and improper material flow. Therefore, for producing a good quality weld, adequate plunge depth and forging pressure are required for deep penetration. To achieve the downward pressure, set an adequate plunge depth for the tool to fully penetrate [12].

2.4.5 D/d ratio

The D/d ratio is defined as the ratio of the tool shoulder diameter divided by the tool pin diameter. During the time of stirring, the D/d ratio plays a vital role during plastic deformation to obtain the desired results. However, the commonly used ratio of shoulder to pin diameter is 3 [15].

2.4.6 Tilt angle

The tilt angle is defined as the inclination of the tool rotational axis with respect to the workpiece surface, as shown in Figure 2.5. In the FSW process, tilt angle affects frictional heat generation, material flow, and the consolidating of flowing material around the tool. When the vertical force is applied by the tool the peak temperature increases with the tool tilt angle. During the FSW, the tool tilt angle helps in preventing the flowing material from spilling out. To achieve adequate downward force, tilt the tool by some degree and set the plunge depth correctly so that the tool enters the weld fully [12].

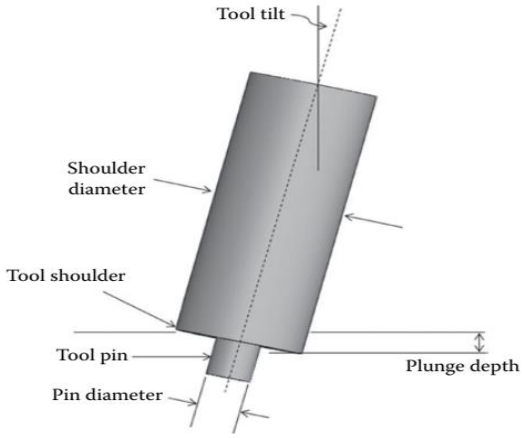

Figure 2. 5: FSW tool with plunge depth and tilt angle [4]

2.5 Joining of dissimilar aluminum alloys

Dissimilar Al-alloys are joined by different methods such as mechanical fastening, brazing, soldering, welding, and adhesive bonding. Of these methods in terms of flexibility, cost, productivity, joint efficiency, and stiffness, welding is the best joining process with both fusion and solid state. Nevertheless, fusion welding methods have many defects like voids, spatters, hot cracking, distortions, work hardening loss, and lack of penetration in the joints that occur during the process. Due to these defects, the joint strength is low because of the higher temperature generated in fusion welding than in solid-state welding and the difference in properties of filler material with both parent materials. New joining processes have developed, such as electron beam welding, laser welding, ultrasonic welding, and FSW to overcome the limits of conventional methods. These are also difficult to join by conventional fusion welding processes. For example, the 5 series is used in automobiles in the inner parts of door panels and on the outer hulls of ships for good corrosion resistance. Similarly, the 6 series is used in the outer parts of door panels and inner structural parts of shipbuilding for appearance and strength. Dissimilar joining of both series of aluminum alloys is required. Therefore, an efficient joining process for dissimilar aluminum alloys is FSW with optimum parameter setting [4].

2.6 Applications of FSW

Application of FSW in several industrial sectors resulted in remarkable benefits in terms of performance and cost reduction. FSW possesses numerous applications in different industries including aerospace, shipbuilding, railways, automobile, etc. Dissimilar material joining is becoming increasingly important to fulfill the requirements of engineering structures and components with reduced weight, improved strength, and functionality. FSW has been adopted extensively for welding al-alloys in various industries owing to economic and environmental benefits [4]. Discussions on some applications areas of FSW are shown on table 2.2.

Table 2. 2: Applications of FSW [4]

No.	Application industry	Aluminum alloys series	Specific application
1	Shipbuilding and Marine Industries	5000 and 6000 series	➢ Panels for decks, sides and floors. ➢ Aluminum hulls ➢ Boat internal surface ➢ Helicopter landing platforms ➢ Ship body structures
2	Aerospace Industry	2000 and 7000	➢ Wings, Fuel tanks, ➢ Stringers
3	Railway Industry	6000 and 7000 series	➢ Bodies of high-speed trains made of high-strength aluminum alloys ➢ Underground carriages and trams ➢ Railway tankers and goods wagons
4	Automobile Industry	5000 and 6000 series	➢ Front portion of an engine ➢ Alloyed wheel rims ➢ Fuel tankers Bodies of heavy-duty vehicles, Tailored blanks
5	Construction Industry	5000 and 6000 series	➢ Facade panels, Window frames ➢ Aluminum bridges ➢ Reactors for power plants ➢ Pipe fabrication
6	Electrical Industry	6000 and 8000 series	➢ Electric motor housings ➢ Encapsulation of electronics, and ➢ Electrical connectors.

2.7 Defects of FSW

The amount of heat used throughout FSW is essential in determining whether a sound weld will produce or whether weld defects will develop. Defects including nugget collapse, surface galling, and excessive weld flash are seen because of high heat input. On the other side, minimal heat input causes defects in the weld such hook, tunneling, and kissing bonds (KB), as well as joint line remnant[16].

Table 2. 3: Types, locations, and causes of FSW defects [16]

S no.	Defect	Location of Defect	Cause
1	Hook defect	TMAZ	➢ High rotation speed ➢ Low weld traverse speed ➢ Improper tool design ➢ Tool tilt being inadequate
2	Kissing Bond	SZ, interface of upper and lower sheet	➢ Low heat input ➢ Insufficient stirring of material ➢ Oxide layer at the interface
3	Tunneling defect	Under the weld surface, on AS near the SZ-TMAZ interface	➢ Low heat input ➢ High weld traverse speed with low rotational speed ➢ Low plunge depth ➢ Inappropriate pin offset
4	Void	On or below the weld surface on the AS of the weld	➢ Incorrect forging pressure ➢ Welding speed too high
5	Incomplete Root Penetration	Below the pin/SZ at the interface of the faying surfaces	➢ Improper tool design ➢ Insufficient plunge depth ➢ Local variation in thickness of the plate
6	Joint Line Remnant	At remnant of original faying surfaces in SZ, At weld root	➢ Poor joint alignment ➢ Inappropriate pin offset ➢ Non-removal of oxide layer on the surfaces

2.8 Application of aluminum alloys

Aluminum alloys are economical in many applications. They are used in the automobile, aerospace, construction, railway, electrical, shipbuilding, and marine industries, as pressure vessels for cryogenic applications, and in a variety of other applications. New developments in aluminum alloys have opened a wide range of applications of wrought aluminum in place of aluminum castings. The improvement of aluminum alloy mechanical properties by adding various alloying elements has opened a wider field of applications for these alloys, particularly in the aerospace and automotive industries [17]. Table 2.4 lists typical applications for some of the more commonly used wrought alloys.

2.8.1 Applications of Al-Alloys in Civil Engineering

The use of Al-alloys as structural materials has grown in recent years due to their advantageous properties, which include a high strength-to-weight ratio, ease of fabrication, a high degree of workability, considerable ductility, excellent thermal conductivity, high corrosion resistance, and an appealing appearance in their natural finish. For this reason, 25% of global aluminium production is currently used in the construction sector. The aforementioned advantageous features have contributed to an increased usage of aluminium alloys in structural applications, where their application can allow for a reduction of the total structural weight [18]. Typical structural aluminium applications along with brief information are presented in Figure 2.6.

St Mary Axe, London, UK
A curved and anodised aluminium skin was used to integrate the raking columns with the curve façade

The Sage Gateshead, Gateshead Quays, UK
Al was used to support the glazing system

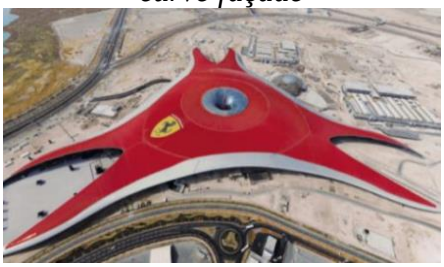

Ferrari World, Abu Dhabi, UAE *The largest aluminium roof in the world.*

Gaylord Texan Resort & Convention Center, Grapevine, Texas, USA *The roof is made of a glazed aluminium framework*

The Crystal, London, UK
The roof is made from 100% recycled aluminium

The Iceberg Skating Palace, Sochi, Russia
Aluminium was one of the key materials used to the construction.

Casablanca Finance City Tower, Casablanca, Morocco
The modular façade elements were made out from aluminium instead of concrete for cost reasons.

The Co-operative Group, Manchester, UK
The anodised exterior aluminium structure holds the glass panels.

Figure 2. 6: Some applications of aluminium alloy structures [18]

2.8.2 Aluminum alloys for automotive applications

Throughout the decade, an increasing demand for vehicles was observed around the world. The advantageous material properties of aluminium alloys led to its significant role in the future of automotive industries. The weldability, formability, high corrosion resistance and high strength of aluminium alloy opened several new ways for new applications in the automotive. Application of semifinished aluminium parts includes engine blocks and power train parts, sheet structures (Jaguar, Honda NSX, Rover), space frames (BMW Z8, Audi A2, A8, Lotus Elise), or as closures and hang-on parts (DC-E-class, Renault, Peugeot) and other structural components. Aluminium part is seen to contribute most on the weight of the vehicle as it gave a share of between 25 and 30% of the complete installed, integrated safety features, and engine size. The most used aluminum alloy series is the non-heat treatable Al-Mg (5 series) and the heat treatable Al-Mg-Si (6 series) alloys. Due to the variations in chemical composition and processing, AA5xxx are optimized for strength and corrosion resistance in vehicle chassis and AA6xxx are optimized for age hardening response and high formability so that efficient auto body sheets panels can be developed [19]. Application of Al-alloy for automotive industry as shown in the figure 2.7.

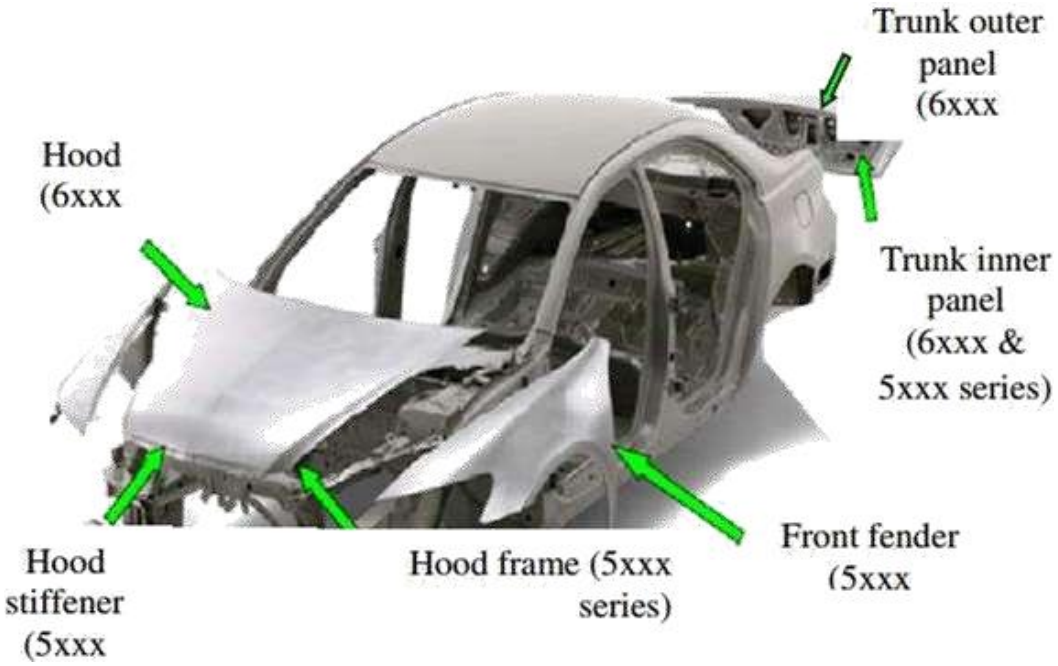

Figure 2. 7: Application of aluminum alloy for automotive [19]

2.8.3 Aerospace applications

In aerospace applications, a material that is lightweight and durable is essential. Henceforth, Aluminum-Lithium (Al-Li) alloys are the most commonly used and applied in aerospace applications. This metal are efficient in critical application of aerospace due to its lightweight, good strength and toughness, excellent corrosion resistance and compatibility with standard manufacturing techniques . Figure 2.8 shows it is applied in several aircrafts parts such as engine, seat track, leading and trailing edges, wing skin, and many other parts. Currently, aircraft and aerospace industry improves their structure by double folding the raw material which will ensure a stronger sheet metal. However, this will thicken the structure and increase the cost of the materials required. Henceforth, aircraft manufacturers had come up with cost reduction program for their existing aircraft version which led to applying new material solution. This new and advanced material will help in facing the new challenges in the future involving the mass air transportation. With the cost reduction programs, the once large assemblies and build up structures consisting of riveted and joined parts were substituted with a single integrated structure which reduced the needs of rivet and joints. This is proven to be advantageous in the cost savings, weight reduction, simplifying storage system and improved production logistics [19].

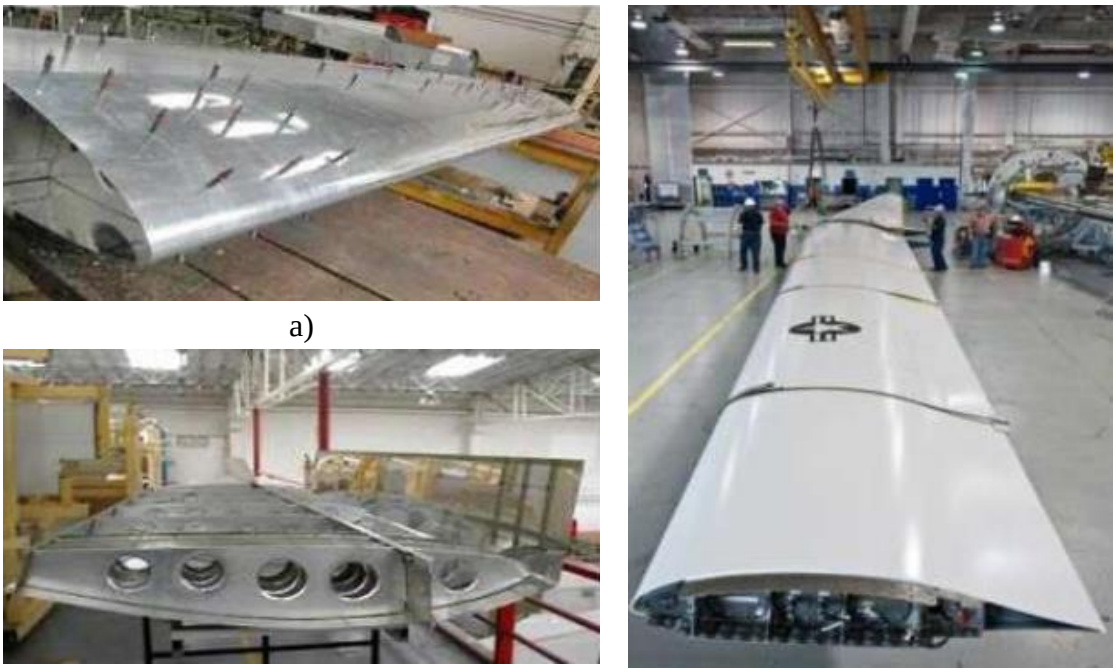

a) b) c)

Figure 2. 8: (a) Wing skin (b) Wing ribs made from aluminum alloys and (c) Final wing, upper skin and ribs are made of aluminum alloys [19]

Table 2. 4: Selected applications for wrought aluminum alloys [17]

Alloy	Description and selected applications
1100	Commercially pure aluminum is highly resistant to chemical attack and weathering. Low cost, ductile for deep drawing, and easy to weld. Used for high-purity applications such as chemical processing equipment. Also for nameplates, fan blades, flue lining, sheet metal work, spun holloware, and fin stock
1350	Electrical conductors
2011	Screw machine products. Appliance parts and trim, ordnance, automotive, electronic, fasteners, hardware, machine parts
2014	Truck frames, aircraft structures, automotive, cylinders and pistons, machine parts, structurals
2017	Screw machine products, fittings, fasteners, machine parts
2024	For high-strength structural applications. Excellent machinability in the T-tempers. Fair workability and fair corrosion resistance. Alclad 2024 combines the high strength of 2024 with the corrosion resistance of commercially pure cladding. Used for truck wheels, many structural aircraft applications, gears for machinery, screw machine products, automotive parts, cylinders and pistons, fasteners, machine parts, ordnance, recreation equipment, screws and rivets
2219	Structural uses at high temperatures (to 315 °C, or 600 °F). High-strength weldments
3003	Most popular general-purpose alloy. Stronger than 1100 with same good formability and weldabilty. For general use including sheet metal work, stampings, fuel tanks, chemical equipment, containers, cabinets, freezer liners, cooking utensils, pressure vessels, builder's hardware, storage tanks, agricultural applications, appliance parts and trim, architectural applications, electronics, fin stock, fan equipment, name plates, recreation vehicles, trucks and trailers. Used in drawing and spinning.
3004	Sheet metal work, storage tanks, agri cultural applications, building products, containers, electronics, furniture, kitchen equipment, recreation vehicles, trucks and trailers.
3105	Residential siding, mobile homes, rain-carrying goods, sheet metal work, appliance parts and trim, automotive parts, building products, electronics, fin stock, furniture, hospital and medical equipment, kitchen equipment, recreation vehicles, trucks and trailers.

5052	Stronger than 3003 yet readily formable in the intermediate tempers. Good weldability and resistance to corrosion. Uses include pressure vessels, fan blades, tanks, electronic panels, electronic chassis, medium strength sheet metal parts, hydraulic tubes, appliances, agricultural applications, architectural uses, automotive parts, building products, chemical equipment, containers, cooking utensils, fasteners, hardware, highway signs, hospital, and medical equipment, kitchen equipment, marine applications, railroad cars, recreation vehicles, trucks and trailers
5056	Cable sheathing, rivets for magnesium, screen wire, zippers, automotive applications, fence wire, fasteners
5083	For all types of welded assemblies, marine components, and tanks requiring high weld efficiency and maximum joint strength. Used in pressure vessels up to 65 °C (150 °F) and in many cryogenic applications, bridges, freight cars, marine components, TV towers, drilling rigs, transportation equipment, missile components, and dump truck bodies. Good corrosion resistance
5086	Used in generally the same types of applications as 5083, particularly where resistance to either stress corrosion or atmospheric corrosion is important
5454	For all types of welded assemblies, tanks, and pressure vessels. ASME code approved to 205 °C (400 °F). Also used in trucking for hot asphalt road tankers and dump bodies; also, for hydrogen peroxide and chemical storage vessels
5456	For all types of welded assemblies, storage tanks, pressure vessels, and marine components. Used where best weld efficiency and joint strength are required. Restricted to temperatures below 65 °C (150 °F).
5657	For anodized auto and appliance trim and nameplates
6061	Good formability, weldability, corrosion resistance, and strength in the T-tempers. Good general-purpose alloy used for a broad range of structural applications and welded assemblies including truck components, railroad cars, pipelines, marine applications, furniture, agricultural applications, aircraft, architectural applications, automotive parts, building products, chemical equipment, dump bodies, electrical and electronic applications, fasteners, fence wire, fan blades, general sheet metal, highway signs, hospital and medical equipment, kitchen equipment, machine parts, ordnance, recreation equipment, recreation vehicles, and storage tanks.
7050	High-strength alloy in aircraft and other structures. Also used in ordnance and recreation equipment.
7075	For aircraft and other applications requiring highest strengths. Alclad 7075 combines the strength advantages of 7075 with the corrosion-resisting properties of commercially pure aluminum clad surface. Also used in machine parts and ordnance.

2.9 FSW of dissimilar 5-series and 6-series Al alloys

Due to the large application of 5- series and 6- series combinations, there has been a growing interest in the welding of these alloys. Various studies on friction stir welding in butt, lap, and spot (FSSW) configurations have been conducted for these systems of the dissimilar joint. The joints between plates with a thickness range of 1 to 6 mm were evaluated. A brief review is presented for FSW of dissimilar aluminum alloys in the 5-series and 6-series is presented in Table 2.5. Generally, high carbon steel of various grades has been employed as a tool material, and important process parameters are reviewed below.

Rajbinder et al. [20] optimized the mechanical properties of dissimilar FSW of AA 5052 and AA 6061 having a thickness of 5 mm plates by using a vertical milling machine and conducted tests on the effect of welding parameters like tool rotation speed and welding speed to get the optimum tensile strength and hardness of the welding joint. The tool used for the FSW process is a high-speed steel tool with a cylindrical pin profile. The result shows that at 1200 rpm and 55 mm/mm, the maximum Rockwell hardness and the highest tensile strength are obtained.

Lakshmikhanth & Subbaiah [21] studied different tool pin profile effects on dissimilar friction stir welded (FSW) AA5083-H111 and AA6061-T6 aluminum alloy plates. The mechanical characterizations and microstructures of 5 mm thick joints were examined to discover the best tool pin profiles. The dissimilar aluminum alloy joints were produced by employing three different tool pin profiles, such as tapered cylinder, threaded cylinder, and Straight Square. The microstructures of different zones were tested using optical microscopy (OM) and SEM. The tensile properties and different zones of hardness survey at transversal locations were examined by using a UTM and a Vickers microhardness testing machine, respectively. The dissimilar Al alloys welded with a straight square produced a defect-free weld with good mechanical behavior and microstructure.

Balamurugan and Subbaiah [22] investigated rotation speed effect on microstructural and mechanical properties of FSW of dissimilar AA5052-H32 and AA6061–T6 Aluminum (Al) alloys. The mechanical properties of the FSW weld were tested by employing a UTM. Besides, the microstructures of FSW welding were observed by using optical microscopy (OM). The defect-free dissimilar Al alloys of a 5 mm thick plate were welded together using a triangular pin at different rotational speeds between 900 and 1100 rpm, with the same 28 mm/min traveling (welding) speed.

Palanivel et al. [9] investigated the effect of pin profile and rotational speed on the tensile and microstructure of dissimilar FSW AA6351-T6 and AA5083-H111 Al alloys. The dissimilar joints were performed by two process parameters, like pin profiles and tool rotational speeds. The dissimilar aluminum alloy joints were done by using five different pin profiles such as tapered square, tapered octagon, Straight Square, straight octagon, and straight hexagon at tool rotational speeds of 600, 950, and 1300 rpm. The maximum tensile strength of AA6351-T6 and AA5083-H111 Al alloy joints was obtained by fabricating the joints using straight square tool pin profiles at a tool speed of 950 rpm. The scholars concluded that the properties of material flow, over aging and dissolution of precipitates of AA6351-T6, the creation of macroscopic defects in the weld zone, and loss of cold work in the HAZ of AA5083-H111 are affected by tool pin profiles and tool rotational speeds.

Deore [23] investigated the effects of the process parameters and tool geometry on the mechanical behaviors and microstructure variations of dissimilar FSW of AA 6061-T6 and AA 5052-O aluminum alloy joints. The FSW of aluminum alloys was performed by using a semi-automatic vertical milling machine. The joints were performed with an H13 square tool pin and a simple cylindrical tool pin at different tool rotational speeds of 700 rpm, 1050 rpm, and 1400 rpm and different feeding rates (tool transversal speeds) of 36 mm/min, 72 mm/min, and 120 mm/min. The microstructure of dissimilar Al alloy welded joints was tested through SEM and OM. The maximum UTS of dissimilar AA6061 and AA5052 joints was observed when the joints were performed by a square pin tool at 1050 rpm tool rotational speed with a 36 mm/min tool travel speed. The tunnel defects were observed when the joints of dissimilar materials were done by a simple cylindrical tool pin, and the hole defects were found in the joints performed by a square tool pin at higher traverse and lower rotational speeds. The author concludes that the better mechanical behaviors and microstructures produced by employing the square tool pin.

Sindhuja et al. [24] identified the effects of process parameters on the welded microstructure and strength of FSW dissimilar AA6061 and AA5052 aluminum alloy plates. The quality of welding joints was controlled by considering different welding process parameters such as tool rotational speed, traverse speed, axial force, and tilt angle. The dissimilar material weld joints were produced by using the cylindrical tool pin profile at five different rotational speeds of the tool (1000 rpm, 1200 rpm, 1400 rpm, 1600 rpm and 1800 rpm), traverse speeds of the tool (20 mm/min, 25 mm/min, 30 mm/min, 35 mm/min, and 40 mm/min), axial forces (1 kN, 1.5 kN, 2 kN, 2.5 kN and 3 kN), and tilt angles (−2°,−1°,0°,1° and 2°). The microstructure and heat

affected zone (HAZ) were observed by using SEM and OE. The chemical characterization at the weld zone (WZ) was analyzed by energy dispersive x-ray analysis (EDS). The maximum tensile strength of weld joints was observed at 1800 rpm tool rotation speed, 30 mm/min tool transverse speed, 1.5 kN axial force, and – 2° tilt angle. Hence, the investigators concluded that the dissimilar FSW aluminum alloy joints were highly influenced by the welding process parameters.

Shunmugasundaram et al. [25] optimized the process parameters using Taguchi L9 orthogonal design of experiments on the welding of dissimilar aluminum alloys of AA6063 and AA5052 having a thickness of 8 mm by FSW. The joints were fabricated using a hexagonal pin profile tool with three rotational speeds of 650, 750, and 850 rpm; welding speeds of 20, 30, and 40 mm/min; and tilt angles of 1, 1.5, and 2 degrees. The result shows that the tensile strength was higher at a tool rotating speed of 850 rpm, a welding speed of 20 mm/min, and a tilt angle of 2 when using independent process parameters to maximize the tensile strength.

RajKumar et al. [26] performed experiments to study the effects of tool design and welding parameters on the FSW of dissimilar aluminum alloys AA5052 and AA6061 with a thickness of 5 mm on a standard milling machine. The parameters used for FSW using a cylindrical pin tool were at a constant speed of 710 rpm and at two different feed rates of 28 and 20 mm/min. The results show that FSW with a cylindrical threaded pin provides excellent bonding between the two alloys (AA 5052 and AA 6061).

Table 2. 5: Summary on the related literature on FSW of dissimilar 5xxx to 6xxx Al alloys

Name of authors (Year of Publication)	Alloy Combinations & thickness	Tool Shape & material	Operating Parameters	Recommended TRS(rpm) & TS (mm/min)	Objective of Study	Ref.
Rajkumar et al. 2014	5052-H32 and 6061 –T6 5mm	SCT AISI H13	TRS and WS	710@28	Investigates on characterizations of the mechanical and metallurgical properties	[26]
Shunmugasundaram. et al. 2020	AA6063 and AA5052 8mm	SH (HSS)	TRS, WS, and Tilt angle	850@20	Optimizations of process parameters on tensile properties	[25]
Rajbinder et al. (2016)	AA5052 & AA6061 5mm thick	SC (HSS)	TRS and WS	55,1200	Joint strength Hardness	[20]
Balamurugan &Subbaiah (2020)	>>	ST (H13)	TRS, WS	28, 1100	Joint strength Hardness	[22]
Sindhuja et al., 2021	>>	SC	TRS, WS, AF and Tilt angle	30,1800	Yield strength, tensile strength, and percentage of elongation	[24]
Palanivel et al., 2012	AA5083-H111 and AA6351-T6 6mm thick	SS, SH, SO, TS and TO	TRS, constant WS and AF	60,950	Effect of TRS and pin profile on microstructure and tensile strength.	[9]
Gupta et al., 2018	5083-O 6063-T6 6mm thick	-	TRS WS SD and PD	900@60	Tensile strength, microhardness, and grain size.	[27]
Kasirajan et al., 2020	6101 T6 5052 6mm	-	TRS and tool offset to advance side	1400	Tensile strength and wear behavior	[28]
Balamurugan et al., 2021	AA5052-H32 and AA6061-T6 5mm	SS, ST, and SC	TRS WS and TP	60, 1100	Tensile Microhardness and microstructure	[29]

Doley & Kore, 2016	5052-H32 and 6061 –T6 3 mm 1 and 1.5 mm	SC	TRS WS SD and PD	1500	Tensile Microhardness and microstructure	[30]
Shunmugasundaram et al., 2020	AA5052-H32 and AA6061-T6	SH	TRS, WS, and Tilt angle	50, 900	Tensile strength	[31]
Deore & Hiwarkar, 2016	AA5052- and AA6061 3mm thick	SC and SS	TP, TRS and WS	36, 1050	Tensile Microhardness and microstructure	[23]
Kumar et al. 2021	AA5083-H111 and AA6061-T6 6mm thick	CTT H13	Constant	60, 1400	Enhancing corrosion resistance and mechanical properties.	[32]
Krishnan and Subramaniam 2019	5083 6063 4-6mm	THC	TRS, WS and PDe	150, 1100	Tensile, and elongation	[33]
Ghaffarpour et al. 2013	5083-H12 and 6061-T6 1.5 mm	-	TRS WS SD and PD	25,1600	Tensile strength	[34]
Babu et al. 2014	5083 6061	THC, TC	RS, WS and AF	40, 900	Tensile strength and impact strength	[35]
Lakshmikhanth and Subbaiah 2020	AA5083-H111 and AA6061-T6 5mm thick	SS, THC, and TC (H13)	TP	80, 800	Tensile Microhardness and microstructure	[21]
Kumar et al. 2021	5083 6061 6mm	CTT (H13)	TRS and WS	60, 1400	Tensile properties, microstructure	[8]
Verma and Kumar 2021	6061 T6 5083-O 6.35mm	(SC), (TC)& (SS)	TP TRS WS and TTA	39.53, 1568	Tensile, and elongation	[36]

*TRS: tool rotational speed; WS: welding speed; TTA: tool tilt angle; PDe: plunge depth; AF: axial force; SD: shoulder diameter; PD: pin diameter; PL: pin length; TPS: pin shape. TH: tool hardness. TP: Tool Profile. SC: straight cylindrical; ST: straight triangular; SS: straight square; SH: straight hexagon; SO: straight octagon; THC: Threaded cylinder; TS: tapered square; TC: tapered cylindrical; TO: tapered octagon; SCT: straight cylindrical threaded; CTT: conical tapered threaded pin; H13: tool steel; HSS: high speed steel; Re: Reference

2.10 Gaps identified

- ✓ Recent studies showed that fusion welding has emissions and smoke, which can cause the environment to pollute and warm, and nowadays environmental pollution and global warming are burning issues, so finding an option that is environmentally friendly manufacturing possibilities. For this reason, friction stir welding is one of the best material joining mechanisms.
- ✓ Most of the previous works were done on the effects of traverse speed, and rotational speed on mechanical and metallurgical properties; so, process parameters like pin profile effects in optimization of FSW dissimilar aluminum alloys of 6061 and 5052 are not adequately done.
- ✓ Limited works were carried out on Taguchi-based grey relational analysis to solve multi-response optimization problems.

For this reason, the optimization of FSW process parameters was further examined and evaluated in this thesis.

CHAPTER THREE

3. MATERIALS AND METHODS

3.1 Methodology

The steps followed for FSW process is as shown in figure 3.1 below.

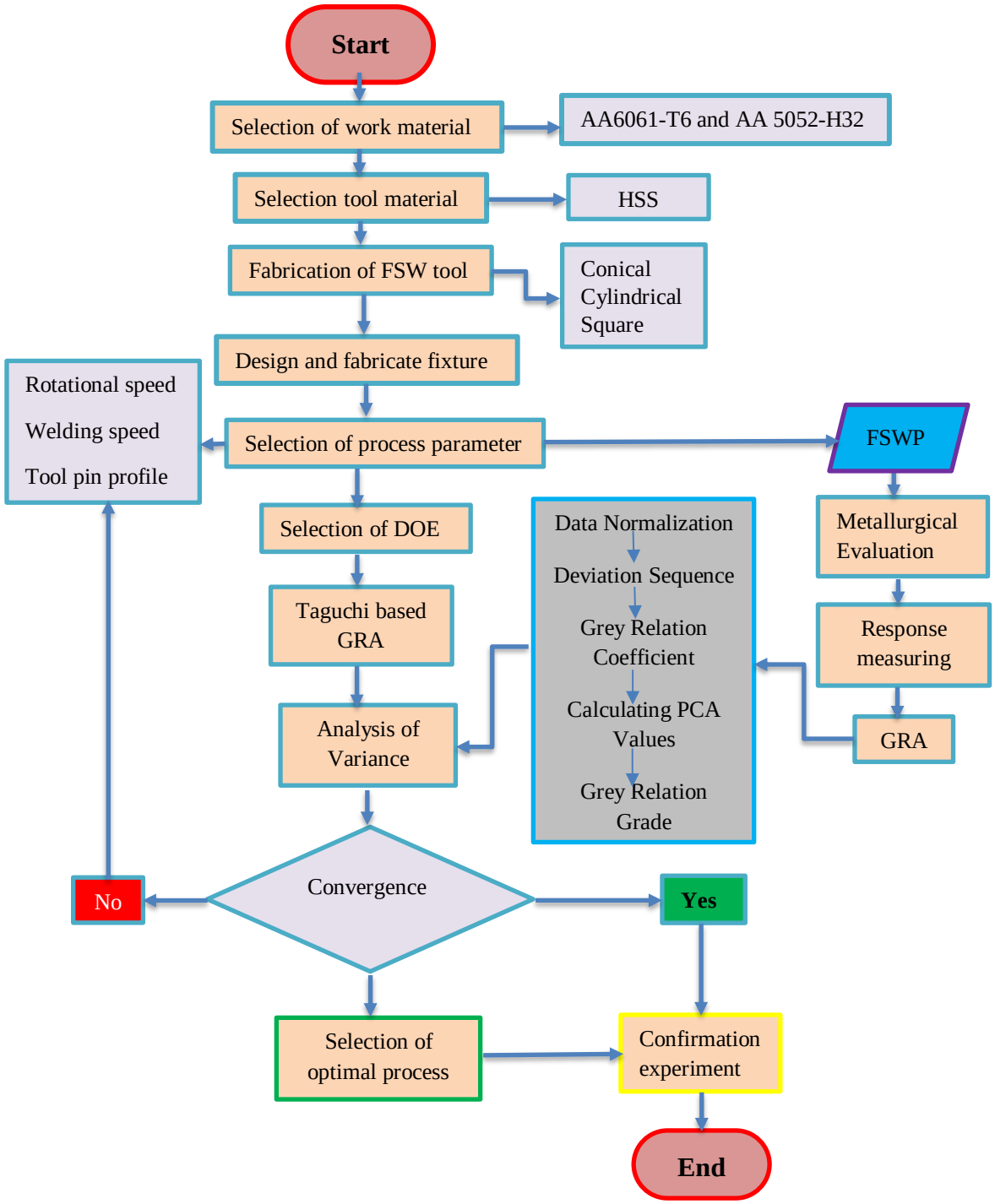

Figure 3. 1: Overall thesis framework

3.2 Materials and Equipment

3.2.1 Selection of materials

In this thesis, dissimilar aluminum alloys 6061 and 5052 selected to find the optimized process parameters to join those by FSW. Nowadays, both aluminum sheets and plates are widely used in the automobile industry, aircraft, and shipbuilding for structural purposes. These dissimilar aluminum alloys have good formability and weldability. The specimens developed by cutting the dissimilar alloys into the required dimensions (150 mm x 110 mm x 6 mm) as shown in fingure 3.2. The chemical composition and mechanical properties of aluminum alloys 6061-T6 and 5052-H32 are displayed in Tables 3.1 and 3.2, respectively.

Table 3. 1: Chemical composition of AA6061 and AA5052 (http://www.hanweilvye.com/en/)

Aluminum alloy	Si	Fe	Cu	Mn	Mg	Cr	Zn	Na	Ti	Al
AA6061-T6	0.616	0.502	0.241	0.083	1.047	0.111	0.125	0.0002	0.027	97.06
AA5052-H32	0.1	0.31	0.01	0.05	2.3	0.17	0.01	_	0.01	Balance

Table 3. 2: Mechanical Properties of AA6061 and AA5052 (http://www.hanweilvye.com/en/)

Materials	Yield Strength (MPa)	Tensile strength (MPa)	Elongation (%)	Microhardness (HV)
AA6061-T6	273	310	15	107
AA5052-H32	158	230	18	68

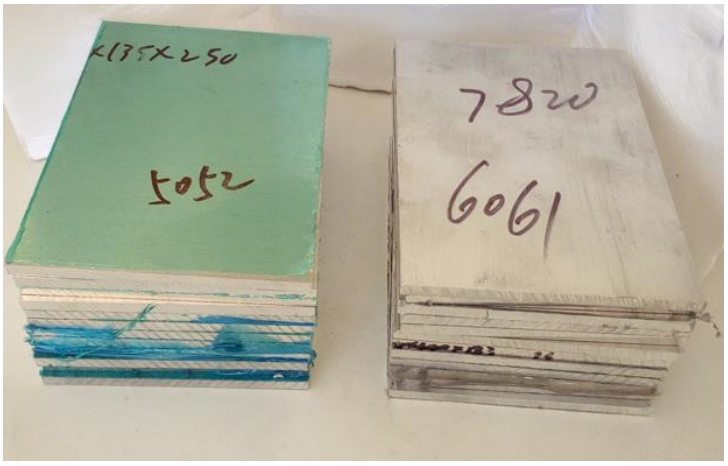

Figure 3. 2: Specimen of AA5052-H32 and AA6061-T6 aluminum plates

3.2.2 Design of Backing Plate and Fixture.

Backing plates are required to resist the normal forces employed in FSW, as well as provide a stiff object to clamp the plates or sheets to be welded. Material diffusivity of the backing plate material is a major element for conducting a proper FSW process [37].

A fixture in FSW is usually the most complicated and critical aspect of the welding process. The workpieces must be fixed to a rigid smooth backing plate and secured to resist the perpendicular and side forces that develop during the welding process. These forces tend to lift and push the workpieces apart. Fixtures are designed to restrain the workpieces and keep them from moving apart. The fixtures that keep the materials to the backing plate should be located as close to the joint as possible to ensure that the workpieces are held in place during the welding procedure.

3.2.2.1 Material for Fixtures

Proper selection of tool traverse and rotational speeds is important for heat generation, and the forces applied to the tool should be minimized to provide material flow around the tool pin. However, selecting the proper material for fixture development is good to get defect-free FSW joints [38]. Materials such as mild steel, stainless steel, aluminum alloys, pure copper, medium carbon steel etc. can be used as a backing plate [37].

During the FSW process, mild steel material is used due to its high strength and toughness [38], this material is used for the manufacturing of fixtures, backing plates, top plates, side supporters, front support plate spacer (adjuster), and bottom plates.

3.2.2.2 Bottom backing plate

The FSW backing plate supports workpieces and is permanently mounted on the CNC milling machine table to prevent blank movement during the welding process. It also ensures that the plasticized material is held within the welding zone because the tool forged it down. It is used for the protection to the milling machine's bed if the tool tip extends beyond the thickness of the workpiece. Support different parts of the fixtures like – the top plate, side supporter, front support, and spacer (adjuster) to make the adjustable fixtures depend on the sheet metal/plate of different similar and dissimilar materials. The backing is placed under workpieces mainly for protection and the stability of blank/workpieces.

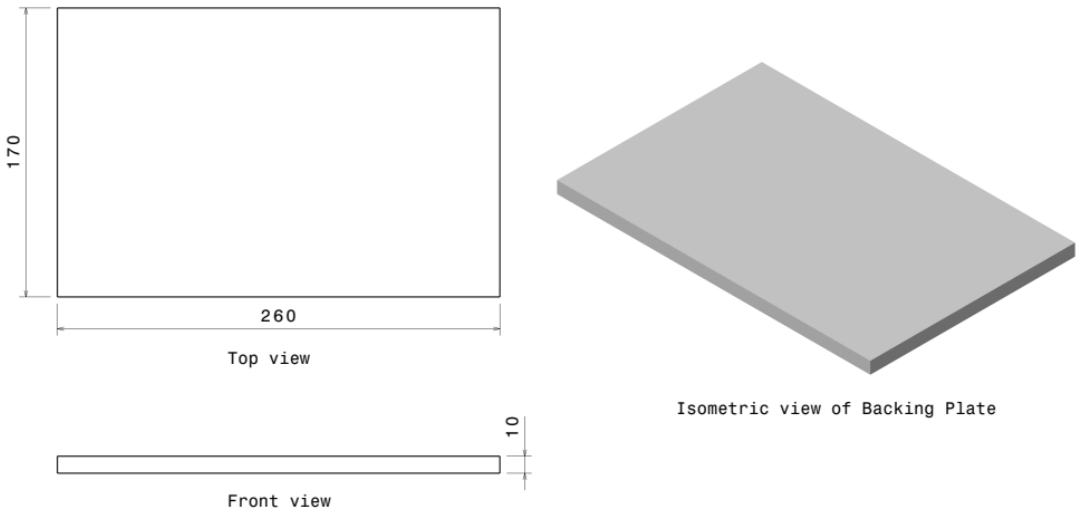

Figure 3. 3: Dimensions & isometric view of bottom backing plate

3.2.2.3 Top plate/ Clamp

The top backing plate is usually adjusting plate thickness in different dimension and hold the workpiece rigidly in right position during welding process by using tightening bots. The dimension of top plate depends on backing plate dimension. There are two top backing plate was welded on both right and left side of side supporter backing plate to fix and provide rigidity of sheet/plate during welding process.

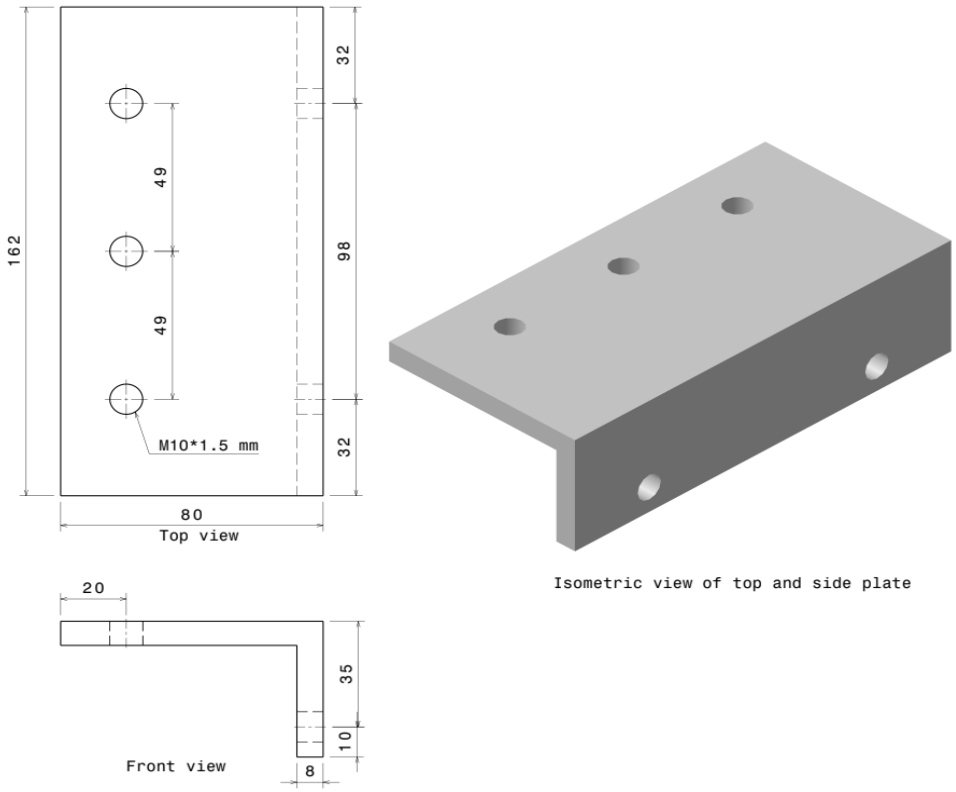

Figure 3. 4: Dimensions of clamp (left side) & 3D model of Top plate/ clamp (right side)

3.2.2.4 Spacer (side adjuster) Plate

The side adjuster plate in this work adjusts the width of sheet/plate to be weld and additionally hold the sheet/plate to be weld against both vertical force and transverse force during plunging and welding time. The side adjuster is moveable and placed between work piece and side support plate. It can be used to adjust the workpiece according to the appropriate welding position.

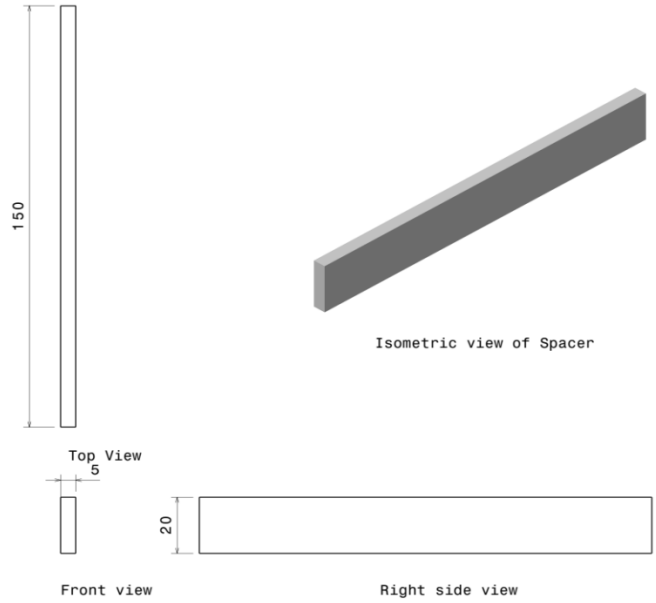

Figure 3. 5: Dimensions of adjuster/spacer

3.2.2.5 Front Supporter plate

This is needed for stopping the longitudinal sliding of workpieces. It also helps the fixture for sustain in the tool axial force and deflection, tool rotational force and separation with this help in preventing the workpiece buckling due to thermal expansion [26]. Front Support Plate, welded on bottom backing plate, side and top plate, is used for securing the workpiece in the welding directions and used as locator.

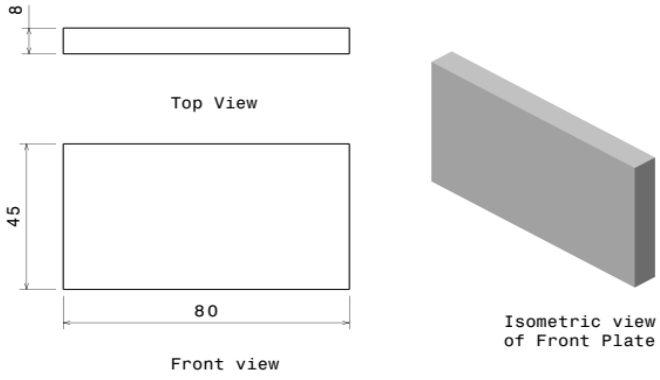

Figure 3. 6: Dimensions of stopper or front Support plate.

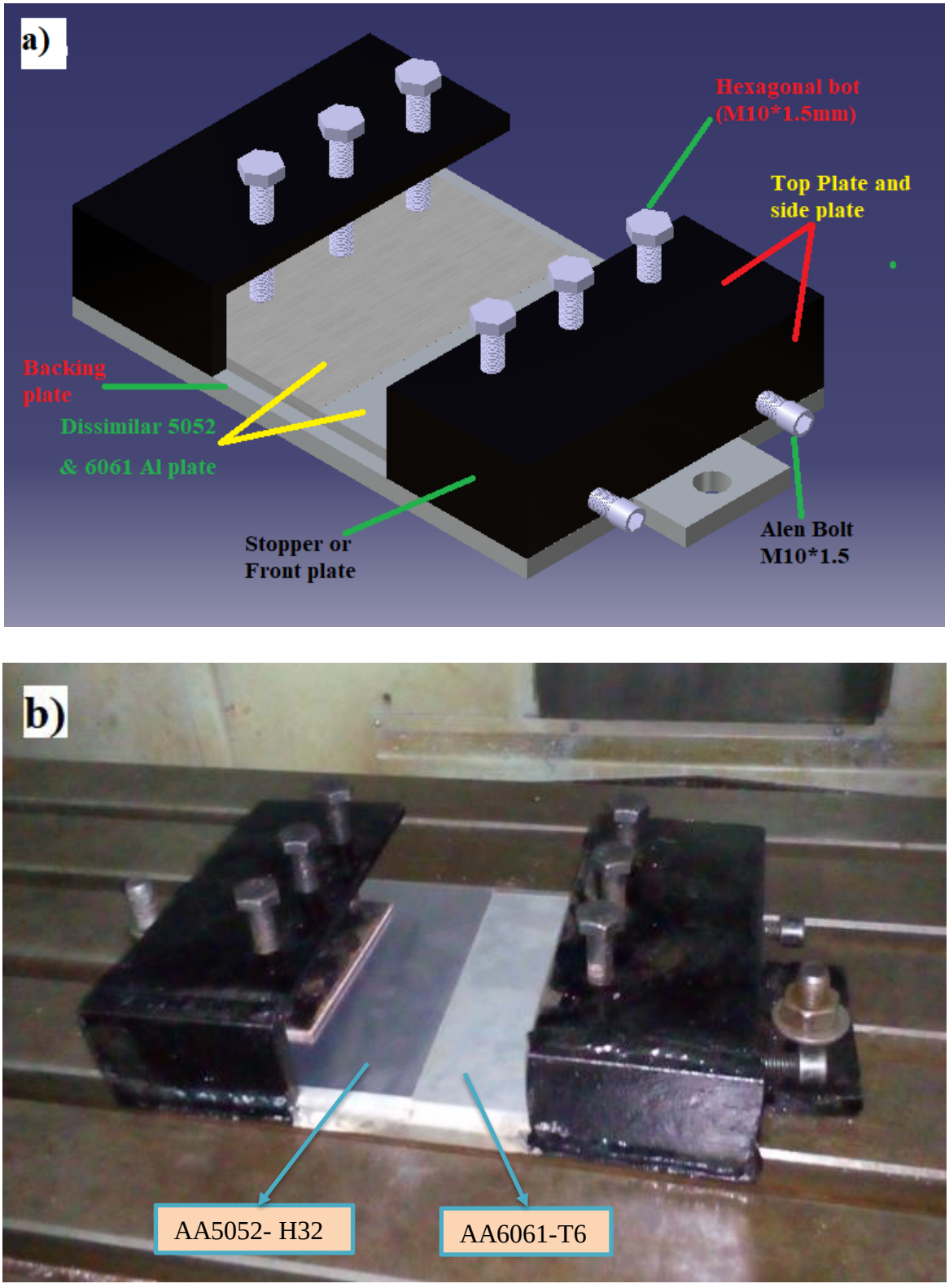

Figure 3. 7: a) 3D Modeling of designed fixture b) actual fixture

3.2.3 Fabrication of tool pin profiles

The tool for the FSW process was developed by a modified hand grinder on the lathe machine. In this experiment, HSS alloy was selected as a welding tool material. It has very high hardness and good wear resistance, with more toughness [25]. There is no functionally working cylindrical grinding machine in the AAiT School of Mechanical and Industrial Engineering workshop. One can design and fabricate a simple attachment on the lathe tool post to handle or clamp the hand grinder on the lathe machine to grind square HSS tool material into a circular or round shape, as shown in figure 3.8.

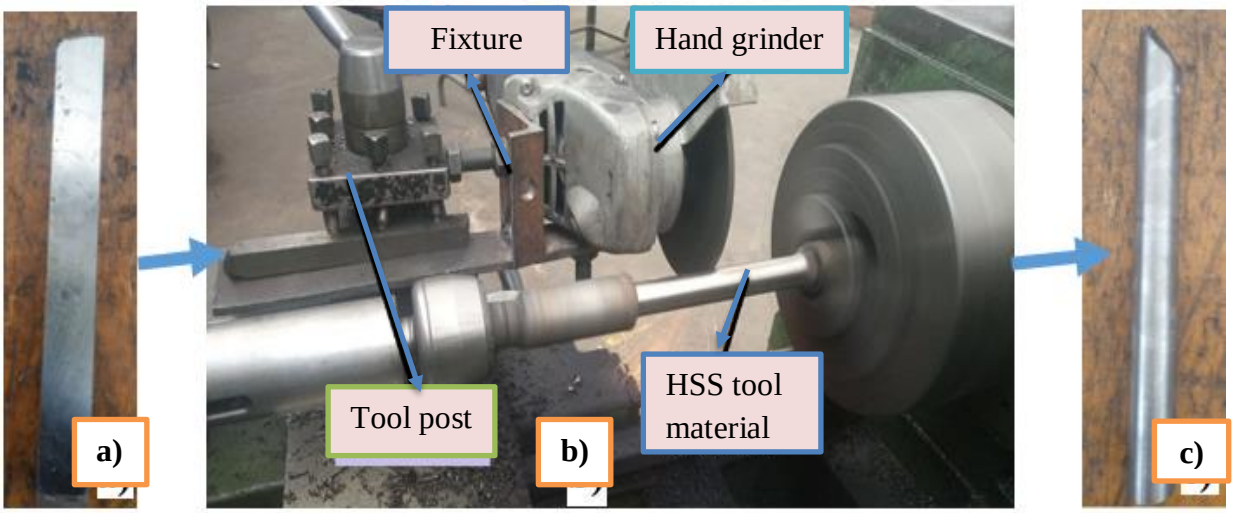

Figure 3. 8 a) square shape HSS tool b) Cylindrical grinding operations setup on lathe machine by using hand grinder by additional attachment. c) After grinding round shape HSS tool material.

The FSW tools that are used to perform all the welds are fabricated with the help of additional attachments on the lathe machine with dimensions [39], based on a different review of literatures, on the tool shown in Table 3.3. This tool consists of two main components: shoulder and pin, which are shown in Figure 3.9.

Table 3. 3: Dimensions of the tool

Tool material	Tool profile	Probe diameter (mm)	Pin length (mm)	Shoulder Diameter (mm)
High Speed Steel	Cylindrical	6mm	5.7	18
	Conical	3 mm through 6 mm		
	Square	6 mm		

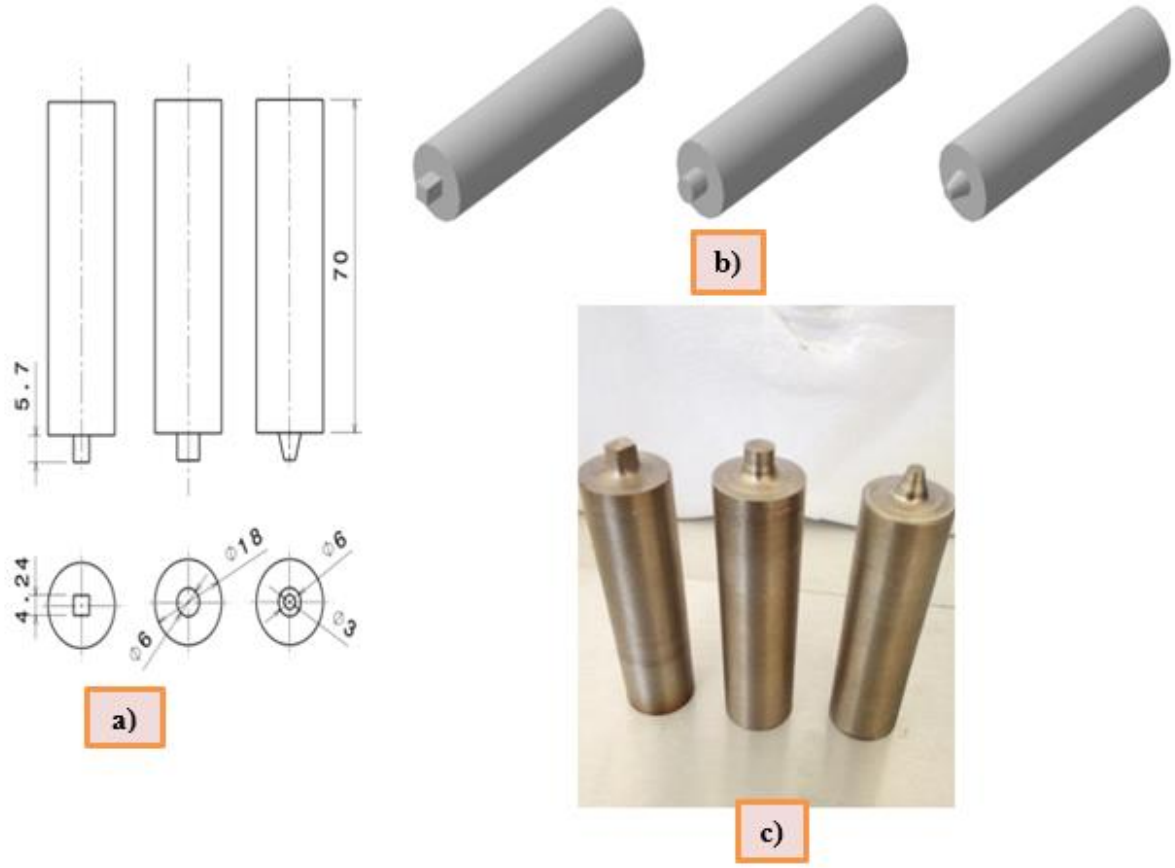

Figure 3. 9: a) 2D with dimensions of the tools b) 3D model of pin profiles c) Actual image of tool Profiles: Square, Cylindrical and Conical

The square pin shapes were formed by encircling inside a circle with a diameter of 6 mm. This value of diameter was also chosen as the diameter of the cylindrical pin. When rotating, square and cylindrical pin shapes occupied the same space.

3.3 Experimental Machines and Setups

3.3.1 FSW using CNC machine

Friction stir welding was performed on the CNC milling machine to weld dissimilar AA6061-T6 and AA5052-H32 6 mm thick. A CNC part program was written using G and M codes for moving the FSW tool in a straight line with welding parameters. The two base plates, which are to be welded, was positioned on the backing plate in the fixture. The CNC program is edited to have different values of welding parameters and performed to obtain welding joints at different weld parameters.

Table 3. 4: XHS7145 CNC milling machine specification (From machine manual)

No	Part Name	Unit	Specification
1	Table working surface	mm	800 * 450
2	Maximum spindle speed	Rpm	8000
3	Spindle motor	HP, KW	7.4, 5.5
4	NC Controller	Type	Fanuc – 0i MD
5	Tool Shank	Type	MAS – 403 BT- 40 Opt.: CAT-40

Figure 3. 10: XHS7145 CNC milling machine

3.3.2 Experimental Work

The target material was selected to be most frequently used in the automotive and marine industries as an AA 6061 and AA5052 plate with a butt joint configuration. All specimens were cut off at dimensions of 150 × 110 × 6 mm. In addition, after welding the specimen, a mechanical test was prepared according to ASTM E8 [40]. The experiment executed with the XHS7145 CNC machining center. The experimental setup is displayed in Figure 3.11 below:

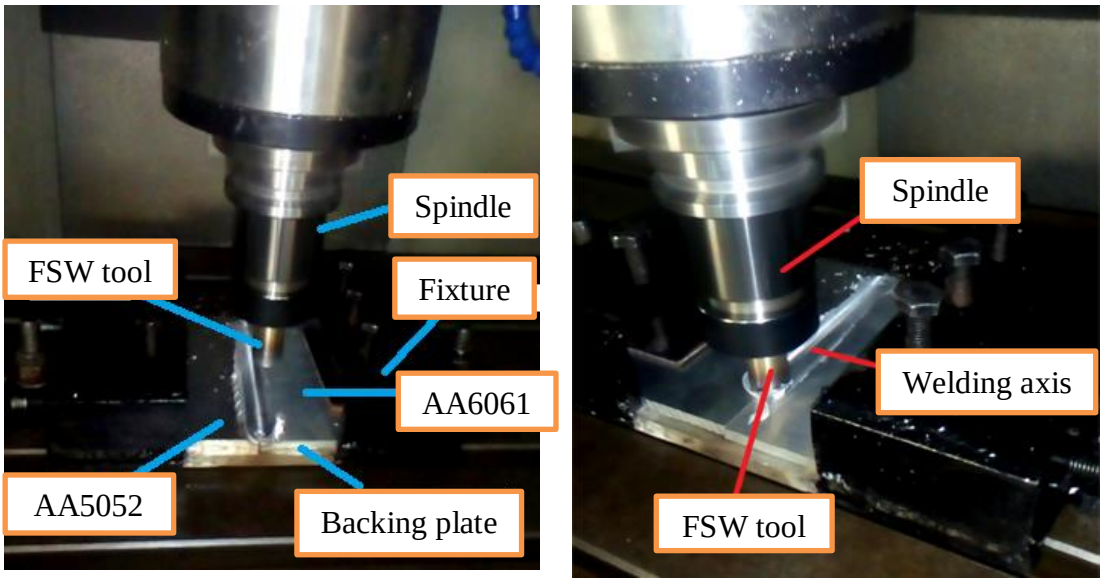

a) Setup for FSW b) Welded joint during FSW process.

Figure 3. 11: Experimental setups for FSW

3.4 Mechanical Testing and Microstructure Examination

3.4.1 Tensile Test

A tensile test is a fundamental mechanical test in which a well-prepared specimen is loaded within controlled conditions while the applied load and the specimen's elongation are measured. The sample dimensions of 200 mm x 20 mm x 6 mm used depend on standard and machine capacity as shown in Figure 3.12. The samples were prepared to the proper dimensions required for the test, according to ASTM E8 standards [40]. This experiment's aim is to gather information about each experiment's result to get the optimum UTS. As shown in figure 3.13, the UTM consists of a load capacity, a maximum piston stroke, and a crosshead having 50KN, 150 mm, and 6 mm/sec, respectively.

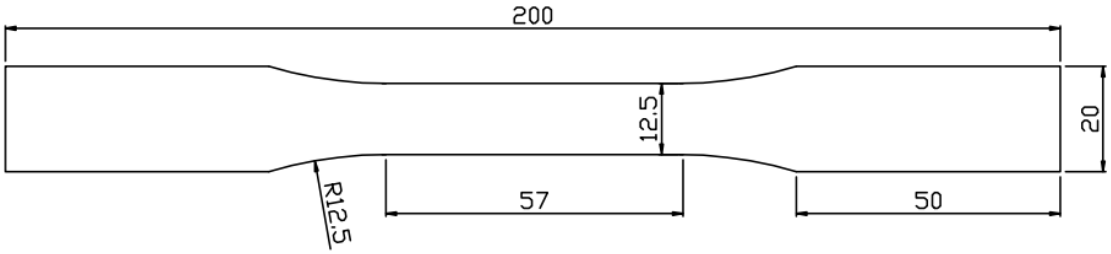

Figure 3. 12: ASTM E8 standard of tensile test specimen

Figure 3. 13: Universal Testing Machine

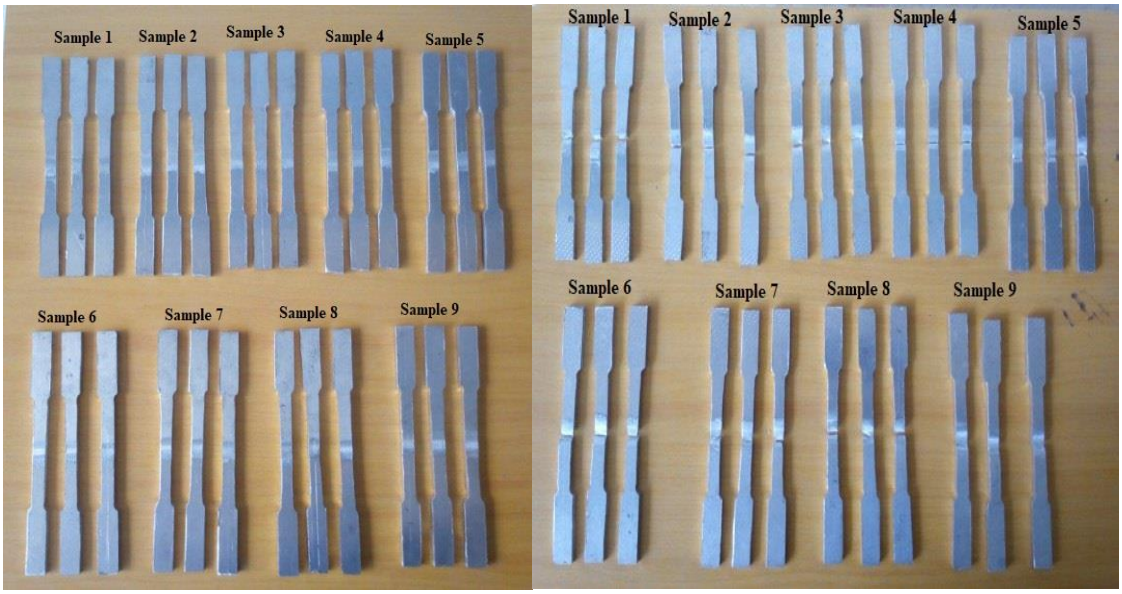

a) b)

Figure 3. 14: a) specimen before tensile test and b) specimen after fracture

3.4.2 Hardness Test

Hardness is the properties of material that allows resisting a plastic deformation, usually measured by penetration. A specially formed indenter is used in all hardness tests; it is much harder than the test material. A force is applied to push this indenter into the sample's external surface. To determine the hardness value, the indenter size or depth must be measured. There are many methods to determine the hardness, among those Brinell, Vickers and Rockwell are frequently used. For this thesis using Vickers hardness test the procedure mentioned as follows.

- ✓ **Vickers test method**

Vickers hardness test an indentation hardness test to force a square-based pyramidal diamond indenter having specified face angles, under a predetermined force, into the surface of the material under test and to measure the diagonals of the resulting impression after removal of the force [41]. The square base pyramidal diamond indenter is forced into the material to be tested while being applied a specified force range of 1 to 129 kgf. Further penetration ends after the forces have reached static or equilibrium conditions, and the force is then maintained in place for a specified period (10 to 15 seconds for normal test times). The indentation diagonals are measured and averaged to obtain a millimeter value. The Vickers hardness number (HV) is calculated using the length.

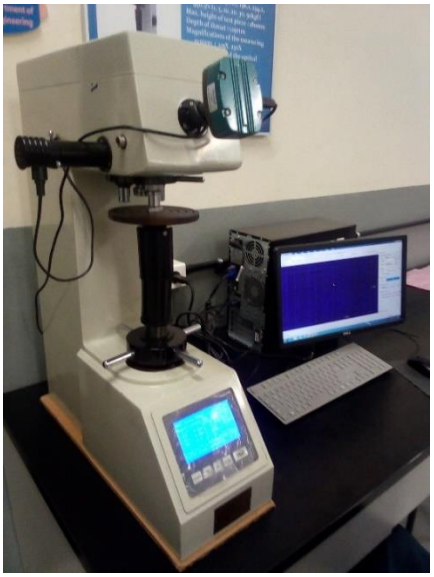

Figure 3. 15: Vickers hardness tester HVS-50

3.4.3 Microstructure Observation

Analyze the effects of grain size and shape, as well as the distribution of various phases and inclusions, on the mechanical properties of the metal. The metallographic test specimen preparation procedure is as follows.

3.4.3.1 Cut Specimen from the Sample

The first step of a microstructural test is to cut the specimen from the sample accurately to the required testing size. A two-centimeter-long specimen is cut from each sample by using a consumable high-speed rotating disc abrasive cutter.

3.4.3.2 Mounting the specimen

The second step of specimen preparation was mounting specimens for microstructural analysis. Specimens cut from each sample were fixed in a holder to be managed easily during polishing, which is necessary to examine the microstructure. The mounting operation was done by the RB 206 Metpress-A machine using MC-PRC (phenolic resin conductive powder). The maximum heating temperature was 250^0C and took 1020 seconds to 17 minutes (i.e., 300 sec for heating time, 300-sec holding time, and 420 sec for cooling time) for each sample. The machine consists of an upper ram, a lower ram, and a heating part and is cooled by water controlled by a solenoid valve. A small piece of the specimen was increased into a 32 mm diameter pellet before grinding and polishing.

Figure 3. 16 a) Hot mounting press(RB 206 Metpress-A) b) Samples of mounted specimen

3.4.3.3 Grinding of Specimen

Two grinding processes were applied to each specimen. The first one is a rough grinding using silicon carbide paper, and the second one is an intermediate grinding process using the RB 204 Metpol-II machine. Firstly, the specimen was grinned on 400 grit size silicon carbide paper for

about two minutes. Again, grinned by the following carbide papers: 800, 1200, and 2000 grit sizes, respectively. The particles are washed with water and removed by a compressor after each grinding step. The sample was continued to be rough grind until the surface was smooth and free of nicks, burrs, etc.

3.4.3.4 Polishing of specimen

The last step is to use a wet rotating wheel to get a free surface without any scratches. In this step of specimen preparation, the specialized liquid sprayed on the surface of the polishing cloth was diamond suspension liquid, which is used in a spray form.

Figure 3. 17: Grinder and polisher RB 204 Metpol-II Machine

3.4.3.5 Etching

This is the final step of specimen preparation to make the sample visible to many structural characteristics of the metal. This is accomplished by using an appropriate reagent which subjects the polished surface to chemical action**.** All samples were etched with 25 ml of hydrochloric acid, 25 ml of nitric acid, 25 ml of methanol, and one droplet of hydrogen fluoride combination. The duration of time for each sample etching is 30 seconds.

Finally, the reflective surface of the specimen is put on the table of optical microscopy to examine its microstructure properties. Optical microscopy has five magnification ranges, which are 50, 100, 200, 500, and 1000. The scanning area covers 104 mm × 102 mm. Microstructural properties are observed by 20 micrometer labels.

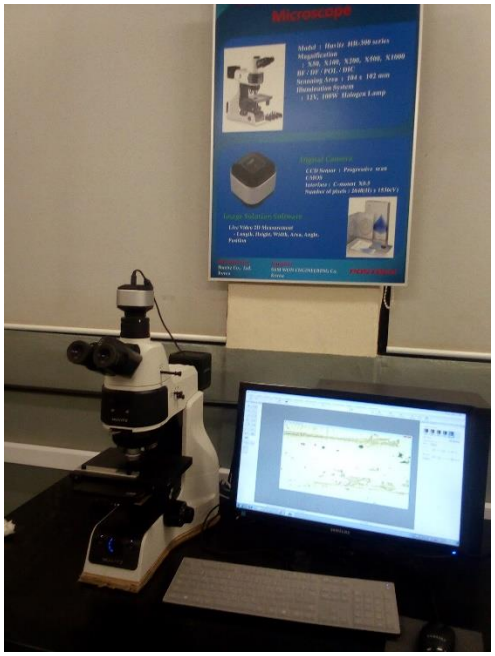

Figure 3. 18: Optical Microscopy during microstructure evaluation.

3.5 Methods

3.5.1 Determination of Working Limits of Parameters

The Analysis of Variance used to identify the process parameters that are statistically significant, which parameters affect the response of the study [42]. Different scholars use ANOVA to identify parameters of how much percent contribute to the response of the study. Therefore, in this thesis, reviewed and determined the most significant process parameters that strongly improved the response of the study. Parameters were collected from a previous similar study of 11 article journals by looking at their average percentage of contribution, and, after that, determined and selected using Pareto principles. The magnitude of RPM levels is also reviewed from previous similar studies and selected based on scholars' highly or repeatedly used magnitudes for dissimilar aluminum alloys. The remaining magnitude levels are chosen based on magnitudes that are extremely close to the selected RPM magnitudes.

Table 3. 5: Parameters with its contribution to the response of mechanical properties of FSW joint.

No	Parameter with % contribution								Ref.
	TS	**TRS**	**TPS**	**TSD**	**PD**	**TTA**	**AL**	**Error**	
1	11.5	5.5	51					32	[43]
2	3.47	3.04		26.56	8.94			57.99	[44]
3	40.5	18.13			25.84			15.25	[33]
4	36.64	55.18				5.63		2.54	[45]
5	5.37	85.1	4.01					5.52	[46]
6	48.7	15.13	27.48					8.52	[47]
7	37.99	25.55		18.26			18.20		[48]
8	29.55	64.08		5.67				0.797	[49]
9		96.24	0.41			0.06			[50]
10	34	36	4			9			[51]
11	8.25	58.05	33.1					0.6	[52]
Average	**25.60**	**42.00**	**20.00**	**16.83**	**17.39**	**4.90**	**18.20**		

*TS – Traverse speed; TRS – Tool Rotational Speed; TPS Tol pin profile; TSD – Tool Shoulder diameter; PD – Plunge Depth; TTA – Tool Tilt Angle; AL - Axial load; D/d - Shoulder diameter-to-pin diameter ratio

Based on the table results to identify the vital parameters from the trivial ones, the Pareto principles are used. The Pareto diagram essentially states that 80% of quality problems in the product or service are caused by 20% of the problems in the production or service processes.

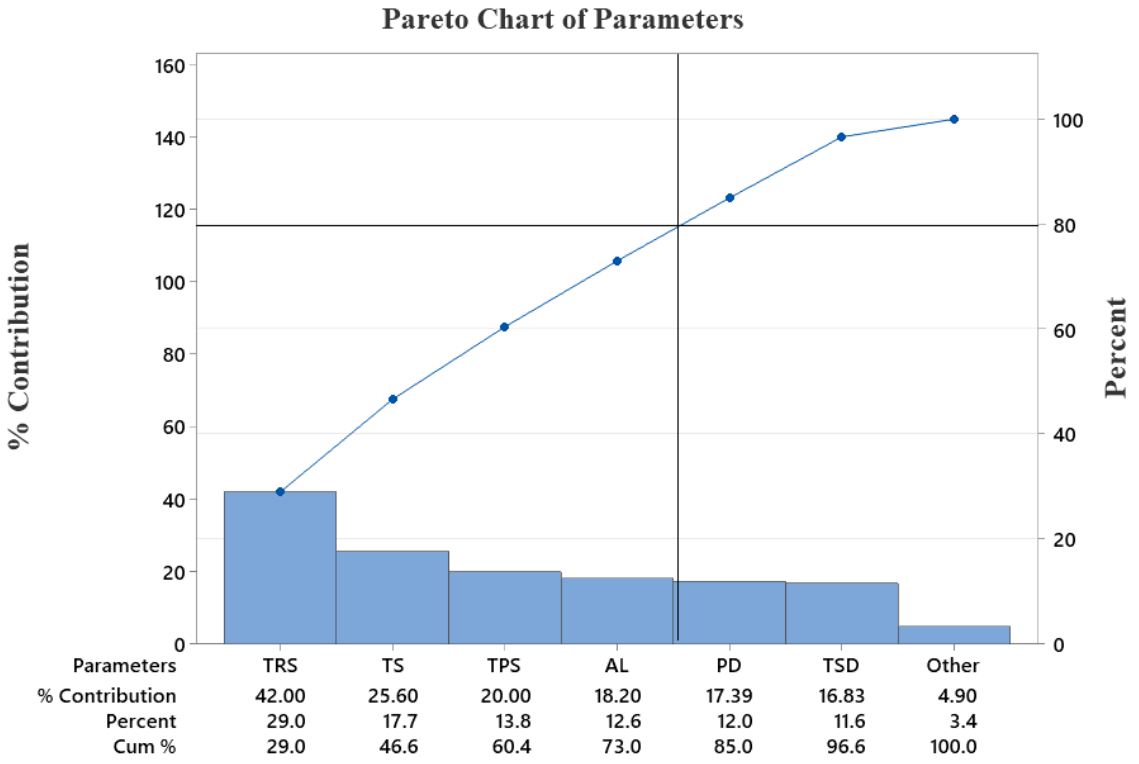

Figure 3. 19: Pareto Chart of parameters

Based on the Pareto diagram, the first four parameters out of seven consist of 80% of the total parameters, namely: tool rotational speed, tool traverse speed, tool pin profiles, and axial load, which are the most vital parameters. However, axial load is not controlled on a 3-axis CNC machine. Instead of axial load, consider plunge depth as a process parameter because plunge depth is directly proportional to axial load.

When increasing plunge depth, the axial force also increases and generates high heat. This high amount of heat affects grain growth in the nugget zone. Low plunge depth decreases the axial load, which leads to low heat supply and improper material flow. Therefore, for producing a good quality weld, adequate plunge depth and forging pressure are required for deep penetration. To achieve the downward pressure, set an adequate plunge depth for the tool to fully penetrate [12,53].

3.5.2 Determination of Working Limits of levels

To select the appropriate rotational and traverse speeds for the target materials of AA 6061 T6 and AA 5052 H32, a review of the existing literature that is like this study was conducted, and the levels were chosen based on their frequency. i.e., which level magnitudes scholars frequently use, and the level magnitudes that impart the highest response value were selected.

3.5.3 Determination of RPM levels

The selection of tool rotational speeds selected from different scolars as shown in the table 3.6.

Table 3. 6: Selections of tool rotational speed

No.	Title	Material thickness	Initial rpm	Optimized	Result	Ref.
1	Investigation of Welding Parameters Effects on Microstructure and Mechanical properties of FSW 5052 and 6061 Dissimilar Al Alloy Welded Joint	5052-H32 and 6061 – T6 5mm	900, 1100	1100@28	165.84MPa 70 HV	[22]
2	Effect of welding speed on mechanical properties and corrosion resistance rates of filler induced FSW AA6082 and AA5052 joints	AA6082 and AA5052 8mm		1150@130	177 Mpa 93 Hv	[54]
3	Studies on effect of tool design and welding parameters on the FSW of dissimilar Al alloys AA 5052 – AA 6061	5052-H32 and 6061 – T6 5mm	710	710@28	180MPa 75Hv	[26]
4	Optimization of FSW for AA5052 and AA6061	5052-H32 and 6061 – T6 5mm	1200	1200@55	175MPa 73.8HRB	[20]
5	FSW parameters and their influence on mechanical properties of welded AA6061 and AA5052 aluminum plates	5052-H32 and 6061 – T6 5mm	1000 1200 1400 1600 1800	1800@30	179MPa	[24]
6	Optimization of process parameters of friction stir welded dissimilar AA6063 and AA5052 Al-alloys by Taguchi technique	6063 and 5052 8mm	650 750 850	850@20	151.78MPa	[25]
7	Effect of tool geometry and process parameters on microstructure and mechanical properties of Dissimilar FSW of AA6061- AA5052	5052-H32 and 6061 – T6 3 mm	700 1050 1400	1050@36	175MPA 65HV	[23]
8	A Study on FSW of Dissimilar Thin Sheets of Al-alloys AA 5052–AA 6061	5052and 60611 and 1.5 mm	1500	1500	210.4 for 1.5mm 172.4 for 1mm	[30]
9	Influence of FSW Parameters on Dissimilar Joints AA6061-T6 and AA5052-H32	AA5052-H32 and AA6061-T6 5mm	800, 950, 1100	1100@60	181 MPa 90 HV	[29]
10	Parametric optimization on tensile strength of friction stir butt joints of dissimilar AA6061 and AA5052 aluminium alloys by Taguchi technique	>>>	560 700 900	900@40	151.78 MPa	[31]
11	Tensile and wear behavior of friction stir welded AA5052 and AA6101-T6 Al-alloys: effect of welding parameters	6101 5052 6mm	765, 980 1190,1400	1400	118 Mpa	[28]

12	Optimization of Tool Pin Profile for Dissimilar FSW of AA5083-H111 and AA6061-T6 Al-alloys	AA5083-H111 and AA6061-T6 5 mm	800	800@80	188.64 Mpa 95 HV	[21]
13	Artificial intelligence-based modeling and multi-objective optimization of FSW of dissimilar AA5083 and AA6063 Al-alloys	5083 6063	700 900 1100	900@60	168Mpa 87HV	[27]
14	Optimization of FSW parameters of dissimilar Al-alloys 6061 and 5083 by using RSM	5083 6063 6mm	1200 1575 1950	1568@39.53	135.83 Mpa	[36]
15	Multi-response optimization of friction stir corner welding of dissimilar thickness AA5086 and AA6061 Al-alloys by Taguchi GRA	5083 6063 4-6mm	900 1000 1100	1100@150	192 Mpa	[33]
16	Effect of FSW parameter on the material flow, mechanical properties, and corrosion behavior of dissimilar AA5083-AA6061 joint	5083 6061	800 1100 1400 1700	1400@60	197Mpa	[8]
17	Dissimilar alloys (AA6082/AA5083) joining by FSW and parametric optimization using Taguchi, grey relational, and weight method	AA6082/AA5083	1200 1950 3080 4600	1200@30	249.5 Mpa	[49]
18	Optimization of Process Parameters during FSW of dissimilar Al-Alloys (AA 5083 & AA 6061) using Taguchi L9 Orthogonal Array	5083 6061	700 800 900	900@40	216mpa	[35]
19	Effect of Welding Speed on Mechanical Properties of Dissimilar FSW AA5083-H321 and AA6061-T6 Aluminum Alloys	AA5083-H321 and AA6061-T6		1120@80	183 84	[55]
20	Examining the Mechanical and Metallurgical Properties of Single Pass FSW Dissimilar Al-Alloys Tee Joints	5052-H32 and 6061 – T6	900 1100 1200	1100@50	314 Mpa	[56]
21	Effect of tool rotational speed and pin profile on microstructure and tensile strength of dissimilar FSW AA5083-H111 &AA6351-T6 Al- alloys	AA5083 and AA6351-T6	600 950 1300	950@60	273Mpa	[9]
22	Dissimilar FSW of thick plate AA5052-AA6061 aluminum alloys: effects of material positioning and tool eccentricity	5052-H32 and 6061 – T6	1120	1120@90	215Mpa 70 HV	[57]
23	Enhancing corrosion resistance and mechanical properties of dissimilar friction stir welded 5083-6061 Al-alloys using external cooling environment	5083 and 6061	1400	1400@60		[32]

The magnitude of parameters is selected based on the frequency of the scholars most used. Table 3.7 shows the parameters selected for this thesis work.

Table 3. 7: Selected tool rotational speed

RPM	Tensile Test	Hardness	Frequency	Rank
710	180Mpa	75Hv	1x	5
800	188.64 Mpa	95 HV	1x	5
850	151.78Mpa	-	1x	5
900	151.78 MPa		3x	2
	168Mpa	87HV		
	216Mpa			
950	273Mpa	-	1x	5
1050	175MPA	65HV	1x	5
1120	215Mpa	70 HV	2x	4
	183	84		
1150	177 Mpa	93 Hv	1x	
1100	165.84Mpa	70 HV	4x	1
	314 Mpa	-		
	192 Mpa	-		
	181 Mpa	90 HV		
1200	175Mpa	73.8HRB	1x	5
1400	-	-	3x	2
	197Mpa	-		
	118 Mpa	-		
1500	210.4 Mpa for 1.5mm 172.4Mpa for 1mm		1x	5
1568			1x	
1800	179Mpa	-	1x	

Based on the above table it is possible to select 900, 1100, or 1400 rpm as the rotational speed magnitude for welding of dissimilar AA6061-T6 and AA5052-H32 materials. The first magnitude gap is not equal to the second and third. The reason for this is that most scholars achieve maximum tensile strength at a rotational speed of 1100 rpm and achieve maximum tensile strength at 900 rpm or 1400 rpm.

3.5.4 Determination of Traverse speed levels

The selection of level magnitudes of traverse speed is based on the selected rpm magnitudes.

Table 3. 8: Selection of Transverse Speed

No	Title	Material thickness	Initial traverse speed	Optimized traverse speed at selected rpm	Result	Ref.
1	Influence of FSW Parameters on Dissimilar Joints AA6061-T6 and AA5052-H32	AA5052-H32 and AA6061	30,60 and 90	60@1100	181 Mpa 90 HV	[29]
2	Artificial intelligence-based modeling and multi-objective optimization of FSW of dissimilar AA5083-O and AA6063-T6 aluminum alloys	5083 6063	40, 60 and 80	60@900	168Mpa 87HV	[27]
3	Effect of FSW parameter on the material flow, mechanical properties, and corrosion behavior of dissimilar AA5083-AA6061 joint	5083 6061	40,60 and 80	60@1400	197Mpa	[8]
4	Optimization of Process Parameters during FSW of dissimilar Aluminum Alloys (AA 5083 & AA 6061) using Taguchi L9 Orthogonal Array	5083 6061	40,50 and 60	40@900	216mpa	[35]
5	Examining the Mechanical and Metallurgical Properties of Single Pass FSW Dissimilar Aluminum Alloys Tee Joints	5052-H32 and 6061 –T6	50	50@1100	314 Mpa	[56]
6	Enhancing corrosion resistance and mechanical	5083 and 6061	60	60@1400		[32]

	properties of dissimilar FSW 5083-6061 aluminum alloys using external cooling environment					
7	Parametric optimization on tensile strength of friction stir butt joints of dissimilar AA6061 and AA5052 aluminum alloys by Taguchi technique	>>>	30, 40 and 50	40@900	151.78 MPa	[31]
8	A Study of the Effect of Tool Pin Profiles on Tensile Strength of Welded Joints Produced Using FSW Process	AA7075-T6 5mm	40, 50 and 63	40@900	290 Mpa	[42]

Table 3. 9: Selected traverse speed

Traverse speed, [mm/min]	**Tensile Mpa**	**Hardness Hv**	**Frequency**	**Rank**
60	181 Mpa	90 HV	4x	**1**
	168Mpa	87HV		
	197Mpa	-		
	-	-		
50	314 Mpa	-	1x	**3**
40	216Mpa	-	2x	**2**
	151.78 MPa	-		

The traverse speed (40, 50 and 60 mm/min) was selected based on the above RPM.

Table 3. 10: Summary of Selected tool rotational speed and traverse speed

Traverse speed (mm/min)	**Rotational Speed (rpm)**
40	900
50	1100
60	1400

3.6 Taguchi approach and grey relational analysis

Many researchers have used different statistical tools for optimization study of FSW process. Taguchi approach is useful techniques for single response optimization studies used for several engineering problems. The present scenario of rapid manufacturing and cost reducing with maximum utilization, complex processes have several quality characteristics [43,46]. In these cases, many multi-response optimization methods are required, and this thesis work has applied Taguchi-based grey relational analysis as shown in the figure 3.20.

Taguchi method has provided three different options to calculate the S/N ratio such as larger is better; nominal is best and smaller is better. However, the selection of an appropriate S/N ratio needs some practical knowledge, expertise, and understanding of the process. The aim of this study is finding the higher hardness and tensile strength that corresponds to a better welding performance. Therefore, larger is better S/N ratio was selected. It was calculated with the following equation [47].

$$\frac{S}{N}(\eta) = -10\log 10\frac{1}{n}\sum_{i=1}^{n}\frac{1}{y^2_{ijk}} \quad (1)$$

Where n is the number of replications and y_{ijk} is the response value of the i^{th} performance characteristic in the j^{th} experiment at the k^{th} trial.

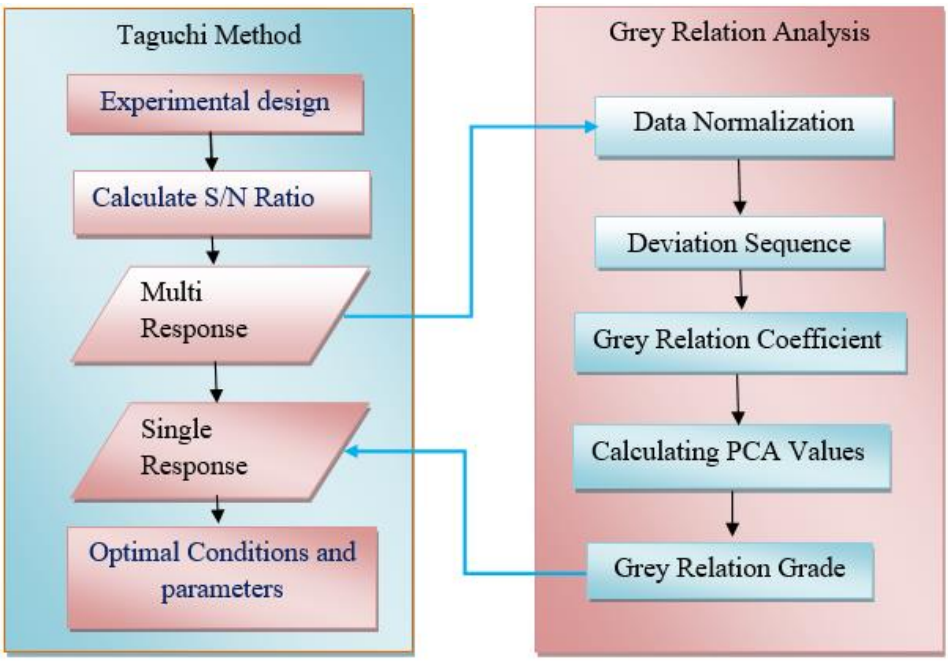

Figure 3. 20: Flow chart showing main steps in combined Taguchi method and GRA model optimization process.

3.6.1 Grey relational analysis

One of the drawbacks of the Taguchi method is used to optimize only a single parameter (i.e., Mono-objective optimization). The combination of Taguchi with a grey relational analysis method can optimize multiple parameters easily and effectively [58]. GRA is an efficient tool for optimizing multi-response conditions. This analysis method used for solving the sophisticated interconnection among the multi-objective responses[48]. Grey relational analysis uses normalization of data to calculate grey relational coefficients and grey relational grades. It analyses optimum arrangement and ANOVA is utilized for the estimate of optimum grey relational grades.

3.6.1.1 Data normalization

In GRA method data normalization is the first step, in this process to get comparable sequence changing original sequence. The experimental results are normalized in the range between zero and one. The process is necessary when the arrangement scatter range is too large, or when the direction of the target in the sequence are different[48]. If the response is to be increased, then larger is better characteristics are expected for normalization to scale it into an adequate range by the following equation (2) [47].

$$x_i(k) = \frac{x_i^0(k) - \min x_i^0(k)}{\max x_i^0(k) - \min x_i^0(k)} \tag{2}$$

where $xi^0(k)$ is the reference sequence, xi*(k) is the sequence after the data preprocessing (comparability sequence), max $xi^0(k)$ is the largest value in the reference sequence, min $xi^0(k)$ is the smallest value in the reference sequence, i = 1, 2, m; k = 1, 2..., n; m is the number of experiment and n is the number of experimental data.

3.6.1.2 Calculation of deviation sequences and grey relational coefficients (GRC)

The next step is to calculate the grey relational coefficient, ξi (k) from the normalized values by the following formula as follows. The GRC is utilized to describe the correlation between the reference sequence and the comparability sequence. The GRC (ξ) is calculated to integrate the data achieved from equations [59,60].

$$\Delta_{0i}(k) = \|x_{o^*}(k) - x_{i^*}(k)\| \tag{3}$$

$$\xi(x_{o^*}(k) - x_{i^*}(k)) = \frac{\Delta_{\min}(k) + \xi\Delta_{\max}(k)}{\Delta_{0i}(k) + \xi\Delta_{\max}(k)} \tag{4}$$

Where $\Delta_{0i}(k)$ is the deviation sequence of the reference sequence $x_{o^*}(k)$ and comparability sequence $x_{i^*}(k)$ and ξ is the distinguishing coefficient that takes a value between 0 and 1, and the value of $\xi = 0.5$ is taken from the calculation result. As given in equation (4), it is necessary to calculate the deviation sequences before the calculation of the GRC. The deviation sequences are calculated using equation (3).

3.6.1.3 Calculation of grey relational grades (GRG)

The GRG represents the level of correlation between the reference sequence and comparability sequence. The GRG is a weighted average of the GRC of multi-objective [59]. It is determined as the following equation [47]:

$$\gamma i(x_{0^*}, x_{1^*}) = \frac{1}{n}\sum_{i=1}^{n} wi\xi\left(x_{0^*}(k), x_{1^*}(k)\right) \quad (5)$$

Where $\gamma i(x_{0^*}, x_{1^*})$ is the GRG for the i^{th} experiment, wi is the weighting value of the i^{th} performance characteristic and n is the number of performance characteristics.

3.7 Design of Experiments

3.7.1 Selections of Orthogonal Array

The selection of a particular orthogonal array was based on the number of levels of various factors. Here, to conduct the experiments 3 factors each at 3 levels were selected. Now the DOF of welding operation can be calculated by the formula as given below.

$$DOF = P * (L - 1)$$

Where, P = number of factors

L = number of levels

DOF = 3(3 – 1) = L9, However, total number of experiments of the OA should be greater than or equal to the total DOF required for the experiment. Thus, L9 orthogonal array was selected from standard design of experiment to make the further experiments were shown in Table 3.11.

Table 3. 11: Standard L9 orthogonal array

Experimental run	Control factors and levels		
	Rotational speed(rpm)	Transverse speed (mm/min)	Tool pin Shape
1	900	40	Conical
2	900	50	Cylindrical
3	900	60	Square
4	1100	40	Cylindrical
5	1100	50	Square
6	1100	60	Conical
7	1400	40	Square
8	1400	50	Conical
9	1400	60	Cylindrical

CHAPTER FOUR

4. RESULT AND DISCUSSION

4.1 Introduction

This chapter gives the overall results of the experiments using the application of the Taguchi and Grey relational analysis method. The experiment was conducted to find the optimum response of hardness and tensile strength of 606-T6 and 5052- H32 aluminum sheets.

The optimum condition is identified by studying the main effects of parameters. The main effects indicate the common trend of influence of each parameter. The ANOVA is the statistical treatment most applied to the results of the experiments in determining the percent contribution of each parameter against a stated level of confidence. In this thesis, the optimization of FSW parameters on the selected quality characteristics has been investigated through the plots of the main effects based on the obtained data from the experiments. The optimum condition for each of the quality characteristics has been established through S/N data analysis.

4.2 Experimental results and discussions

Table 4.1 shows the results of the tests on the effect of process factors on the output response characteristics of hardness and tensile strength. A series of welding tests were found out to see how welding parameters affected the hardness and tensile strength of AA 6061-T6 and AA 5052-H32 materials. MINITAB 20 software packages were used to perform statistical analysis on the data.

Table 4. 1: Experimental result

Sample No.	Rotational speed(rpm)	Welding speed (mm/min)	Tool pin Shape	Ultimate Tensile Strength (MPa)	Hardness value (HV)
1	900	40	Conical	135.94	61.03
2	900	50	Cylindrical	163.89	63.27
3	900	60	Square	172.46	64.77
4	1100	40	Cylindrical	176.87	67.67
5	1100	50	Square	154.25	62.77
6	1100	60	Conical	122.87	56.63
7	1400	40	Square	183.04	76.40
8	1400	50	Conical	131.85	59.43
9	1400	60	Cylindrical	181.47	68.93

4.2.1 Tensile strength

The maximum tensile or ultimate strength is the maximum stress that a material can withstand while being stretched or pulled before failure or fracture. The test was conducted at room temperature for dissimilar FS welded Al-alloys (6061-T6 and 5052-H32). The highest tensile strength was 183.04 MPa obtained from a square pin profile tool at a rotational speed of 1400 rpm with a traverse speed of 40 mm/min. Correspondingly, the lowest tensile strength value of 122.87 MPa was observed from the Conical tool pin profile at a rotational speed of 1100 rpm with a traverse speed of 60 mm/min. The tensile strength of FSW weld joint has achieved 79.58% with AA5052-H32 and 59.05% with AA6061-T6 individually. The ultimate tensile strength of the weld joint has reached 183.04 MPa, indicating the weld joint efficiency of 79.58% to the weak base metal with 1400 rpm 40mm/min, and square pin profile. In all joints, fracture occurred inside the weld line due to reduced thickness caused by forging action of tool[43]. The result shows that the tensile strength increases, the traverse speed of the tool decreases, and the rotational speed of the tool increases because the lower traverse speed and higher rotational speed produce adequate heat for joining the base metal.

Tensile test was carried out for as received and welded samples with various process parameters with ASTM E8 standard. A tensile test was performed on a UTM machine.

It was observed that tool geometry, rotational speed, and traverse speed are very important parameters of the friction stir welding process. Amongst these, tool geometry is found to be the most influential parameter. Square tool geometry shows better UTS values compared to that of the conical and cylindrical tools.

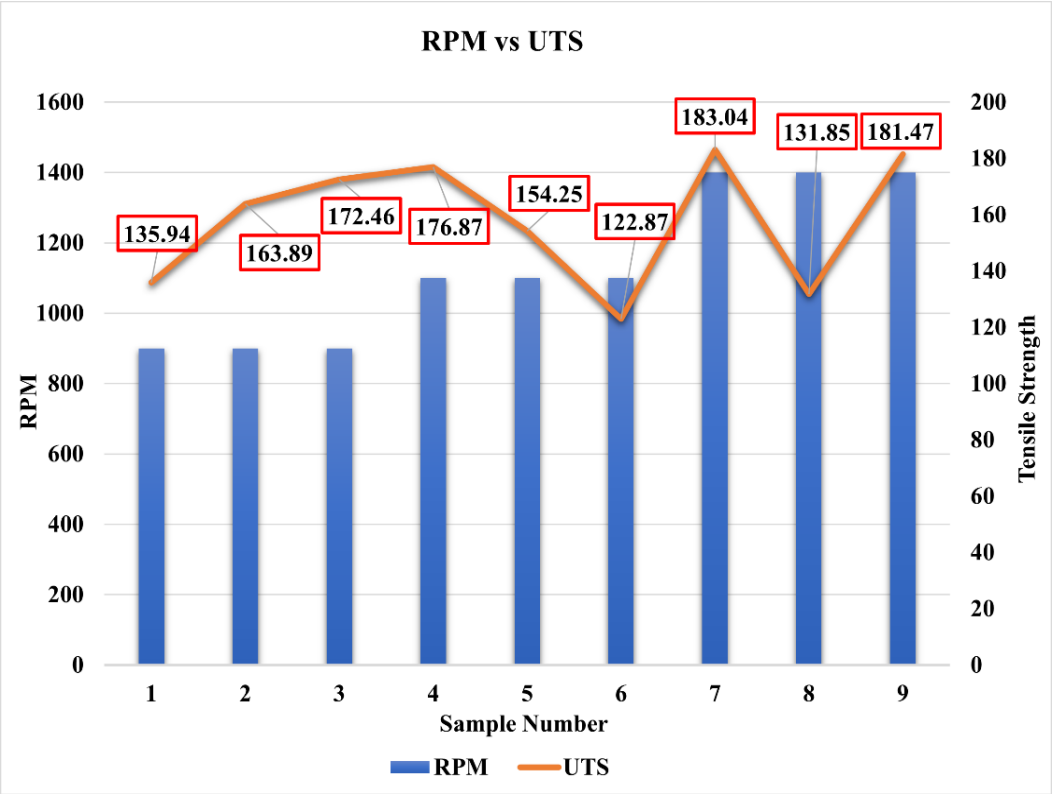

Figure 4. 1: Influence of rotational speed on the tensile strength

The graph shows that the tensile strength was increased at a combination setting of the higher rotational speed and the lower traverse speed.

4.2.2 Hardness

The hardness was measured three times at the stir zone of the FSW joint. The higher hardness value of 76.40 HV was obtained at a rotational speed of 1400 rpm, traverse speed of 40 mm/min and square tool pin profile. Similarly, the minimum hardness value of 56.63 HV was recorded at a rotational speed of 1100 rpm, traverse speed of 50 mm/min and conical tool pin profile. The maximum rotational speed with a combination of a square tool pin provides the highest hardness. The rotational speed with a combination of traverse speed and tool shape contributes a great influence on the hardness of the joint.

As shown in the figure 4.2, the higher rotational speed of 1400 rpm imparts the maximum hardness for the dissimilar FS welding of AA6061 and AA5052. This is because of the hardness of the joint which was depended on the amount of heat that develops during the stirring process.

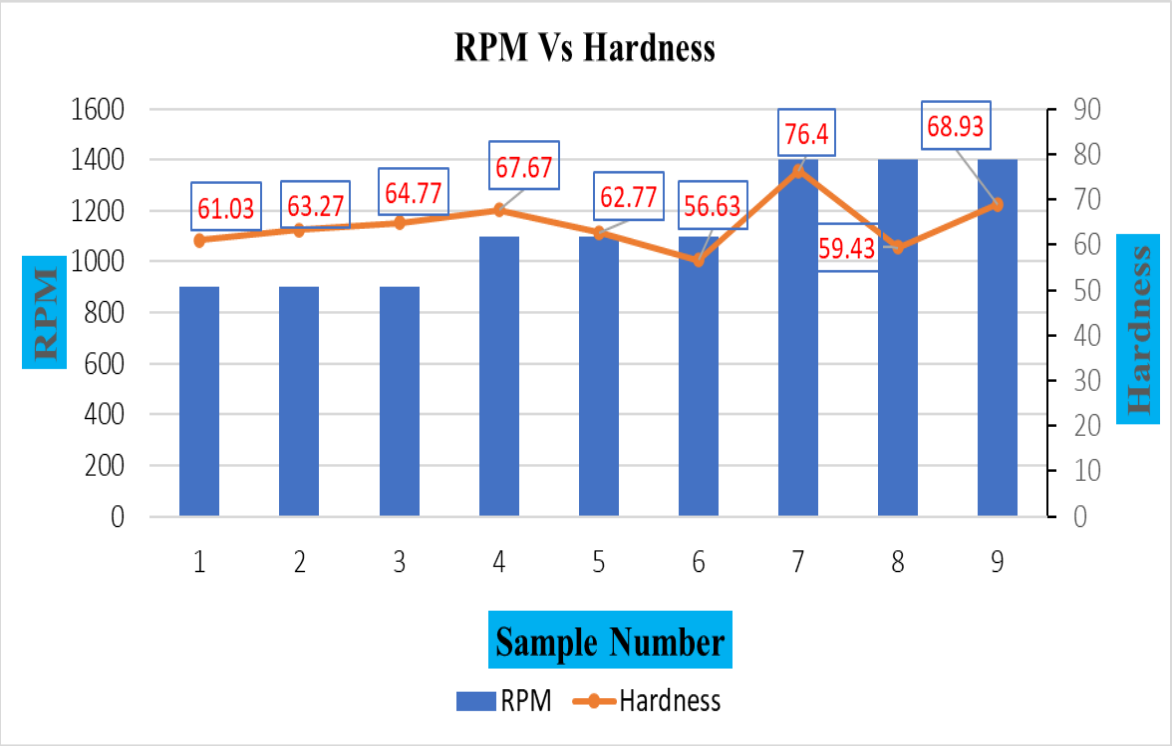

Figure 4. 2: Effect of rotational speed on the hardness

As shown in the Figure 4.3, the rotational speed is kept constant while the effect of varying transverse speed on hardness is measured. The increase in tool traverse speed from 40 to 60 mm/min at a constant tool rotation rate causes a decrease in the hardness of the stir zone for conical and square-shaped tools; however, the hardness under the same conditions for cylindrical-shaped tools shows a decrease.

As shown in the Figure 4.4, the transverse speed is kept constant while the effect of varying rotational speed on hardness is measured. The increase in tool rotation rate at constant tool traverse speed results in increased hardness of the stir zone for cylindrical and square-shaped tools; however, the hardness under the same conditions for conical-shaped tools shows a decrease.

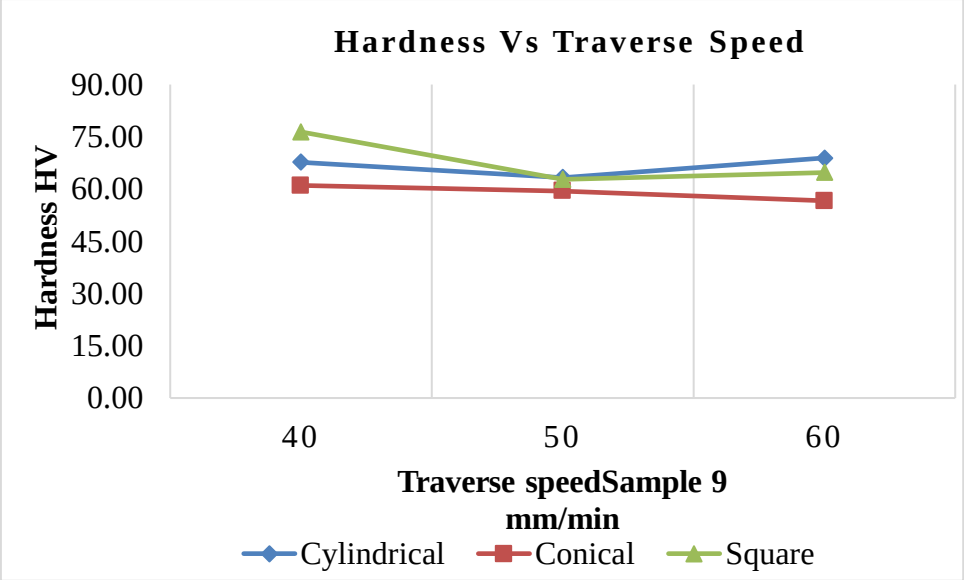

Figure 4. 3: The influence of traverse speed on hardness

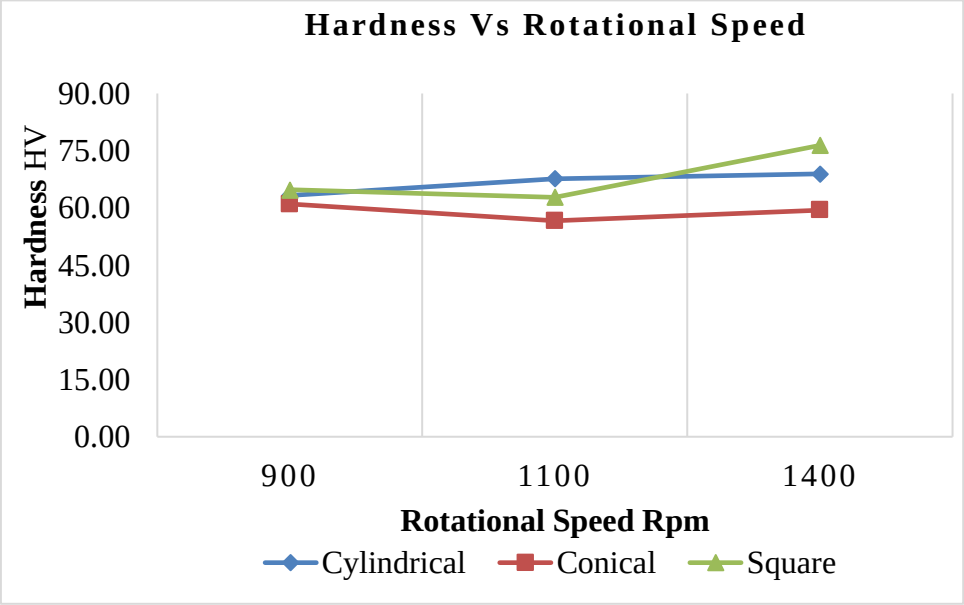

Figure 4. 4: The influence of rotational speed on hardness

4.2.3 Influence of Process Parameters on Microscopic Examination

Friction stir welding has four distinct regions of metallographic properties, such as the stir zone or nugget zone (SZ), the Thermo-mechanical heat affected zone (TMAZ), the heat affected zone (HAZ), and base metal. Recrystallization of grains occurs due to high deformations during tool moves in the regions. In the stir zone, small-sized grains or fine grains are formed due to recrystallization. In TMAZ, the shape and size of the grains changed. The region after TMAZ is a heat-affected zone, in this region precipitation that impacts the properties of this zone. Microstructural and physical properties are not changed in the last region, which is the base metal [4].

The SEM micrographs taken from stir zone of lower and higher mechanical properties of welded jonits (experment 6 and 7) are shown in Figure 4.5. From the micrographs it is understood that although all of the identified particles in the parent alloy appear in the sample 6 and 7, the number and size of the particles of each type present at the sample 6 and 7 areas are different. The size and distribution of the Al (Fe-Mn), Al-Mg and Al (Fe-Mn-Cr) particles decrease in the sample 6 region with increasing the welding speed from 40 to 60 mm/min. sample 6 have void defect occur due to low heat input and the higher transvers speed. Whereas, sample 7 have defect free due to low transvers speed, higher rotational speed.

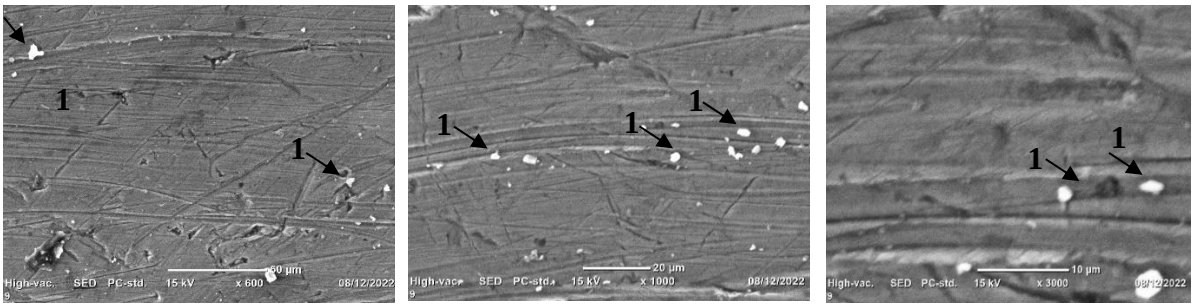

Sample 7: welded at 1400 rpm, 40 mm/min and square pin profile

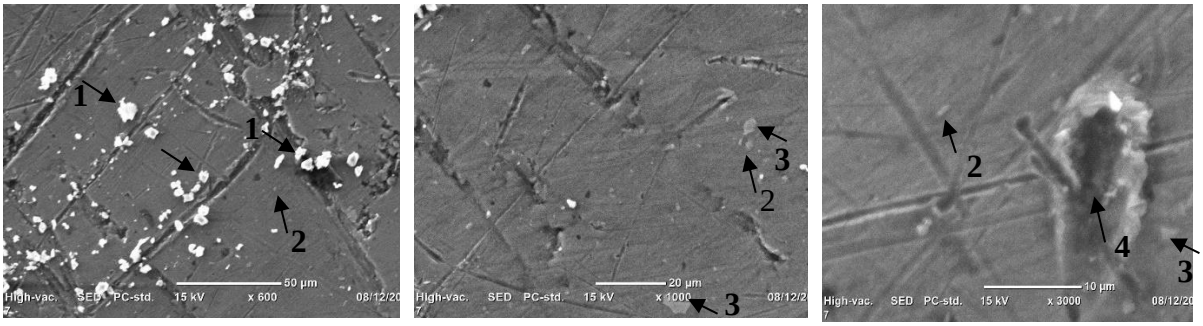

Sample 6: welded at 1100 rpm, 60 mm/min and conical pin profile

Figure 4. 5: SEM micrograph images of intermetallic identified in the nugget zone at different welding condtions: (1) Al (Fe-Mn) (2) Al (MgSi) (3) Al-Mg (4) void defect

Tensile properties of the FSW joints are improved by microstructural features and grain refinement [24]. Samples 4, 7 and 9 have the higher tensile strength because in the nugget zone the grain structure of the samples are defect free as shown in figures 4.6. This is because more tool rotation speed produce more heat. In samples 2, 3, 5 and 6, void defects occur due to lack of sufficient heat in the weld line which in turn lowers the tendency of plastic deformation as shown in figure 4.6. In the nugget zone, using a higher welding speed produced some cracks because of poor stirring of materials during the process. Welding time decreases or tool travel speed increases the contact time between tool and work pieces is reduced results lower heat generation causes reduction of grain growth. Low welding time and high travel speed imparts the contact between tool and work pieces is reduced. The tensile strength of the weld joint is also reduced because the time of stirring the materials is low. In sample 3 and 6 the effects of transverse speed on nugget zone microstructure shown in figure 4.6.

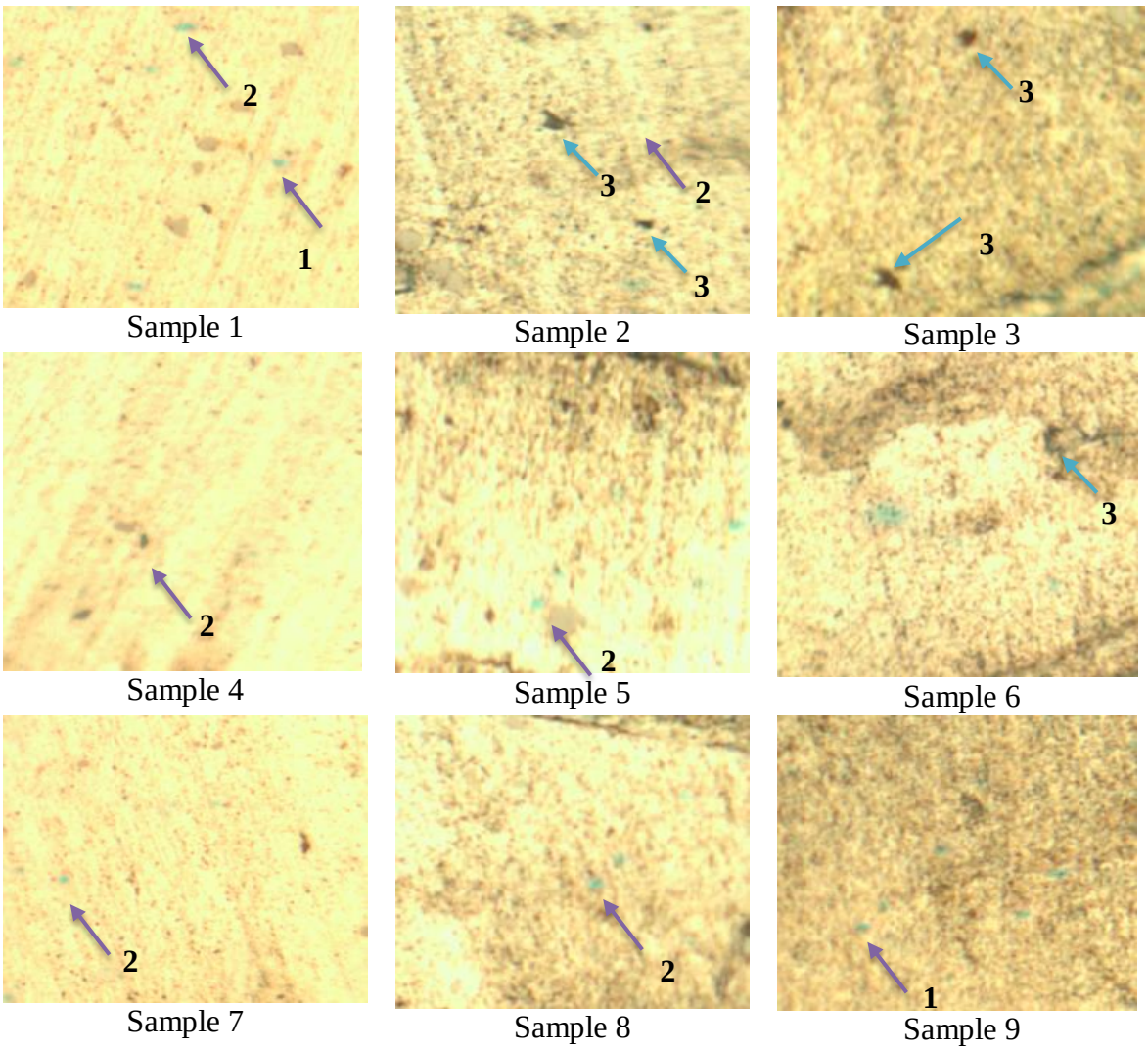

Figure 4. 6: Optical microscope of stir zone of different FSW jonits: (1) Al (MgSi) (2) Al-Mg (3) void defect

4.3 Effect of welding parameters on the joint quality

The following table 4.2 shows the effect of welding parameters on the joint strength of the dissimilar FSW of AA6061 and AA5052 aluminum alloys.

Table 4. 2: Effect of RPM and traverse speed on the joint strength

No	Process parameters	Mechanical property	Welding Joint	Observation
1	900 rpm 40 mm/min Conical pin profile	UTS = 135.94 Hv = 61.03		Surface defect Reason for the defect: Low heat & improper pressure[61]
2	900 rpm 50 mm/min Cylindrical pin profile	UTS = 163.89 Hv = 63.27		Flash defect ✓ Low heat
3	900 rpm 60 mm/min Square pin profile	UTS = 172.46 Hv = 64.77		Flash defect
4	1100 rpm 40 mm/min Cylindrical pin profile	UTS = 176.87 Hv = 67.67		Defect free

5	1100 rpm 50 mm/min Square pin profile	UTS = 154.25 Hv = 62.77		Defect free
6	1100 rpm 60 mm/min Conical pin profile	UTS = 122.87 Hv = 56.63		Surface defect Reason for the defect: Low heat & improper pressure[61]
7	1400 rpm 40 mm/min Square pin profile	UTS = 183.04 Hv = 76.40		Defect free
8	1400 rpm 50 mm/min Conical pin profile	UTS = 131.85 Hv = 59.43		Surface defect
9	1400 rpm 60 mm/min Cylindrical pin profile	UTS = 181.47 Hv = 68.93	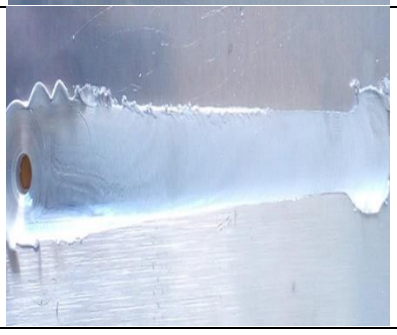	Flash defect ✓ High tool rotation speed. ✓ High vertical force

4.4 Result of Grey Relation Analysis

4.4.1 The results of S/N ratios

The results of UTS, Hv and their S/N ratios are given in Table 4. 3.

Table 4. 3: Results of UTS, Hv and their S/N ratios

Sample No.	Ultimate Tensile Strength (MPa)	Hardness value (HV)	S/N UTS	S/N HV
1	135.94	61.03	42.6669	35.7109
2	163.89	63.27	44.2910	36.0240
3	172.46	64.77	44.7338	36.2275
4	176.87	67.67	44.9531	36.6079
5	154.25	62.77	43.7645	35.9550
6	122.87	56.63	41.7889	35.0609
7	183.04	76.40	45.2509	37.6619
8	131.85	59.43	42.4016	35.4801
9	181.47	68.93	45.1761	36.7682

4.4.2 Principal Component Analysis (PCA)

The PCA has been used to eliminate the response correlation. This matrix consists of Eigenvalues, Eigenvectors, and quality characteristics contributions. The elements of the array for multiple performing characteristics shown in table 4.4 and 4.5 represent the GRC matrix and find the corresponding Eigenvalue.

Table 4. 4: Eigen values and explained variation (Appendices 12)

Principal components	Eigen Values	Explained Variation (%)
UTS	1.8930	94.7
HV	0.1070	5.3

The principal component with the greatest Eigen values is selected to replace the original responses for further analysis. In this case, the highest Eigen values were obtained in the UTS first principal component. Then, the contribution of every single quality characteristic for the first principal components Quality characteristic contribution was 0.49 for both UTS and HV. Therefore, the grey relational coefficients values are taken $\xi = 0.5$ is used.

Table 4. 5: The Eigenvectors for principal component (Appendices 12)

Quality Characteristics	Eigenvector	
	Principal component one	Principal component two
UTS	0.707	- 0.707
Hv	0.707	0.707

Table 4. 6: Data normalization and deviation sequence

Step 1: Data normalized			Step 2: Deviation sequence	
S no.	UTS	Hv	UTS	Hv
1	0.2536	0.2499	0.7464	0.7501
2	0.7227	0.3703	0.2773	0.6297
3	0.8506	0.4485	0.1494	0.5515
4	0.9140	0.5948	0.0860	0.4052
5	0.5706	0.3438	0.4294	0.6562
6	0.0000	0.0000	1.0000	1.0000
7	1.0000	1.0000	0.0000	0.0000
8	0.1770	0.1612	0.8230	0.8388
9	0.9784	0.6564	0.0216	0.3436

Table 4. 7: The result of GRC and GRD

Step 3: Grey relational Coefficient			Step 4: Grey relational grade and it is rank	
S no.	UTS	Hv	GRG	Rank
1	0.40116	0.39996	0.4006	7
2	0.64329	0.44258	0.5429	5
3	0.76997	0.47552	0.6227	4
4	0.85320	0.55235	0.7028	3
5	0.53801	0.43244	0.4852	6
6	0.33333	0.33333	0.3333	9
7	1.00000	1.00000	1.0000	1
8	0.37792	0.37346	0.3757	8
9	0.95857	0.59269	0.7756	2
Average GRG = 0.5821				

4.4.3 Determination of the optimal level of each parameter

The main effect analysis of GRG is adopted to figure out the response table for grey relational analysis, as indicated in table 4.9 shows the average of each response characteristic for each level of each factor. The delta static is shown that the highest minus the lowest average of each factor. Minitab assigns the ranks of optimum parameters based on delta values, for instance, rank 1 is the highest delta value, rank two is the second delta value and so on. These ranks indicate that the relative importance of each factor to the response and the mean response refers to the average value of the performance characteristic for each parameter at different levels.

Table 4. 8: Main Effects means of GRG

Level	**Rotational Speed[A]**	**Welding (transverse) Speed[B]**	**Tool Pin Profile[C]**
1	0.5221	**0.7011***	0.3699
2	0.5071	0.4679	0.6738
3	**0.7171***	0.5772	**0.7027***
Delta	0.2100	0.2332	0.3328
Rank	3	2	1

* Indicates the optimum value in each parameter

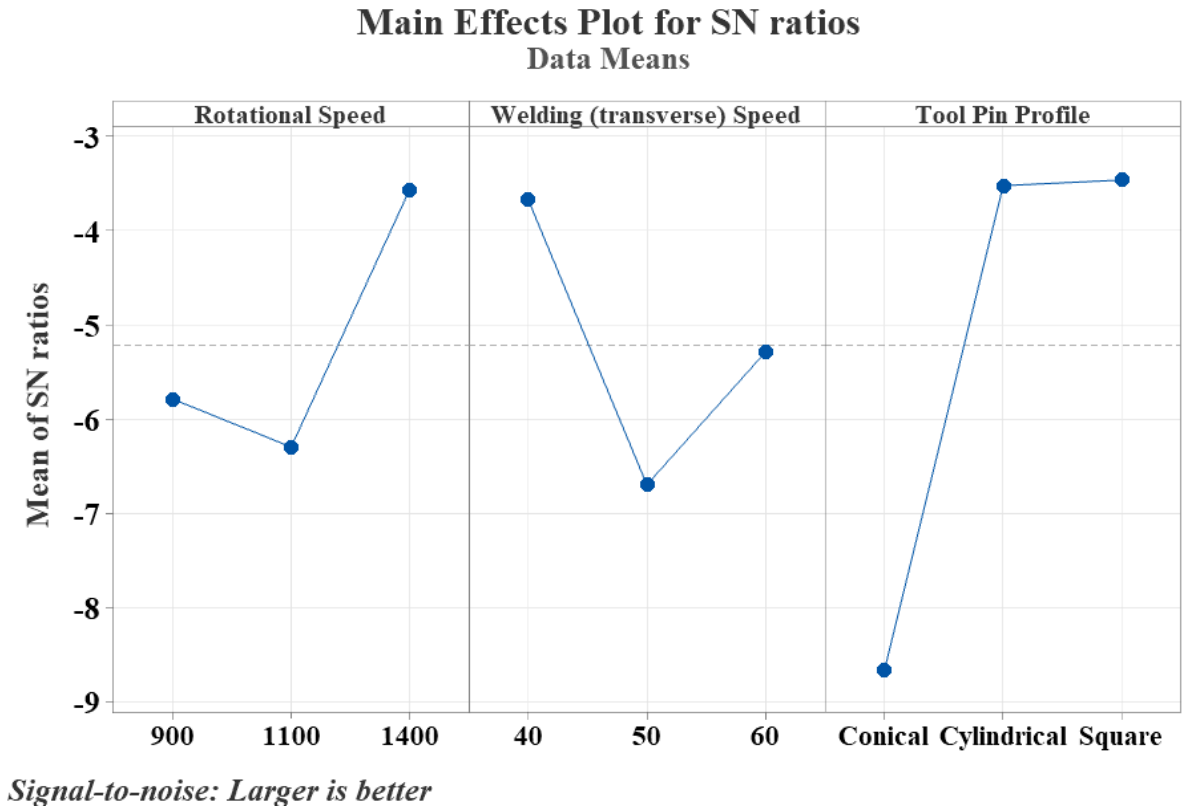

Figure 4. 7: Main effects plot for S/n ratios

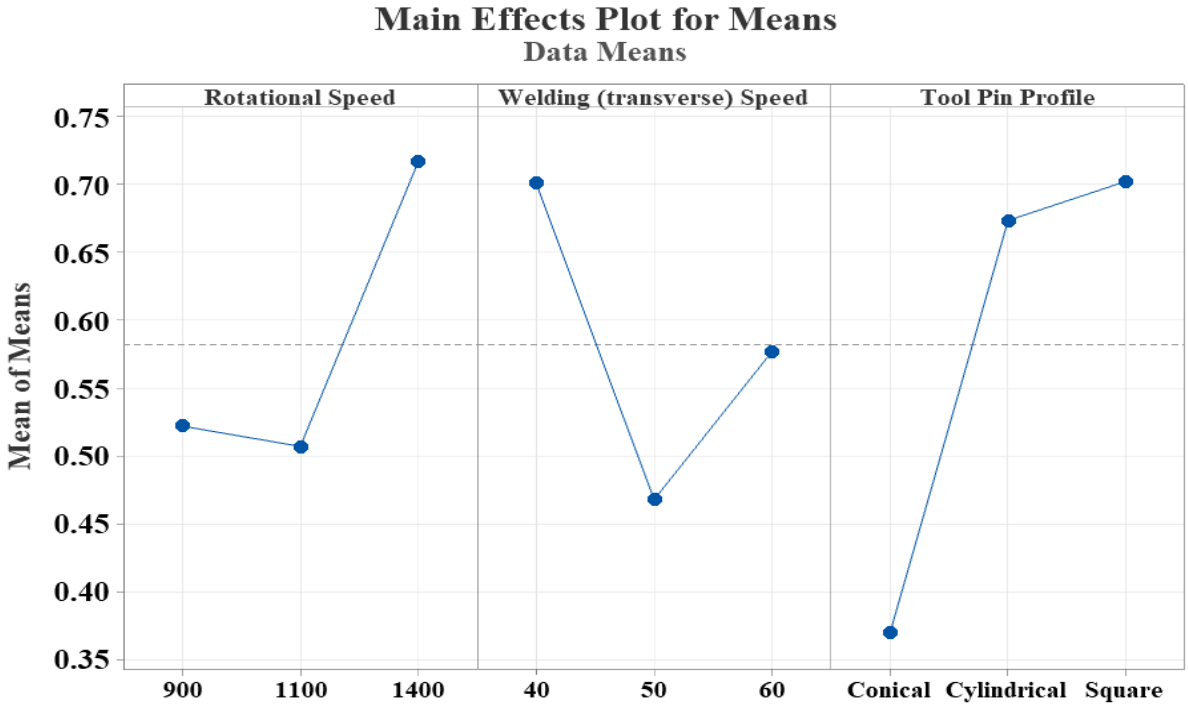

Figure 4. 8: Main effects of (GRG)

4.4.4 ANOVA for GRG

The percentage effects of the FSW parameters on the mean GRG were obtained using an ANOVA. The analysis was employed at a 95% confidence level and is listed in Table 4.10. The percentage contribution of individually parameter to the average GRG is calculated and presented in the last column of Table 4.10. As seen in Table 4.10, tool pin profile, tool rotational speed, and weld traverse speed influenced the average GRG values by 54.15%, 21.86% and 21.68%, respectively. Therefore, the tool pin profile was the most important parameter affecting the average GRG values. Another finding is that tool pin profiles have a statistical significance on average GRG results at a reliability level of 95% because the P value results are lower than 0.05. According to the ANOVA results, the tensile strength and hardness of FSW joints are significantly influenced by the process parameters under investigation, and the effect is determined to be in the following order: 1) the tool pin profile; 2) the tool rotational speed; and 3) the weld traverse speed.

Table 4. 9: Analysis of Variance results for GRG

Source	DF	Seq SS	Adj SS	Adj MS	F-Value	P-Value	PC
Rotational Speed	2	0.082358	0.082358	0.041179	9.46	0.096	21.86%
Welding (transverse) Speed	2	0.081654	0.081654	0.040827	9.37	0.096	21.68%
Tool Pin Profile	2	0.203951	0.203951	0.101975	23.42	0.041	54.15%
Error	2	0.008710	0.008710	0.004355			2.31%
Total	8	0.376673					100.00%

*DF-Degree of Freedom; SS-Sum of Square; MS-Mean Square; PC- Percentage contribution

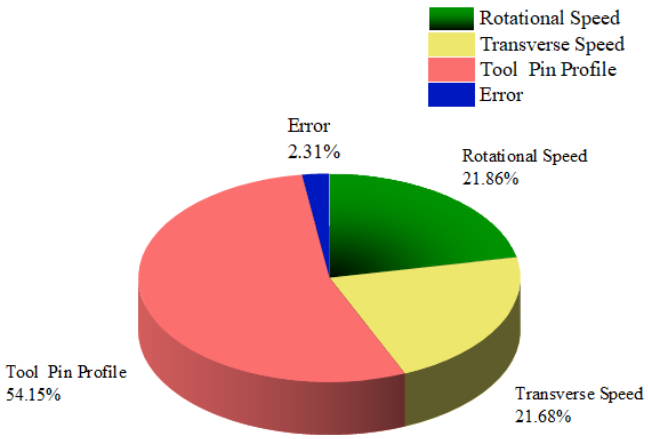

Figure 4. 9: Contribution of each welding parameters in ANOVA

4.4.5 Interactions plot of GRG

The combined effect of all parameters considered in the thesis is shown in Figure 4. 10. The tool rotation and transverse rate affect the grain size and quality of the weld. An increase in rotational speed increases strength, while an increase in transverse speed decreases weld strength.

For tool pin profile versus rotational speed, square and cylindrical pin profile tools show high weld strength at a high rotational rate. The conical-shaped tool shows high strength at the lowest rotational speed.

For tool pin profile versus transverse speed, an increase in transverse speed results in a decrease in weld strength for square pin profile; for cylindrical pin profile an increase in transverse speed results in an increase in weld strength, and conical pin profile tool produces the least strength at the highest transverse speed.

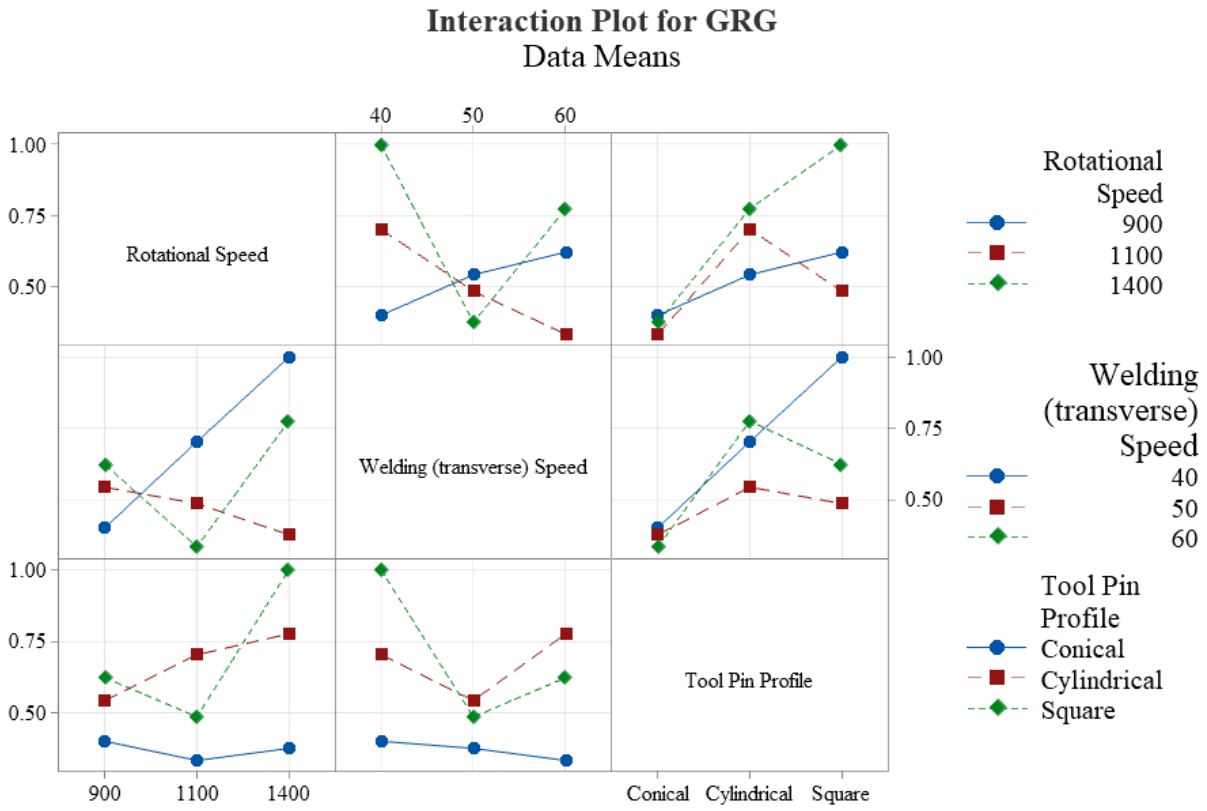

Figure 4. 10: Interaction plot showing influence of rotational speed, transverse speed, and pin profile on GRG of welded parts.

4.4.6 Confirmation Experiment

The results obtained at optimum process parameter setting have been validated through confirmation experimental runs. To get the average values three confirmation experiments were performed for every quality characteristic (Tensile strength and hardness). The predicted mean value of GRG at optimum level of parameter setting was computed by using equation (6). The estimated values for multi-response optimization at optimum level of parameter setting were confirmed through confirmation experimental results. The average values of the response variables must lie within the 95% confidence interval, obtained from confirmation experiments CI.

$$\hat{\gamma} = \gamma_m + \sum_{i=1}^{v} (\gamma_i - \gamma_m) \quad (6)$$

$$\hat{\gamma} = 0.5821 + (0.7171 - 0.5821) + (0.7011 - 0.5821) + (0.7027 - 0.5821) = \mathbf{0.9567}$$

Where; $\hat{\gamma}$ – predicted mean GRG value, γ_m – total mean of GRG, γ_i – mean GRG at optimum level, v –Number of process parameters.

$$CI = \hat{\gamma} = \pm \sqrt{F_\alpha; (1: f_e) * Ve(\frac{1}{n_{eff}} + \frac{1}{R})} \quad (7)$$

Calculation for CI using Equations (7) is as follows:

N = Total number of experiments = 9

R = Sample size for confirmation experiments = 3

Ve = Error variance = 0.004355 (Table 4.10)

f_e = Error DOF = 2 (Table 4.10)

$F_\alpha; (1: f_e)$ $F_{0.05}; (1: 2)$= 18.51 (from Appendix E Tabulated F- critical value)

DOF associated in the significant effect of mean response = 2 (Table 4.10)

$$n_{eff} = \frac{N}{1+DOF} = \frac{9}{1+2} = 3$$

Therefore, the calculated CI is

$$CI = \hat{\gamma} \pm \sqrt{F_{0.05}; (1:2) * Ve(\frac{1}{n_{eff}} + \frac{1}{R})}$$

$$= 0.9567 \pm \sqrt{18.51 * 0.004355(\frac{1}{3} + \frac{1}{3})} = 0.9567 \pm 0.2318$$

where, $F_{\alpha}; (1: f_e)$ is the F ratio at confidence level of (1-α) against DOF 1 and error degree of freedom f_e, R is the Number of confirmations runs (R = 3), N is total No. of experiments (N = 9), Ve is error variance and n_{eff} = N/1 + DOF associated in the significant effect of mean response. Therefore, the predicted confidence interval and the 95% confirmation interval of the predicted mean for confirmation experiments is:

$$\text{Mean } \hat{\gamma} - \text{CI} < CI < Mean\, \hat{\gamma} + \text{CI}$$

$$(0.9567 - 0.2318) < 0.9567 < 0.9567 + 0.2318$$

$$0.7249 < 0.9567 < 1.1885$$

Based on the confidence of interval analysis at 95 % of the confidence level, the mean GRG confirmation result is between 0.7249 and 1.1885. The effectiveness of the optimal condition can be ensured if the predicted and observed GRG values of the different performance parameters are close to each other. To put the theory to the test, the predicted outcomes were confirmed three times under optimum conditions. The grey relational grade for the conformation test experiment is 0.7550, which is in the range of the 95 % confidence level.

The confirmation test achieved tensile strength and hardness of 183.23 MPa and 76.51 HV respectively. Hence, the results of the confirmatory experiment tests show that the experiment is safest. Table 4.11 indicates the grey relational grade value for both the conformation test and for the predicted value.

Table 4. 10: Predicted optimal values, confidence intervals and results of confirmation test

Optimal parameter setting	Predicted optimal value (GRG)	Predicted confidence intervals at 95% confidence level	Actual value (Avg. of 3 confirmation test)
A3B1C3	0.9567	CI: $0.7249 < \hat{\gamma} < 1.1885$	0.7550

CHAPTER FIVE

5. CONCLUSIONS AND RECOMMENDATIONS

5.1 Conclusions

In this thesis, FSW is used to join the two dissimilar Al-alloys, 6061 and 5052, plates. The Taguchi L9 orthogonal array was used to determine the number of welding tests in the experiment conducted. The sheets are welded successfully, and the welded dissimilar Al-plates are measured at room temperature using a standard testing machine to test the tensile strength and Vickers hardness. Similarly, the results of Taguchi Grey relational analysis can be used to optimize the process parameters of the weld process, and it can be applied extensively to find out the most important factor. Testing is conducted out to achieve the most optimal (optimum) set of chosen parameters and their effects on the welded joints of the tensile strength and hardness.

- ✓ The result shows that the tool rotational speed is 1400 rpm, the welding speed is 40 mm/min, and square pin profiles are the optimized independent process parameters to maximize the tensile strength and hardness of the welded joints.
- ✓ The percentage of contribution of these FSW process parameters were determined by ANOVA, and it was found that the tool pin profile has a major contribution compared to tool rotational speed and weld traverse speed.
- ✓ Based on the ANOVA results, the percentage contribution of process parameters in joint efficiency
    - Tool pin profile has a greater effect, with an 54.15% contribution,
    - Tool rotational speed has an 21.86% contribution and
    - The traverse speed effect has an 21.68% contribution.
- ✓ The joint fabricated using with 1400 rpm, 40mm/min, and square pin profile maximum tensile strength of 183.04 MPa, which is 79.58% with AA5052-H32 and 59.05% with AA6061-T6 independently of the base material.
- ✓ The higher strength of joints fabricated using square tool pin profile is attributed to the development of finer recrystallized grains in stir zone of FSW joints due to frictional heat generated by the shoulder and pin caused by the stirring action of tool pin.
- ✓ Microstructural examinations revealed that square pin profile showed finer and equiaxed grains as compared to other pin profiles. Crack defects occur in the microstructure at high transverse speeds because of low stirring of material.

- ✓ Overall square tool produces better microstructure and mechanical properties compared to cylindrical tool and conical tool because of pulsating stirring action.

5.2 Recommendations

- ✓ Further work in 5 axis CNC milling machines involves using appropriate combined plunge depth and tilt angle as process parameters to get more defect-free and high-strength joints.
- ✓ Tool material also has more impact on joint quality, so one can use H13 tool steel for better joint integrity.
- ✓ Axial load is also not controlled in CNC milling machines, so use an axial load-controlled machine like the latest CNC machine having force controller machine. Currently, this machine is not available in Ethiopia.

5.3 Future Works

- ✓ This thesis is only performed for butt welding configurations, but it can be applied for lap welding and T-welding.
- ✓ Investigate simulation of friction stir welding to determine the thermal analysis.

REFERENCES

[1] T. Senthilnathan, B. Sujay Aadithya, K. Balachandar, Prediction of mechanical properties and optimization of process parameters in friction-stir-welded dissimilar aluminium alloys, World J. Eng. 17 (2020) 519–526. https://doi.org/10.1108/WJE-01-2020-0019.

[2] S. Verma, J.P. Misra, A Critical Review of Friction Stir Welding Process, (2015) 249–266. https://doi.org/10.2507/daaam.scibook.2015.22.

[3] W. M. Thomas, E. D. Nicholas, C.N. James, S. Walden, M. G. Murch, P. Temple-Smith, C. J, Dawes, Friction welding, Weld. J. (Miami, Fla). 78 (1991) 56. https://doi.org/10.31399/asm.hb.v06.a0001381.

[4] K.N. Zaman, A.N. Siddiquee, Z.A. Khan, Friction Stir Welding: Dissimilar Aluminium Alloys, 2017.

[5] A.. Mousa, S.. Abdallah, A comparative study between friction stir welding and metal inert gas welding of 2024-T4 aluminum alloy, J. Eng. Appl. Sci. 6 (2019) 36–40.

[6] D. Baffari, G. Buffa, D. Campanella, L. Fratini, F. Micari, Friction based solid state welding techniques for transportation industry applications, Procedia CIRP. 18 (2014) 162–167. https://doi.org/10.1016/j.procir.2014.06.125.

[7] D.M. Rodrigues, A. Loureiro, C. Leitao, R.M. Leal, B.M. Chaparro, P. Vilaça, Influence of friction stir welding parameters on the microstructural and mechanical properties of AA 6016-T4 thin welds, Mater. Des. 30 (2009) 1913–1921. https://doi.org/10.1016/j.matdes.2008.09.016.

[8] K.K. Kumar, A. Kumar, M.V.N.V. Satyanarayana, Effect of friction stir welding parameters on the material flow, mechanical properties and corrosion behavior of dissimilar AA5083-AA6061 joints, Proc. Inst. Mech. Eng. Part C J. Mech. Eng. Sci. 236 (2021) 2901–2917. https://doi.org/10.1177/09544062211036102.

[9] R. Palanivel, P. Koshy Mathews, N. Murugan, I. Dinaharan, Effect of tool rotational speed and pin profile on microstructure and tensile strength of dissimilar friction stir welded AA5083-H111 and AA6351-T6 aluminum alloys, Mater. Des. 40 (2012) 7–16. https://doi.org/10.1016/j.matdes.2012.03.027.

[10] R.S. Mishra, Z.Y. Ma, Friction stir welding and processing, Mater. Sci. Eng. R Reports. 50 (2005) 1–78. https://doi.org/10.1016/j.mser.2005.07.001.

[11] P. Avinash, M. Manikandan, N. Arivazhagan, R.K. Devendranath, S. Narayanan, Friction stir welded butt joints of AA2024 T3 and AA7075 T6 aluminum alloys, Procedia Eng. 75 (2014) 98–102. https://doi.org/10.1016/j.proeng.2013.11.020.

[12] S.L. J, G. Bharathiraja, V. Jayakumar, A review on Friction Stir Welding in Aluminium Alloys, IOP Conf. Ser. Mater. Sci. Eng. (2020) 15. https://doi.org/10.1088/1757-899X/954/1/012007.

[13] W.M. Thomas, D.G. Staines, I.M. Norris, R. De Frias, Friction Stir WeldingTools And Developments, 47 (2003) 10–17.

[14] Y.N. Zhang, X. Cao, S. Larose, P. Wanjara, Review of tools for friction stir welding and processing, Can. Metall. Q. 51 (2012) 250–261. https://doi.org/10.1179/1879139512Y.0000000015.

[15] N.Z. Khan, Z.A. Khan, A.N. Siddiquee, Effect of Shoulder Diameter to Pin Diameter (D/d) Ratio on Tensile Strength of Friction Stir Welded 6063 Aluminium Alloy, Mater. Today Proc. 2 (2015) 1450–1457. https://doi.org/10.1016/j.matpr.2015.07.068.

[16] N. Bhardwaj, R.G. Narayanan, U.S. Dixit, M.S.J. Hashmi, Recent developments in friction stir welding and resulting industrial practices, Adv. Mater. Process. Technol. 5 (2019) 461–496. https://doi.org/10.1080/2374068X.2019.1631065.

[17] J.R. Davis, Aluminum and Aluminum Alloys, ASM Int. (2001) 351–416. https://doi.org/10.1361/autb2001p351.

[18] Georgantzia, Gakantou, M, Kamaris, Aluminium alloys as structural material: A review of research, LJMU Res. Online Eng. Struct. (2021) 1–40.

[19] Ng, M.N.Y. S, M.A. A., Reviews on aluminum alloy series and its applications, Acad. J. Sci. Res. 5 (2017) 708–716. https://doi.org/10.15413/ajsr.2017.0724.

[20] Rajbinder, V. Rathi, Singh Kuldeep, Optimization of Friction Stir Welding for AA5052 and AA6061, Int. J. Sci. Res. Dev. 4 (2016) 29–31.

[21] R.S. Lakshmikhanth, K. Subbaiah, Optimization of Tool Pin Profile for Dissimilar

Friction stir welding of AA5083-H111 and AA6061-T6 aluminum alloys, 40 (2020) 460–473.

[22] S. Balamurugan, K. Subbaiah, Investigation of Welding Parameters Effects on Microstructure and Mechanical properties of FSW AA5052-H32 and AA6061 – T6 Dissimilar Al Alloy Welded Joint, 40 (2020) 1305–1314.

[23] H. Deore, V. Hiwarkar, Effect of tool Geometry and process parameters on microstructure and mechanical properties of Dissimilar Friction stir welding of AA6061- AA5052, Int. J. Precis. Eng. Manuf. 18 (2016) 445–452.

[24] M. Sindhuja, S. Neelakrishnan, B.S. Davidson, Friction stir welding parameters and their influence on mechanical properties of welded AA6061 and AA5052 aluminium plates, Mater. Res. Express. 8 (2021) 106525. https://doi.org/10.1088/2053-1591/ac2daf.

[25] M. Shunmugasundaram, A.P. Kumar, L.P. Sankar, S. Sivasankar, Optimization of process parameters of friction stir welded dissimilar AA6063 and AA5052 aluminum alloys by Taguchi technique, Mater. Today Proc. 27 (2020) 871–876. https://doi.org/10.1016/j.matpr.2020.01.122.

[26] V. RajKumar, M. VenkateshKannan, P. Sadeesh, N. Arivazhagan, K. Devendranath Ramkumar, Studies on effect of tool design and welding parameters on the friction stir welding of dissimilar aluminium alloys AA 5052 - AA 6061, Procedia Eng. 75 (2014) 93–97. https://doi.org/10.1016/j.proeng.2013.11.019.

[27] S.K. Gupta, K.N. Pandey, R. Kumar, Artificial intelligence-based modelling and multi-objective optimization of friction stir welding of dissimilar AA5083-O and AA6063-T6 aluminium alloys, Proc. Inst. Mech. Eng. Part L J. Mater. Des. Appl. 232 (2018) 333–342. https://doi.org/10.1177/1464420715627293.

[28] G. Kasirajan, S. Rengarajan, R. Ashok Kumar, G.R. Raghav, V.S. Rao, K.J. Nagarajan, Tensile and wear behaviour of friction stir welded AA5052 and AA6101-T6 aluminium alloys: Effect of welding parameters, Metall. Res. Technol. 117 (2020) 405. https://doi.org/10.1051/metal/2020039.

[29] S. Balamurugan, K. Jayakumar, K. Subbaiah, Influence of Friction Stir Welding Parameters on Dissimilar Joints AA6061-T6 and AA5052-H32, Arab. J. Sci. Eng. 46

(2021) 11985–11998. https://doi.org/10.1007/s13369-021-05773-7.

[30] J.K. Doley, S.D. Kore, A Study on Friction Stir Welding of Dissimilar Thin Sheets of Aluminum Alloys AA 5052-AA 6061, J. Manuf. Sci. Eng. Trans. ASME. 138 (2016) 1–6. https://doi.org/10.1115/1.4033691.

[31] Shunmugasundaram., A.P. Kumar, N.K. Amudhavalli, S. Sivasankar, Parametric optimization on tensile strength of friction stir butt joints of dissimilar aa6061 and aa5052 aluminium alloys by taguchi technique, Mater. Today Proc. 27 (2020) 1258–1262. https://doi.org/10.1016/j.matpr.2020.02.166.

[32] K.K. Kumar, A. Kumar, M.V.N.V. Satyanarayana, Enhancing corrosion resistance and mechanical properties of dissimilar friction stir welded 5083-6061 aluminium alloys using external cooling environment, Proc. Inst. Mech. Eng. Part L J. Mater. Des. Appl. 235 (2021) 2692–2708. https://doi.org/10.1177/14644207211032335.

[33] K. Manigandan, S. Subramaniam, Multi-response optimization of friction stir corner welding of dissimilar thickness AA5086 and AA6061 aluminum alloys by Taguchi grey relational analysis, Proc. Inst. Mech. Eng. Part C J. Mech. Eng. Sci. 233 (2019) 3733–3742. https://doi.org/10.1177/0954406218806032.

[34] M. Ghaffarpour, S. Kolahgar, B.M. Dariani, K. Dehghani, Evaluation of dissimilar welds of 5083-H12 and 6061-T6 produced by friction stir welding, Metall. Mater. Trans. A Phys. Metall. Mater. Sci. 44 (2013) 3697–3707. https://doi.org/10.1007/s11661-013-1739-2.

[35] S.R. Babu, P. Karthik, S. Karthik, S.A. Kumar, J. Morris, Optimization of process parameters during friction stir welding of dissimilar aluminium alloys (AA 5083 & AA 6061) using Taguchi L9 orthogonal array, Appl. Mech. Mater. 592–594 (2014) 630–635. https://doi.org/10.4028/www.scientific.net/AMM.592-594.630.

[36] S. Verma, V. Kumar, Optimization of friction stir welding parameters of dissimilar aluminium alloys 6061 and 5083 by using response surface methodology, Proc. Inst. Mech. Eng. Part C J. Mech. Eng. Sci. 235 (2021) 7009–7020. https://doi.org/10.1177/09544062211005804.

[37] A. Mishra, A.K. Sharma, H. Kapoor, J. Singh, K. Kumar, Investigation on the Tensile Strength of the Friction Stir Welded similar joint of Al / Al alloy using high thermal

diffusivity backing plate material, Int. J. Therm. Technol. 8 (2018) 100–102.

[38] A. Mishra, S. Rizvi, R. Singh, Fabrication and vibration analysis on friction stir welding fixture for mass production, Mech. Mech. Eng. 21 (2017) 531–540.

[39] M. Masoumi, Y. Zedan, D. Texier, M. Jahazi, The Influence of Tool Geometry on Mechanical Properties of Friction Stir Welded AA-2024 and AA-2198 Joints, Int. Comm. Study Bauxite, Alumina Alum. (2016).

[40] ASTM E8, ASTM E8/E8M standard test methods for tension testing of metallic materials 1, Annu. B. ASTM Stand. 4. (2010) 1–27. https://doi.org/10.1520/E0008.

[41] ASTM E92-82, Standard Test Method for Vickers Hardness of Metallic Materials, ASTM Int. 82 (2004) 1–9.

[42] C.N. Suresha, B.M. Rajaprakash, S. Upadhya, A study of the effect of tool pin profiles on tensile strength of welded joints produced using friction stir welding process, Mater. Manuf. Process. 26 (2011) 1111–1116. https://doi.org/10.1080/10426914.2010.532527.

[43] S.Y. Abbasi, I. Shahid Butt, G. Hussain, S. Husain Imram, A. Mohammad Khan, R. Abdul Baseer, Optimization of parameters for micro friction stir welding of aluminum 5052 using Taguchi technique, Int. J. Adv. Manufacuring Technol. (2019) 1–10. https://doi.org/https://doi.org/10.1007/s00170-018-3138-8.

[44] P.K. Sahu, S. Pal, Multi-response optimization of process parameters in friction stir welded AM20 magnesium alloy by Taguchi grey relational analysis, J. Magnes. Alloy. 3 (2015) 36–46. https://doi.org/10.1016/j.jma.2014.12.002.

[45] J. Kundu, H. Singh, Friction stir welding: multi-response optimisation using Taguchi-based GRA, Prod. Manuf. Res. 4 (2016) 228–241. https://doi.org/10.1080/21693277.2016.1266449.

[46] K. Palani, C. Elanchezhian, Multi response Optimization of Friction stir welding process parameters in dissimilar alloys using Grey relational analysis, IOP Conf. Ser. Mater. Sci. Eng. 390 (2018) 1–9. https://doi.org/10.1088/1757-899X/390/1/012061.

[47] Ş. Kasman, Optimisation of dissimilar friction stir welding parameters with grey relational analysis, Proc. Inst. Mech. Eng. Part B J. Eng. Manuf. 227 (2013) 1317–1324. https://doi.org/10.1177/0954405413487729.

[48] N.D. Ghetiya, K.M. Patel, A.J. Kavar, Multi-objective Optimization of FSW Process Parameters of Aluminium Alloy Using Taguchi-Based Grey Relational Analysis, Trans. Indian Inst. Met. 69 (2016) 917–923. https://doi.org/10.1007/s12666-015-0581-1.

[49] S. Jain, N. Sharm, R. Gupta, Dissimilar alloys (AA6082/AA5083) joining by FSW and parametric optimization using Taguchi, grey relational and weight method, Eng. Solid Mech. 6 (2018) 51–66. https://doi.org/10.5267/j.esm.2017.10.003.

[50] S. Kumar, S. Kumar, Multi-response optimization of process parameters for friction stir welding of joining dissimilar Al alloys by gray relation analysis and Taguchi method, J. Brazilian Soc. Mech. Sci. Eng. 37 (2015) 665–674. https://doi.org/10.1007/s40430-014-0195-2.

[51] K.N. Wakchaure, A.G. Thakur, V. Gadakh, A. Kumar, Multi-Objective Optimization of Friction Stir Welding of Aluminium Alloy 6082-T6 Using hybrid Taguchi-Grey Relation Analysis- ANN Method, Mater. Today Proc. 5 (2018) 7150–7159. https://doi.org/10.1016/j.matpr.2017.11.380.

[52] C. Chanakyan, S. Sivasankar, S. V. Alagarsamy, S.D. Kumar, S. Sakthivelu, M. Meignanamoorthy, M. Ravichandran, Parametric optimization for friction stir welding with AA2024 and AA6061 aluminium alloys by ANOVA and GRG, Mater. Today Proc. 27 (2020) 707–711. https://doi.org/10.1016/j.matpr.2019.11.257.

[53] R.P. Singh, S. Dubey, A. Singh, S. Kumar, Materials Today : Proceedings A review paper on friction stir welding process, Mater. Today Proc. 38 (2021) 6–11. https://doi.org/10.1016/j.matpr.2020.05.208.

[54] A. Sasikumar, S. Gopi, D.G. Mohan, Effect of welding speed on mechanical properties and corrosion resistance rates of filler induced friction stir welded AA6082 and AA5052 joints, Mater. Res. Express. 8 (2021) 066531. https://doi.org/10.1088/2053-1591/ac0c9e.

[55] D. Devaiah, K. Kishore, P. Laxminarayana, Effect of Welding Speed on Mechanical Properties of Dissimilar Friction Stir Welded AA5083-H321 and AA6061-T6 Aluminum Alloys, Int. J. Adv. Eng. Res. Sci. 4 (2017) 22–28. https://doi.org/10.22161/ijaers.4.3.4.

[56] D.G. Mohan, S. Gopi, A. Sasikumar, Examining the Mechanical and Metallurgical

Properties of Single Pass Friction Stir Welded Dissimilar Aluminium Alloys Tee Joints, 3 (2021) 6–12. https://sciencevolks.com/materials-science/pdf/SVOA-MST-03-019.pdf.

[57] L.H. Shah, S. Sonbolestan, A.R.H. Midawi, S. Walbridge, A. Gerlich, Dissimilar friction stir welding of thick plate AA5052-AA6061 aluminum alloys: effects of material positioning and tool eccentricity, Int. J. Adv. Manuf. Technol. 105 (2019) 889–904. https://doi.org/10.1007/s00170-019-04287-9.

[58] J. Kundu, H. Singh, Friction stir welding of AA5083 aluminium alloy: Multi-response optimization using Taguchi-based grey relational analysis, Adv. Mech. Eng. 8 (2016) 1–10. https://doi.org/10.1177/1687814016679277.

[59] U. Çaydaş, A. Hasçalik, Use of the grey relational analysis to determine optimum laser cutting parameters with multi-performance characteristics, Opt. Laser Technol. 40 (2008) 987–994. https://doi.org/10.1016/j.optlastec.2008.01.004.

[60] D. Ju-Long, Control problems of grey systems, Syst. Control Lett. 1 (1982) 288–294. https://doi.org/10.1016/S0167-6911(82)80025-X.

[61] I. Abdulaziz, Albannai, Review The Common Defects In Friction Stir Welding, Int. J. Sci. Technol. Res. 9 (2020) 318–329. www.ijstr.org.

APPENDICES

Appendix: A

Table A1: Chemical Composition and Mechanical Properties of AA 5052 -H32

河 南 明 泰 产 品 质 量 证 明 书

HE NAN MING TAI PRODUCT QUALITY CERTIFICATE

订 货 单 位 Customer			编 号: Serial No:	17120520013
产品名称 Product	批 号 Lot No	合 金 状 态 Alloy And Temper	规格（mm） Dimension	
	1706521	5052-H32	6*1250*2500mm	
技 术 标 准 Technique Standard		GB/T3880-2012	化 学 成 分 标 准 Composition Standard	GB/T3190-2020

化学成分% Chemical Composition

元 素 Element	Si	Fe	Cu	Mn	Mg	Cr	Ni	Zn	Ti	Al
标 准 值 Standard Value	0.25	0.40	0.10	0.1	2.2-2.8	0.15-0.35	---	0.1	0.15	余量 Remainder
实测值 Actual Value	0.1	0.31	0.01	0.05	2.3	0.17		0.01	0.010	

机械性能 Mechanical Property

取样方法 Sampling Method	抗拉强度（MPa） Tensile Strength		屈服强度（MPa） Yield Strength		延伸率（%） Elongation	
——	标 准 值 Standard Value	实测值 Actual Value	标 准 值 Standard Value	实测值 Actual Value	标 准值 Standard Value	实测值 Actual Value
	210-260	230	≥130	158	≥7	18

杯 突 Cup Bulge	——	——	90° 折弯 90° bend	——
制耳率 Earing（%）	——	——	其他 Others	——

表面质量 Surface Control	良	几何尺寸 Dimension Control	符合标准
氯含量标准值（ml/100gAl） Hydrogen Content Standard Value	——	氯含量实测值（ml/100gAl） Hydrogen Content Actual Value	——
备注 Note			

质量、环境、职业健康安全分别通过 ISO9001、TS16949 管理体系认证。本产品的铝、汞、镉、六价铬的含量均符合欧盟 ROHS 指令 2005/618/EC 的要求，砷＜1000PPm。

Quality，Environment and Professional Health &Safety Management System have Certified as per ISO9001、TS16949。Content of Plumbum、Mercury、Cadmium and sexivalent Chrome conforms to ROHS 2005/618/EC,arsenic is less than 1000PPm。

检查员： 曹万军 日期： 2021 年 09 月 03 日

Inspector: Date:

河南明泰铝业股份有限公司

地址:河南省巩义市回郭镇开发区北部

邮编:451283 电话:0371-67554997 67554995 传真:0371-67554518

Table A2: Chemical Composition and Mechanical Properties of AA 6061- T6

明 泰 铝 业 产 品 质 量 证 明 书

CE

MING TAI AL. PRODUCT QUALITY CERTIFICATE

订货单位 Customer	—			编 号: Serial No:	MT21061664
产品名称 Product	批 号 Lot No	合 金 状 态 Alloy And Temper	规格（mm） Dimension		
铝板/铝带	SYK2105N60258	6061 T6	6.0000*1250.00*2500		
技 术 标 准 Technique Standard		GB/T 3880-2012	化 学 成 分 标 准 Composition Standard		GB/T 3190-2020

化学成分 % Chemical Composition

元素 Element	Si	Fe	Cu	Mn	Mg	Cr	Zn	Na	Ti	Al
标准值 Standard Value	0.4-0.8	≤0.7	0.15-0.4	≤0.15	0.8-1.2	0.04-0.35	≤0.25	---	≤0.15	余量
实测值 Measured Value	0.616	0.502	0.241	0.083	1.047	0.111	0.125	0.0002	0.027	97.06

力学性能 Mechanical Property

取样方法 Sampling Method	抗拉强度（MPa） Tensile Strength		屈服强度（MPa） Yield Strength		延伸率（%） Elongation	
横向	标准值 Standard Value	实测值 Measured Value	标准值 Standard Value	实测值 Measured Value	标准值 Standard Value	实测值 Measured Value
	≥290	310	≥240	273	≥10	15

杯 凸 Cup Bulge	标准值 Standard Value	——	制耳率（%） Earing	标准值 Standard Value	——
	实测值 Measured Value	——		实测值 Measured Value	——

表面硬度(HV) Hardness(HV)	107	其他 Others	合格
表面质量 Surface Control	合格	几何尺寸 Dimension Control	合格
综合判定 Overall Conlusion	合格		

郑州明泰实业有限公司 技术质量处

填表人： 刘盈鸽 审批人： 魏豪杰 日期： 2021年06月12日

Inspector: Approver: Date:

郑州明泰实业有限公司

地址:河南省郑州市高新区长椿路6号 邮编：450000

电话:86-371-67898721 传真:86-371-67898178

Appendix: B

The part programs used for FSW of dissimilar Al-alloys 6061 and 5052

```
O0101;
G21 G90 G40 G80 G49;
MO6 T02;
M03 S1100 ;
G54 ;
G00 X0 Y0 ;
G00 Z5 ;
G01 Z -5.72 F40 ;
G01 Y-1
G04 P10000;
G01 Y -133;
G01 Z5;
G00 Z300;
G00 X0 Y0;
M05;
M30;
%
```

Appendix: C

Table C1: Eigen analysis of the Correlation Matrix

Eigen analysis of the Correlation Matrix

Eigenvalue	1.8930	0.1070
Proportion	0.947	0.053
Cumulative	0.947	1.000

Table C2: Eigenvectors

Eigenvectors

Variable	PC1	PC2
SN_{UTS}	0.707	-0.707
SN_{RA4}	0.707	0.707

Appendix: D

Mechanical test results

Table D1: Tensile strength Experiment result

Experiment number	Trial 1	Trial 2	Trial 3	Average tensile strength in MPa
1	143.72	137.61	126.5	135.94
2	148.89	166.94	175.83	163.89
3	166.83	169.96	180.58	172.46
4	168.17	182.61	179.83	176.87
5	152.71	161.33	148.72	154.25
6	114.17	128.61	125.83	122.87
7	184.17	183.33	181.63	183.04
8	137.05	133	125.5	131.85
9	181.71	183.75	178.94	181.47

Table D2: Hardness test experiment result

Experiment number	Trial 1	Trial 2	Trial 3	Average Vickers hardness HV
1	66	58.3	58.8	61.03
2	62.8	61.7	65.3	63.27
3	63	68.5	62.8	64.77
4	61.8	70.5	70.7	67.67
5	61	62.7	64.6	62.77
6	58.7	55.3	55.9	56.63
7	78.4	72	78.8	76.40
8	61.8	59.4	57.1	59.43
9	67.6	72.5	66.7	68.93

Table D3: Confirmation test result

Optimal Combination	**The response of quality characteristics**				
A3B1C3	UTS(MPa)	UTS $_{S/N}$	Hardness (Hv)	Hardness $_{S/N}$	GRG
Replication 1	183.55	45.2751	76.77	37.7038	0.9316
Replication 2	183.56	45.2756	76.83	37.7106	1.0000
Replication 3	182.57	45.2286	75.93	37.6083	0.3333
Average	183.23		76.51		**0.7550**

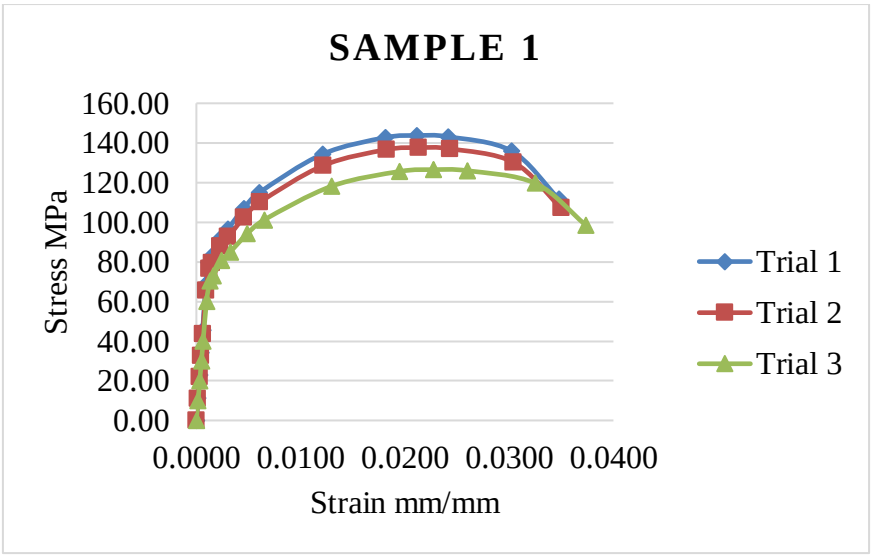
SAMPLE 1
160.00
140.00
120.00
100.00
80.00
60.00
40.00
20.00
0.00
Stress MPa
0.0000
0.0100
0.0200
0.0300
0.0400
Strain mm/mm
Trial 1
Trial 2
Trial 3

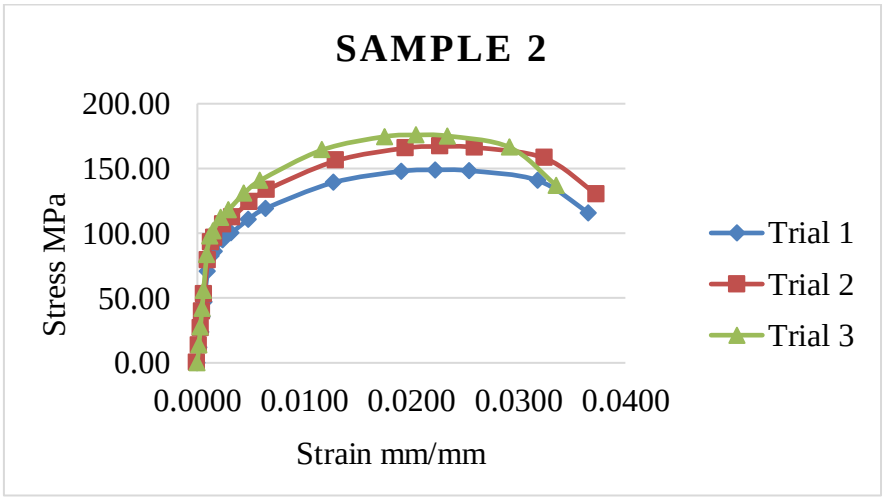
SAMPLE 2
200.00
150.00
100.00
50.00
0.00
Stress MPa
0.0000
0.0100
0.0200
0.0300
0.0400
Strain mm/mm
Trial 1
Trial 2
Trial 3

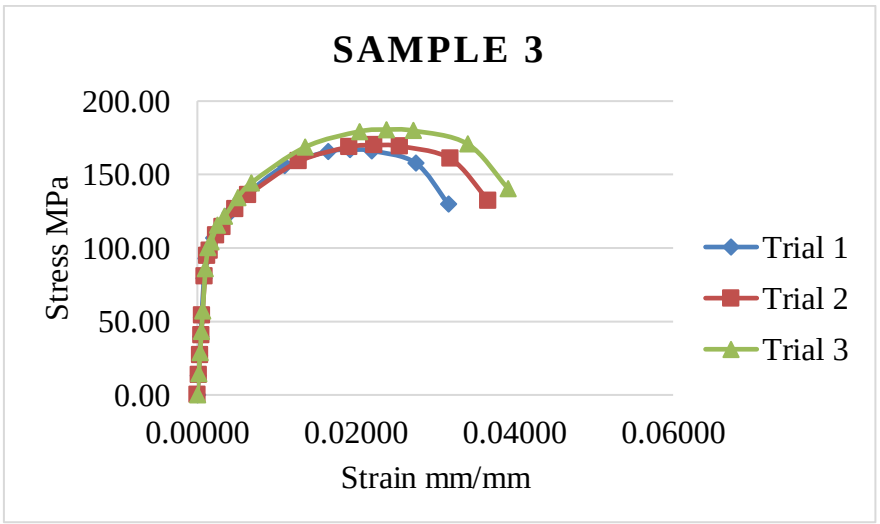
SAMPLE 3
200.00
150.00
100.00
50.00
0.00
Stress MPa
0.00000
0.02000
0.04000
0.06000
Strain mm/mm
Trial 1
Trial 2
Trial 3

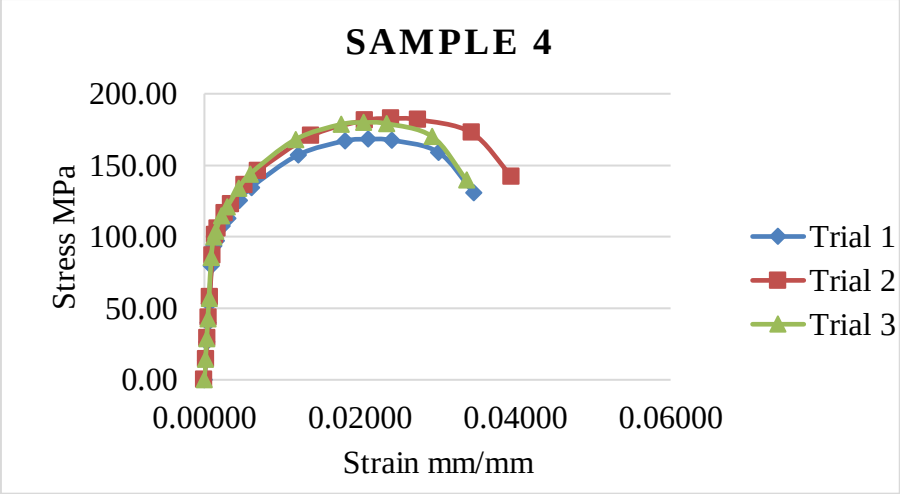
SAMPLE 4
200.00
150.00
100.00
50.00
0.00
Stress MPa
0.00000
0.02000
0.04000
0.06000
Strain mm/mm
Trial 1
Trial 2
Trial 3

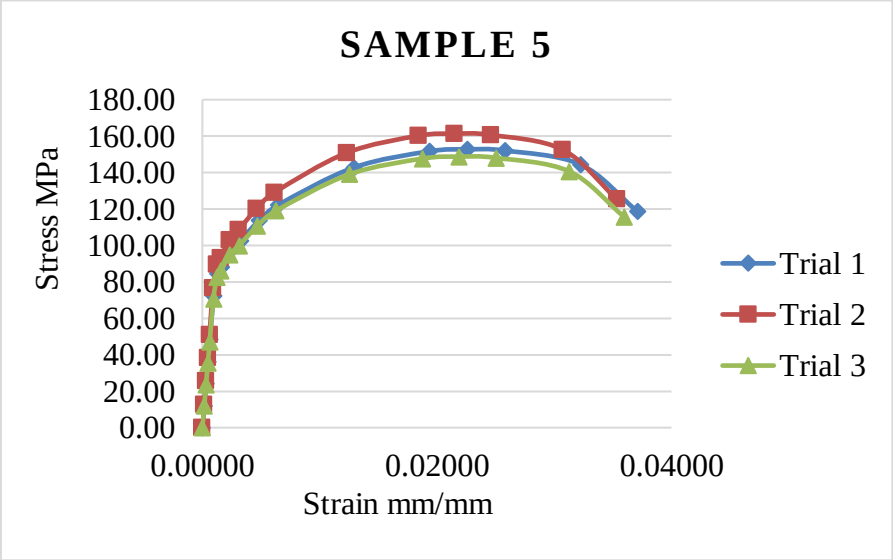
SAMPLE 5
180.00
160.00
140.00
120.00
100.00
80.00
60.00
40.00
20.00
0.00
Stress MPa
0.00000
0.02000
0.04000
Strain mm/mm
Trial 1
Trial 2
Trial 3

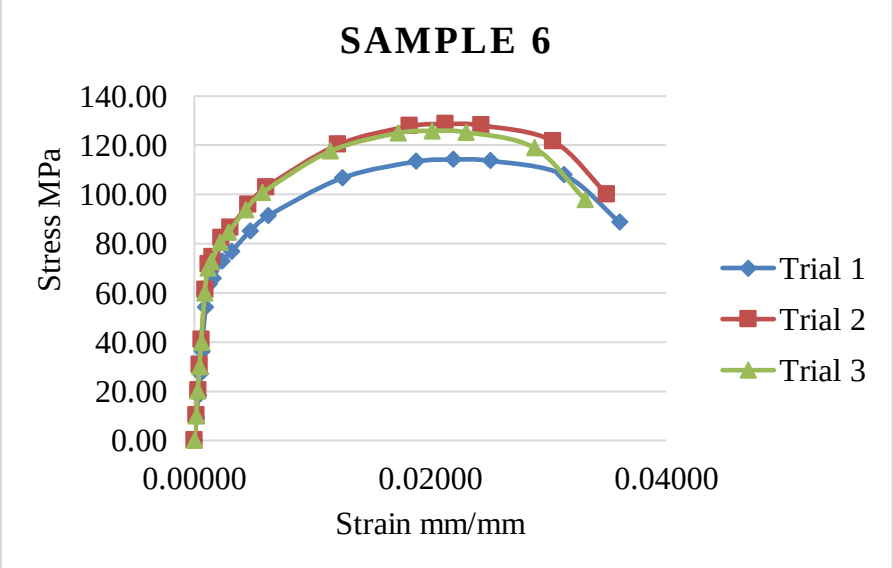
SAMPLE 6
140.00
120.00
100.00
80.00
60.00
40.00
20.00
0.00
Stress MPa
0.00000
0.02000
0.04000
Strain mm/mm
Trial 1
Trial 2
Trial 3

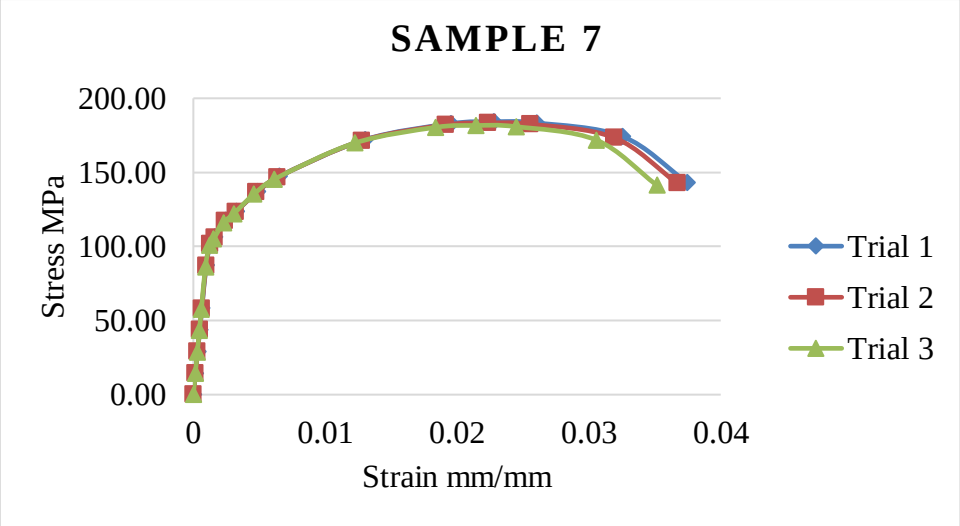

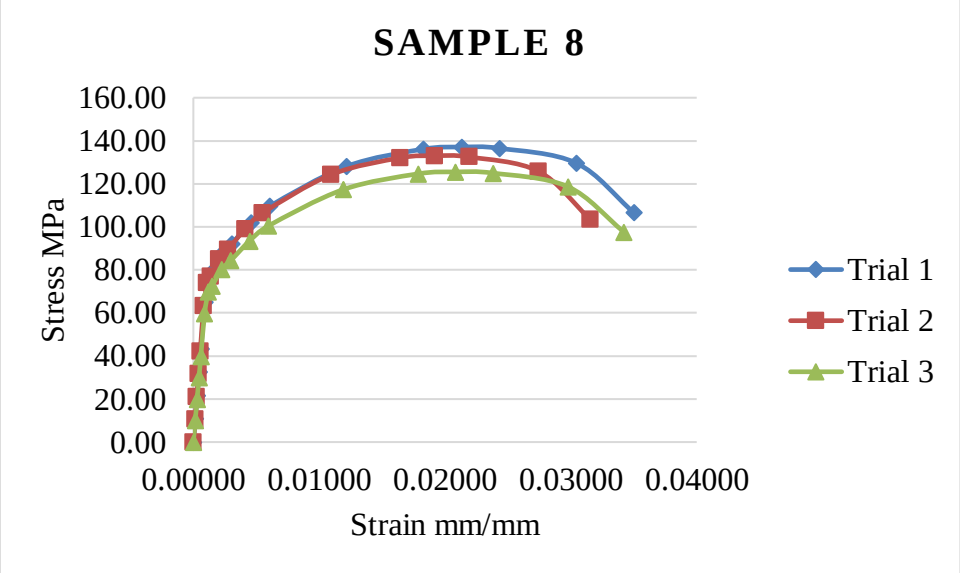

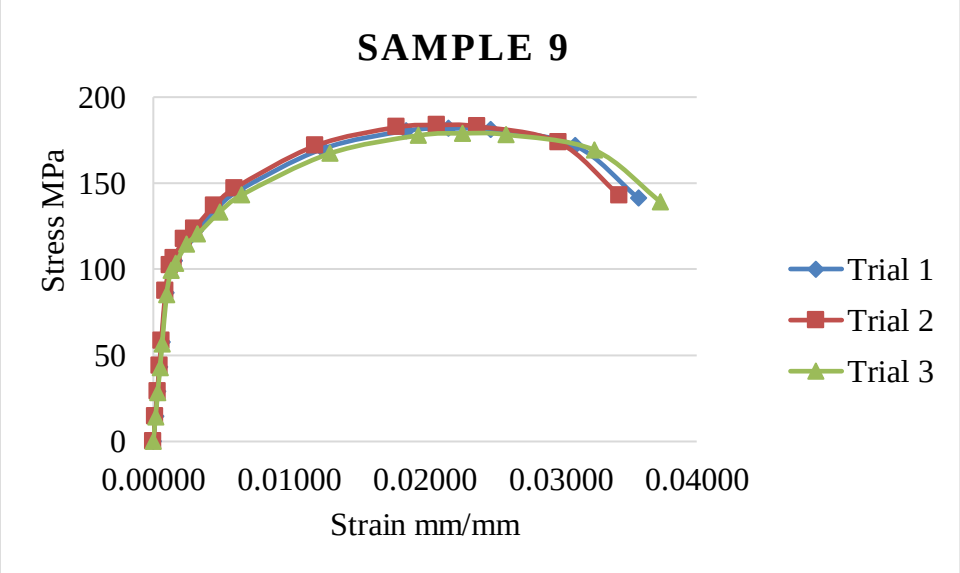

Figure D1: Stress-strain diagram of tensile test results

Appendix: E

Table E1: F-Critical values

TABLE E

F critical values

Degrees of freedom in the denominator		Degrees of freedom in the numerator								
	p	1	2	3	4	5	6	7	8	9
1	.100	39.86	49.50	53.59	55.83	57.24	58.20	58.91	59.44	59.86
	.050	161.45	199.50	215.71	224.58	230.16	233.99	236.77	238.88	240.54
	.025	647.79	799.50	864.16	899.58	921.85	937.11	948.22	956.66	963.28
	.010	4052.2	4999.5	5403.4	5624.6	5763.6	5859.0	5928.4	5981.1	6022.5
	.001	405284	500000	540379	562500	576405	585937	592873	598144	602284
2	.100	8.53	9.00	9.16	9.24	9.29	9.33	9.35	9.37	9.38
	.050	18.51	19.00	19.16	19.25	19.30	19.33	19.35	19.37	19.38
	.025	38.51	39.00	39.17	39.25	39.30	39.33	39.36	39.37	39.39
	.010	98.50	99.00	99.17	99.25	99.30	99.33	99.36	99.37	99.39
	.001	998.50	999.00	999.17	999.25	999.30	999.33	999.36	999.37	999.39
3	.100	5.54	5.46	5.39	5.34	5.31	5.28	5.27	5.25	5.24
	.050	10.13	9.55	9.28	9.12	9.01	8.94	8.89	8.85	8.81
	.025	17.44	16.04	15.44	15.10	14.88	14.73	14.62	14.54	14.47
	.010	34.12	30.82	29.46	28.71	28.24	27.91	27.67	27.49	27.35
	.001	167.03	148.50	141.11	137.10	134.58	132.85	131.58	130.62	129.86
4	.100	4.54	4.32	4.19	4.11	4.05	4.01	3.98	3.95	3.94
	.050	7.71	6.94	6.59	6.39	6.26	6.16	6.09	6.04	6.00
	.025	12.22	10.65	9.98	9.60	9.36	9.20	9.07	8.98	8.90
	.010	21.20	18.00	16.69	15.98	15.52	15.21	14.98	14.80	14.66
	.001	74.14	61.25	56.18	53.44	51.71	50.53	49.66	49.00	48.47
5	.100	4.06	3.78	3.62	3.52	3.45	3.40	3.37	3.34	3.32
	.050	6.61	5.79	5.41	5.19	5.05	4.95	4.88	4.82	4.77
	.025	10.01	8.43	7.76	7.39	7.15	6.98	6.85	6.76	6.68
	.010	16.26	13.27	12.06	11.39	10.97	10.67	10.46	10.29	10.16
	.001	47.18	37.12	33.20	31.09	29.75	28.83	28.16	27.65	27.24
6	.100	3.78	3.46	3.29	3.18	3.11	3.05	3.01	2.98	2.96
	.050	5.99	5.14	4.76	4.53	4.39	4.28	4.21	4.15	4.10
	.025	8.81	7.26	6.60	6.23	5.99	5.82	5.70	5.60	5.52
	.010	13.75	10.92	9.78	9.15	8.75	8.47	8.26	8.10	7.98
	.001	35.51	27.00	23.70	21.92	20.80	20.03	19.46	19.03	18.69
7	.100	3.59	3.26	3.07	2.96	2.88	2.83	2.78	2.75	2.72
	.050	5.59	4.74	4.35	4.12	3.97	3.87	3.79	3.73	3.68
	.025	8.07	6.54	5.89	5.52	5.29	5.12	4.99	4.90	4.82
	.010	12.25	9.55	8.45	7.85	7.46	7.19	6.99	6.84	6.72
	.001	29.25	21.69	18.77	17.20	16.21	15.52	15.02	14.63	14.33

TABLE E

F critical values (continued)

Degrees of freedom in the denominator		Degrees of freedom in the numerator								
	p	1	2	3	4	5	6	7	8	9
8	.100	3.46	3.11	2.92	2.81	2.73	2.67	2.62	2.59	2.56
	.050	5.32	4.46	4.07	3.84	3.69	3.58	3.50	3.44	3.39
	.025	7.57	6.06	5.42	5.05	4.82	4.65	4.53	4.43	4.36
	.010	11.26	8.65	7.59	7.01	6.63	6.37	6.18	6.03	5.91
	.001	25.41	18.49	15.83	14.39	13.48	12.86	12.40	12.05	11.77
9	.100	3.36	3.01	2.81	2.69	2.61	2.55	2.51	2.47	2.44
	.050	5.12	4.26	3.86	3.63	3.48	3.37	3.29	3.23	3.18
	.025	7.21	5.71	5.08	4.72	4.48	4.32	4.20	4.10	4.03
	.010	10.56	8.02	6.99	6.42	6.06	5.80	5.61	5.47	5.35
	.001	22.86	16.39	13.90	12.56	11.71	11.13	10.70	10.37	10.11
10	.100	3.29	2.92	2.73	2.61	2.52	2.46	2.41	2.38	2.35
	.050	4.96	4.10	3.71	3.48	3.33	3.22	3.14	3.07	3.02
	.025	6.94	5.46	4.83	4.47	4.24	4.07	3.95	3.85	3.78
	.010	10.04	7.56	6.55	5.99	5.64	5.39	5.20	5.06	4.94
	.001	21.04	14.91	12.55	11.28	10.48	9.93	9.52	9.20	8.96
11	.100	3.23	2.86	2.66	2.54	2.45	2.39	2.34	2.30	2.27
	.050	4.84	3.98	3.59	3.36	3.20	3.09	3.01	2.95	2.90
	.025	6.72	5.26	4.63	4.28	4.04	3.88	3.76	3.66	3.59
	.010	9.65	7.21	6.22	5.67	5.32	5.07	4.89	4.74	4.63
	.001	19.69	13.81	11.56	10.35	9.58	9.05	8.66	8.35	8.12
12	.100	3.18	2.81	2.61	2.48	2.39	2.33	2.28	2.24	2.21
	.050	4.75	3.89	3.49	3.26	3.11	3.00	2.91	2.85	2.80
	.025	6.55	5.10	4.47	4.12	3.89	3.73	3.61	3.51	3.44
	.010	9.33	6.93	5.95	5.41	5.06	4.82	4.64	4.50	4.39
	.001	18.64	12.97	10.80	9.63	8.89	8.38	8.00	7.71	7.48
13	.100	3.14	2.76	2.56	2.43	2.35	2.28	2.23	2.20	2.16
	.050	4.67	3.81	3.41	3.18	3.03	2.92	2.83	2.77	2.71
	.025	6.41	4.97	4.35	4.00	3.77	3.60	3.48	3.39	3.31
	.010	9.07	6.70	5.74	5.21	4.86	4.62	4.44	4.30	4.19
	.001	17.82	12.31	10.21	9.07	8.35	7.86	7.49	7.21	6.98
14	.100	3.10	2.73	2.52	2.39	2.31	2.24	2.19	2.15	2.12
	.050	4.60	3.74	3.34	3.11	2.96	2.85	2.76	2.70	2.65
	.025	6.30	4.86	4.24	3.89	3.66	3.50	3.38	3.29	3.21
	.010	8.86	6.51	5.56	5.04	4.69	4.46	4.28	4.14	4.03
	.001	17.14	11.78	9.73	8.62	7.92	7.44	7.08	6.80	6.58
15	.100	3.07	2.70	2.49	2.36	2.27	2.21	2.16	2.12	2.09
	.050	4.54	3.68	3.29	3.06	2.90	2.79	2.71	2.64	2.59
	.025	6.20	4.77	4.15	3.80	3.58	3.41	3.29	3.20	3.12
	.010	8.68	6.36	5.42	4.89	4.56	4.32	4.14	4.00	3.89
	.001	16.59	11.34	9.34	8.25	7.57	7.09	6.74	6.47	6.26
16	.100	3.05	2.67	2.46	2.33	2.24	2.18	2.13	2.09	2.06
	.050	4.49	3.63	3.24	3.01	2.85	2.74	2.66	2.59	2.54
	.025	6.12	4.69	4.08	3.73	3.50	3.34	3.22	3.12	3.05
	.010	8.53	6.23	5.29	4.77	4.44	4.20	4.03	3.89	3.78
	.001	16.12	10.97	9.01	7.94	7.27	6.80	6.46	6.19	5.98
17	.100	3.03	2.64	2.44	2.31	2.22	2.15	2.10	2.06	2.03
	.050	4.45	3.59	3.20	2.96	2.81	2.70	2.61	2.55	2.49
	.025	6.04	4.62	4.01	3.66	3.44	3.28	3.16	3.06	2.98
	.010	8.40	6.11	5.19	4.67	4.34	4.10	3.93	3.79	3.68
	.001	15.72	10.66	8.73	7.68	7.02	6.56	6.22	5.96	5.75